

**University of Bergen
Geophysical Institute**

**Using a Rayleigh Distillation Framework to
Investigate the Evolution of Stable Water
Isotopes in a Precipitation Event across
Western Norway**

Emili Carin Rønning

Supervisors: Hans Christian Steen-Larsen and Harald Sodemann

Submission: 1st of June 2023

Abstract

Stable water isotope signals in precipitation show spatial and temporal patterns which are visible with high-frequency sampling. Several different processes affect the isotopic signals in precipitation, and investigating these, further the understanding of the hydrologic cycle. As stable water isotopes experience fractionation during evaporation and condensation, the phase changes leaves imprints on the isotopic signals. These imprints makes tracking of moisture in the atmosphere possible, providing a way to determine the location of the moisture source where water first was evaporated. Daily precipitation measurements fails to represent the variations during a single precipitation event so there is a need for high-frequency measurements to investigate which factors affect the isotopic composition in precipitation. The aim of this thesis is to sample high-frequency measurements at different stations and show how the isotopic signals in precipitation change as a result of increasing altitude, rain-out and different below-cloud processes. Samples and measurements were gathered from four stations going west to east on the west coast of Norway during an incoming front on 27/11/22. Relative humidity, temperature and rainfall was measured to look at the different atmospheric processes which affected the isotopic signals. These measurements were compared and with the MetCoOP ensemble prediction system (MEPS) model. The MEPS model was also used to investigate cloud cover, rain generation height, saturation mixing ratio and water vapor, and how these factors potentially affected the final isotopic composition of precipitation. Applications of a Rayleigh distillation model showed that significant rain-out and increase in altitude gave decreasing depletion west to east. The Rayleigh processes were investigated together with the integrated water vapor (IWV) and saturation mixing ratios from the MEPS model. The moisture source was determined under assumption that the condensation temperature during the Rayleigh condensation process was 5 °C and that the initial saturation mixing ratio in the source region was 9 gkg⁻¹. The condensation temperature in the moisture region was calculated to 12.5-15 °C and the source region was narrowed down to around 50°N. The measurements from this field work along with the MEPS model allowed an insight in the atmospheric processes and possible travel distance of moisture in the atmosphere. The orographic effects on isotope signals have few studies in Norway, and this thesis could help broaden the understanding of these processes in a spaitotemporal framework.

Acknowledgement

My deepest gratitude goes to Marlén, Torunn, Sofie and Constance for helping me with my field work and for sampling precipitation. Thank you to my parents for providing me with company during the windy conditions at Finse and for all your support. I would also like to extend my thanks to my supervisors Hans Christian and Harald for guidance and providing useful feedback.

Contents

1	Introduction	5
2	Theory	7
2.1	Fractionation	7
2.2	Equilibrium Processes	8
2.3	Rayleigh Distillation Processes	8
2.3.1	Mixing Ratios	10
2.4	Non-equilibrium processes	12
2.4.1	d-excess	12
2.5	Isotopic composition in precipitation	13
2.5.1	Temperature-, amount-, altitude, and rain-out effects	13
2.6	Isotopic composition of a front	14
2.6.1	Front characteristics	14
2.6.2	Isotopic signals in frontal structures	15
2.6.3	Below-cloud effects	17
2.7	Snow Isotopes	18
3	Method	19
3.1	Stations	19
3.2	Instrumentation	19
3.3	Equipment and techniques for sampling of precipitation	22
3.3.1	Collecting precipitation	22
3.3.2	Snowfall rate	22
3.4	Lab analysis	22
3.5	Weather Forecasting with MEPS	23
3.5.1	ERA5	23
3.6	Statistical methods and model verification	23
4	Results	26
4.1	The incoming front on the 27/11/22	26
4.2	Model verification	26
4.3	Daily precipitation measurements	28
4.4	Meteorological ground observations during the fieldwork	30
4.5	Fieldwork samples and measurements	31
4.5.1	Ågotnes	31
4.5.2	Bergen	32
4.5.3	Voss	33
4.5.4	Finse	34
4.6	Precipitation weighted mean and rain intensity	35
4.7	Integrated water vapor	38
4.8	Rayleigh distillation model	39
4.8.1	Rayleigh model from an IWV framework	39
4.8.2	Rayleigh model from a mixing ratio framework	42
4.9	Generation of precipitation with the MEPS model	44
4.10	d-excess	45
5	Discussion	47

5.1	MEPS model verification and weather forecast	47
5.2	Role of daily precipitation	48
5.3	The evolution of the isotopic in precipitation	48
5.3.1	Patterns and evolution of isotopic signals at Ågotnes	49
5.3.2	Patterns and evolution of isotopic signals in Bergen	50
5.3.3	Patterns and evolution of isotopic signals at Voss	51
5.3.4	Patterns and evolution of isotopic signals at Finse	52
5.3.5	Impacts of humidity and temperature	53
5.4	Processes expanding on the evolution of isotopic signals within the front	54
5.4.1	Amplitudes of the variations of the isotopic composition	54
5.4.2	Precipitation weighted mean and precipitation intensity	54
5.4.3	Altitude effect	56
5.4.4	Cloud shape and evolution	56
5.5	Rayleigh model	57
5.5.1	IWV perspective	59
5.5.2	Saturation mixing ratio perspective	59
5.6	Locating the moisture source	60
5.7	What happens when a rain drop leaves the cloud base?	61
6	Summary and conclusion	64

1 Introduction

Studies on stable water isotopes in precipitation can give insights in how water is transported in the atmosphere, which is a useful tool when studying the hydrologic cycle (Galewsky et al., 2016; Gat, 1996). Observations of isotopic composition in precipitation or vapor can provide useful diagnostics on the physical processes in the atmosphere like evaporation, condensation, mixing of air masses, below-cloud processes, identification of water sources and seasonality of precipitation (Yoshimura et al., 2010; Graf et al., 2019; Dansgaard, 1964; Weng et al., 2021). Stable water isotopes like $^2H^1H^{16}O$ (also called deuterium, HDO) and $H_2^{18}O$ (oxygen-18) are the most abundant of the heavy stable water isotopes. These stable water isotopes have been studied in precipitation since the 50s when Dansgaard (1953) investigated the abundance of oxygen-18 in a warm front and revealed atmospheric processes of fractionation. The fractionation process is connected to phase changes and occurs because of the different masses of the heavy stable water isotopes. Because of the properties that fractionation provides, the condensation history of water vapor can be traced (Dütsch et al., 2017).

Sherwood et al. (2010) noted the need for better isotopic observations to aid in understanding the water vapor processes. High-frequency measurements of water isotopes in precipitation and vapor reveals unique spatial and temporal patterns which could further the knowledge of the processes in the atmospheric water cycle. Studies have shown (Weng et al., 2021; Gedzelman and Lawrence, 1990) that different fronts and cloud structures produce distinct isotopic patterns. Therefore, goal for this thesis is to find these distinct patterns, and investigate their persistence with increasing altitude, rain-out and distance from the coast.

I aim to investigate how oxygen-18 in precipitation change during a frontal passage with field observations and samples surface precipitating from four different stations. Studies investigating isotopic signals at several locations along a topographic rise has not been explored at the west coast of Norway. The main part of this project is the field observations and the analysis of the field measurements. The inquiry was to determine how the isotopic signals will change and which factors contribute to the change. The field observations will be compared with forecasts from the MetCoOP Ensemble Prediction system (MEPS). The goal of using the MEPS model was to investigate the atmospheric processes and to determine if the model could contribute in explaining the changes in the isotopic signals. Prior to the fieldwork, I predicted that the isotopic signals would become more diffuse with increasing distance from the coast and lose the characteristic "W" pattern observed by Weng et al. (2021).

The Rayleigh distillation model was used to investigate the spatiotemporal evolution of the isotopic signals in precipitation. The Rayleigh distillation model offer an simple and effective way of investigating at the isotopic evolution under equilibrium conditions (Gat, 1996; Dansgaard, 1964). The model describes a simplified condensation processes in the atmosphere, and I aim to investigate if the moisture source can be determined with the Rayleigh model and to discuss how accurate this approach is. I will use the Rayleigh model in combination with the MEPS model outputs of integrated water vapor (IWV) and the saturation mixing ratios to determine if the isotopic signals can be explained by the Rayleigh framework. In recent studies (Yoshimura et al., 2010; Weng et al., 2021), the validity of the Rayleigh model is questioned based on its simplicity and that factors like mixing and below-cloud evaporation are neglected in the model due to its idealistic approach. The contributions from the below-cloud effects and how they affect the isotopic composition in precipitation have been discussed in several papers (Graf et al., 2019; Aemisegger et al., 2015; Weng et al., 2021) and will be investigated in this thesis.

During an atmospheric river (AR) event, Coplen et al. (2008) noted that the high variations in isotopic values in precipitation and the sharp drop in the isotopic signals was attributed to change from high cloud to low clouds. Yoshimura et al. (2010) looked at the same AR-event and determined that the below-cloud processes and mixing of air masses caused the change and that the higher isotopic, less depleted, values in the beginning of the AR-event was caused by below-cloud evaporation. Different frontal structures produce different cloud types, and the different cloud types have different isotopic signals (Gedzelman and Lawrence, 1990). The isotopic composition of surface precipitation in relation to deep stratiform clouds needs more investigation (Weng et al., 2021). During analysis of the field observations, the contributing factors from below-cloud effects or changing cloud structures will be discussed, and the plausible explanations for altering isotopic signals will be determined qualitatively.

Measurements of the rainfall throughout the field work can be utilized in rainfall intensity-duration-frequency (IDF) curves which gives a representation of the probability that a given rainfall intensity will occur in a given time (Sun et al., 2019). IDF curves rely on high-frequency measurements of precipitation over longer time periods. One of the problems with IDF is the lack of available data and the small number of stations in Norway makes it difficult to accurately forecast the rainfall intensity over a large area (Dyrrdal, 2021). IDF curves are used in urban planning Sun et al. (2019), and contributing data from this thesis could help improve the IDF curves at the different sampling location used in this field work. There will be an attempt to investigate if there are connection with isotopic signals in a precipitation event, and the potential contributions this could have on predicting intense precipitation in the future.

2 Theory

Water molecules consist of hydrogen and oxygen atoms. On its most common form water consist of hydrogen with 1 proton in the hydrogen atom nuclei while oxygen has 8 protons and 8 neutrons in the atom nuclei. This standard water molecule is written as $H_2^{16}O$. Water can have two naturally occurring isotopes for hydrogen, and three for oxygen (Araguas-Araguas et al., 2000). The two most abundant isotopes after $H_2^{16}O$ are oxygen-18, $H_2^{18}O$ and deuterium, $^1H^2H^{16}O$ which is often referenced as HDO (Gat, 1996). Oxygen-18 have 8 protons and 10 neutrons while HDO have 1 proton and 1 neutron in one of the hydrogen nuclei. The different mass properties between the light and abundant $H_2^{16}O$ and the heavy and rare $H_2^{18}O$ and HDO give the heavy isotopes different physical properties.

The standard amount on heavy to light isotopes in water are $\frac{H_2^{18}O}{H_2^{16}O} = 2005.95 \cdot 10^{-6}$ and $\frac{HDO}{H_2^{16}O} = 155.95 \cdot 10^{-6}$ (Galewsky et al., 2016; Gat, 1996). This is determined by the International Atomic Energy Agency (IAEA) and called the Vienna Standard Mean Ocean Water (VSMOW or SMOW). Water isotopes are most commonly referenced with the δ -notation (eq.1), and measured in units of parts per thousand (‰). δ is the relative deviation of the heavy isotope content in a sample from the standard (Dansgaard, 1964).

$$\delta = \left(\frac{R_{sample}}{R_{standard}} - 1 \right) \cdot 1000 [‰] \quad (1)$$

In eq. 1, δ describes the ratio of a sample R_{sample} to the standard isotopic value, $R_{standard}$. R can be the ratio of $\frac{O^{18}}{O^{16}}$ or $\frac{D}{H}$ (Gat, 1996). A positive δ value indicates enrichment in isotopic composition compared to SMOW, while a negative δ value indicates depletion relative to SMOW. In nature, the amount of HDO is almost an order of magnitude larger than $H_2^{18}O$ ($\delta D = 8\delta^{18}O$) (Dütsch et al., 2017; Gat, 1996), and they are linearly related in precipitation (Merlivat and Jouzel, 1979).

$$d = \delta D - 8 \cdot \delta^{18}O \quad (2)$$

The δD and $\delta^{18}O$ can be expressed with the d-excess (eq. 2) (Dansgaard, 1964) The d-excess is an expression of the departure from the linear relationship and is the result of different evaporation rates of the different isotopes (Galewsky et al., 2016). The proportion of d-excess in precipitation is approximately 10 ‰ globally (Yoshimura, 2015; Araguas-Araguas et al., 2000) and $\delta D = 8 \cdot \delta^{18}O + 10‰$ is called the global meteoric water line (GMWL).

2.1 Fractionation

A significant process in the water cycle, with respect to water isotopes, is when vapor changes to liquid or ice or visa versa (Gat, 1996). Evaporation and condensation are mass dependent processes (Galewsky et al., 2016) and gives rise to fractionation. Fractionation occurs because the weaker molecular bonds and higher diffusive velocities in light isotopes, $\delta^{16}O$. This makes evaporation easier for the lighter isotopes while the increased mass of the heavy isotopes, $\delta^{18}O$ and δD , makes condensation easier (Gat, 1996). Fractionation could therefore be a used to investigate the condensation history of the air parcel (Dütsch et al., 2017).

2.2 Equilibrium Processes

In an equilibrium processes, liquid and vapor phases coexist in a system under thermodynamic equilibrium. Equilibrium fractionation can be expressed as the ratio of liquid and vapor stable water isotopes, $\alpha = \frac{R_{liquid}}{R_{vapor}}$ or $\alpha = \frac{R_{vapor}}{R_{liquid}}$ (Gat, 1996). The equilibrium fractionation is dependent on temperature (eq. 3) and lower temperatures are more affected by the fractionation processes (Gat, 1996). Temperatures above and below freezing affect the fractionation coefficient differently, and for $T < 0$ °C the phase change is between vapor and solid ice (eq. 4). The fractionation coefficient for $\delta^{18}\text{O}$ is given in eq. 3 and 4.

$$\alpha_{v,l}^{18} = \exp\left(\frac{1137}{T^2} - \frac{0.4156}{T} - 0.002067\right) \quad (3)$$

$$\alpha_{v,i}^{18} = \exp\left(\frac{11.839}{T^2} - 0.028224\right) \quad (4)$$

Subscripts of l,v and i in eq. 3 and 4 are for liquid, vapor and ice, respectively, for the equilibrium fractionation coefficient for $\delta^{18}\text{O}$ (Majoube (1971), after Yoshimura (2015)). T is the temperature in kelvin. The fractionation that occurs at all stages in the hydrologic cycle determines the isotopic composition of the atmospheric water. Equilibrium processes occurs mostly through condensation in clouds (Muller et al., 2015).

Condensation is one of the most important processes for the isotopic composition in precipitation (Dansgaard, 1964). The continuous removal of condensate from vapor creates depleted values for both the condensate and the remaining vapor in the air parcel. For example, precipitation formed from the newly removed condensate or solids ice, becomes increasingly more depleted with time as the cloud vapor becomes increasingly depleted.

2.3 Rayleigh Distillation Processes

The Rayleigh distillation model is a model used to describe the fractionation processes (Gat, 1996; Galewsky et al., 2016) and subsequently the evolution of the isotopic composition under equilibrium conditions. There are several different variations of the Rayleigh model, but I will only be using the open system model in this thesis. The open system model represents an ideal situation where newly formed condensation or vapor is immediately removed from the system (Gat, 1996). The Rayleigh model for an open system can be described through the mass balance approach (fig. 1).

A cloud (fig. 1) will have N amounts of molecules and R_v represents the ratio of isotopes in the vapor phase. As vapor turns to cloud condensate, the isotope ratio of condensate R_c , will immediately be removed from the system as precipitation. The evolution of vapor and condensate in the cloud can therefore be expressed as:

$$R_v N = (R_v + dR_v)(N + dN) - R_c dN \quad (5)$$

Writing out eq. 5, with addition of the equilibrium fractionation because of the phase change from vapor to condensate, $R_c = \alpha R_v$, yields:

$$\frac{dR_v}{R_v} = (\alpha - 1) \frac{dN}{N} \quad (6)$$

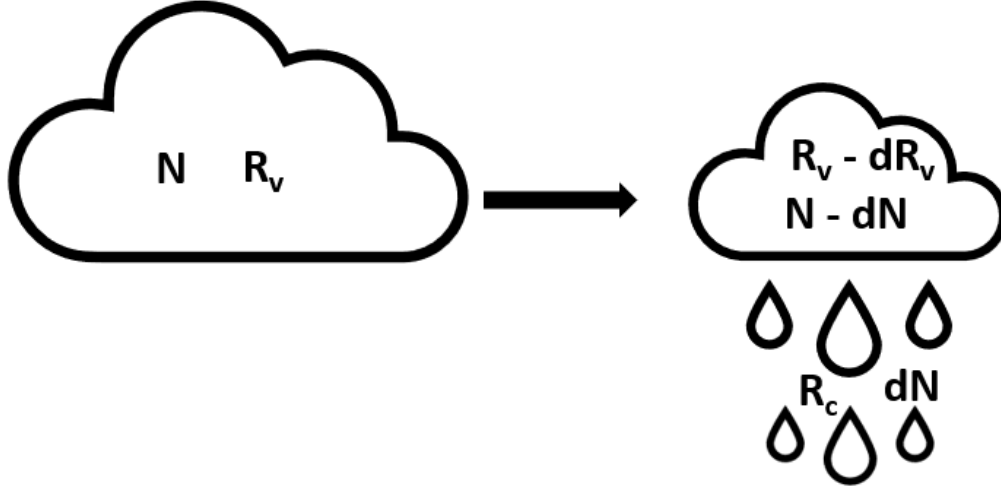


Figure 1: The open system Rayleigh model can be described for a condensation process in clouds with the mass balance approach. R_v ratio of isotopes in the vapor phase and R_c if the cloud condensate, while N is the number of molecules in the system.

Eq. 6 can be described for both evaporation and condensation by looking at a mixed system containing molecules N_i and N_j , of the different isotopes species (Gat, 1996). Under the following assumptions, the system can be described by $N \gg N_i$ where $N_i + N_j = N$. R (R_v or R_c) is the same ratio of rare to abundant isotope, at any given stage (eq. 7).

$$\frac{dR}{dN} = \frac{1}{N} \left(\frac{dN_i}{dN} - \frac{N_i}{N} \right) = \frac{R}{N} (\alpha - 1) \quad (7)$$

$$\frac{d(\ln R)}{d(\ln N)} = (\alpha - 1) \quad (8)$$

Eq. 8 can be integrated from the initial conditions, R_0 and N_0 at any given stage, provided that α remains unchanged. This leads to eq. 9:

$$R = R_0 \cdot \left(\frac{N}{N_0} \right)^{(\alpha-1)} = R_0 \cdot f^{(\alpha-1)} \quad (9)$$

$f = \frac{N}{N_0}$ is the fraction of the remaining material in the system (Gat, 1996), and in this case, the fraction of the initial moisture content that remains in the air mass (Araguas-Araguas et al., 2000). The Rayleigh distillation rises from this concept, and when the isotopic species removed are in thermodynamic equilibrium with the remaining system. Eq. 9 can be easier applicable by using the δ -notation from eq. 1:

$$\delta = (\delta_0 + 1) \cdot f^{\alpha-1} - 1 \quad (10)$$

Using the Rayleigh distillation model to predict the isotopic evolution an air parcel with eq. 10 requires knowledge of the initial conditions, δ_0 . The initial condition are water vapor in equilibrium with water, i.e. the ocean. The isotopic composition of vapor can be defined with eq. 11 (Jouzel and Merlivat, 1984), between the isotopic compositions of vapor, δ_v , and condensate, δ_c . Eq. 11 can also be applied between vapor and liquid phase, δ_l . This relation gives an expression for δ_v in the source region since $\delta_l = 0 \text{ ‰}$ at the sea surface. δ_v is then only dependent on the equilibrium fractionation factor α , until condensation occurs at a later stage.

$$1 + \delta_v = \frac{1}{\alpha}(1 + \delta_c) \quad (11)$$

Different temperatures changes α and subsequently alters eq. 10. This gives rise to different Rayleigh curves (fig. 2). The curve from eq. 10 shows how an air parcel with δ_v or $\delta_c \rightarrow -\infty$ while $f \rightarrow 0$ (Dansgaard, 1964). In figure 2 the Rayleigh curve is expressed for a parcel undergoing isobaric cooling in a saturated environment at different condensation temperatures. The Rayleigh model will therefore lead to higher fractionation compared to the equilibrium fractionation where the two phases are allowed to equilibrate.

A simple description of the atmospheric water cycle through the Rayleigh framework, is that a given observation of an air parcel will reflect the history of evaporation and Rayleigh condensation (Worden et al., 2007). Most δ values in an air parcel will lie between theoretical extremes of the curve for condensation from moisture originating from a warmer oceanic source and the curve of evaporation toward equilibrium with a cold oceanic source. The Rayleigh process can be found inside clouds in the phase shift from vapor to condensate or vapor to solid (ice).

2.3.1 Mixing Ratios

The amount of water vapor in the air can be expressed by the ratio of the mass of moist air, m_v and the mass of dry air, m_d , in the atmosphere (Wallace and Hobbs, 2006). This is called the mixing ratio, w (eq. 12). The mixing ratio is constant if there is no evaporation or condensation.

$$w = \frac{m_v}{m_d} [gkg^{-1}] \quad (12)$$

If the system is fully saturated with respect to liquid, the saturation mixing ratio, w_s , (eq. 13) can be expressed with the surface pressure, p , and the saturation pressure e_s (eq. 14). The saturation mixing ratio can be used to determine the condensation temperature by using the Clausius Clapeyron relation (CC-relation) (Noone, 2012). The CC-relation can show the relationship between saturation pressure e_s and T. e_s can be defined by eq. 14.

$$w_s = 621.97 \frac{e_s}{p - e_s} [gkg^{-1}] \quad (13)$$

$$e_s = 6.11 \cdot \exp\left(\frac{L_v M_w}{1000 R^*} \left(\frac{1}{273} - \frac{1}{T}\right)\right) [Pa] \quad (14)$$

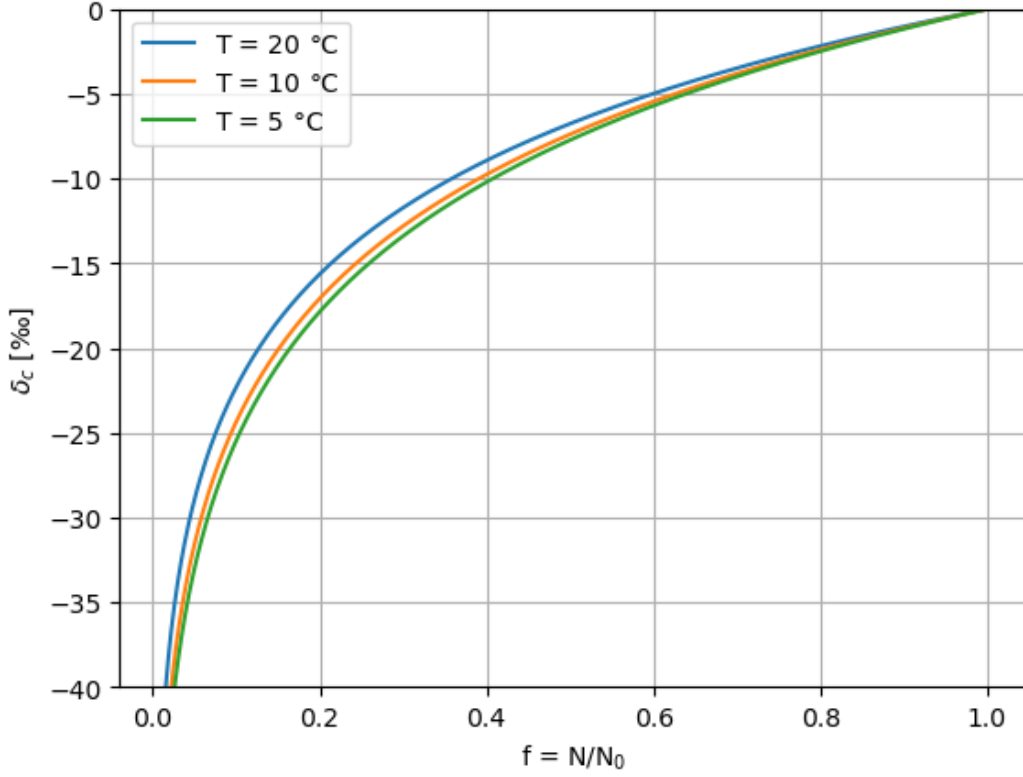


Figure 2: Examples of Rayleigh curves in a saturated environment for condensate δ_c which is isobaric cooled at $T = 20\text{ }^\circ\text{C}$ (blue curve), $T = 10\text{ }^\circ\text{C}$ (orange curve) and $T = 5\text{ }^\circ\text{C}$ (green curve) using eq. 10. f is the ratio of vapor in a reservoir where 1 is equal to a full reservoir and 0 is an empty reservoir. δ_c is the newly formed condensate from vapor

$$e_s \approx 6.11 \cdot \exp(5.42 \cdot 10^3 \left(\frac{1}{273} - \frac{1}{T} \right)) [Pa]$$

L_v , M_w and R^* in eq. 14 are the latent heat of vaporization at $T = 0^\circ\text{C}$ ($2.5 \times 10^6 \text{ Jkg}^{-1}$), the molecular weight of water (18.016 gmol^{-1}) and the universal gas constant ($8.3145 \text{ JK}^{-1}\text{mol}^{-1}$), respectively. e_s is given in Pa and T is given in K (Wallace and Hobbs, 2006).

The mixing of air parcels changes the isotopic composition of the water vapor (Galewsky et al., 2016). With the Rayleigh processes, the isotopic composition can be expressed as a function of the saturation mixing ratio, w_s and we can follow the same Rayleigh curves as in figure 2 for $f = \frac{w_s}{w_{s0}}$. w_s is the saturation mixing ratio in the cloud, when condensate is removed and w_{s0} is the initial saturation mixing ratio in the source region where the evaporation first occurred. Defining f with the saturation mixing ratio accounts for variations in f due to changes in temperature and pressure (Dansgaard, 1964).

The w_s - δ framework provides a synopsis of the water cycle because observations are shown to reflect a history of both condensation and mixing processes associated with the source (Noone, 2012). Partial evaporation of condensate after the precipitation has left the cloud base can make the

δ values lower than expected. The lower values would then lie below the Rayleigh curve in the w_s - δ framework, indicating more depletion compared to the simple Rayleigh distillation, which gives rise to the "Super Rayleigh"-curves. These curves are the product of vapor that have been exposed to fractionation more than once before the precipitation is removed (Noone, 2012). The air masses can be identified by their w_s - δ position, which is established by the different cloud processes.

2.4 Non-equilibrium processes

The equilibrium processes are an idealized way of looking at the hydrological cycle, but, in nature, the system can rarely be assumed to be in equilibrium. The non-equilibrium processes are governed by the kinetic effects. The kinetic effects gives rise to the kinetic fractionation factor $\alpha_k = \mu\alpha$, μ reflects the ratios of diffusion rates between the heavy and light isotopes (Dansgaard, 1964). An example of kinetic fractionation is when water evaporates into unsaturated air. A strong gradient in relative humidity (RH) between the ocean surface and the lower layers of the atmosphere, or winds advecting the newly formed evaporate before equilibrium is reached, can alter the isotopic composition of vapor (Dansgaard, 1964; Muller et al., 2015).

Precipitation falling through unsaturated air below the cloud base or from convective downdrafts might fully or partially re-evaporate. These non-equilibrium fractionation effects are caused by unstable environments. In these cases, the precipitation will experience enrichment relative to the surrounding vapor (Galewsky et al., 2016).

2.4.1 d-excess

The d-excess is a second order isotope parameter. HDO is less sensitive to kinetic effects than $H_2^{18}O$ (Dansgaard, 1964). The slower movements of $H_2^{18}O$ during molecular diffusion leads to enrichment of $H_2^{18}O$ relative to HDO in the gas phase during evaporation. The different molecular diffusivities of the heavy isotopes rises from the different masses, HDO is lighter than $H_2^{18}O$. Merlivat and Jouzel (1979) found that the relationship between δD and $\delta^{18}O$ in precipitation is depended on the physical characteristics of the air masses at the origin of the precipitation. The isotopic signals in precipitation is affected by sea surface temperature (SST) and RH in the source region (Merlivat and Jouzel, 1979), and RH was found to be the main driver of the d-excess (Pfahl and Sodemann, 2014). RH determines if the air is saturated. When there is high humidity there is less evaporation, and the system reaches for equilibrium between the liquid and vapor phases. A high d-excess can therefore indicate if there was a large RH gradient over the ocean which would lead to kinetic fractionation from evaporation. Because of its sensitivity to the conditions in the moisture source, the d-excess can help detect changes in the moisture source conditions. Another trait is to detect the locations associated with reorganizations of the atmospheric circulation (Dütsch et al., 2017).

Supposing condensation is an equilibrium process, the d-excess is assumed to be conserved during transport. The averaged d-excess of precipitation will then reflect the rate of evaporation in the source region (Gat, 1996; Dansgaard, 1964). However, local processes can alter the final d-excess in precipitation. Evaporation of rain drops below the clouds will alter the d-excess dependent on the conditions below the cloud. If the RH is low, the rain drops will experience enhanced evaporation of HDO compared to $H_2^{18}O$. The d-excess in the rain drops will become more negative while the d-excess in the surrounding vapor would become increasingly positive compared to the rain drop. d-excess is also altered when air parcels mix, even if there is no phase transition (Dütsch et al., 2017).

2.5 Isotopic composition in precipitation

Understanding the large and small scale atmospheric processes connected to precipitation will aid the understanding of isotopic signals in precipitation. Water vapor can be subjected to several processes throughout its journey through the hydrologic cycle, and many of these processes will change the isotopic composition. The isotopic composition of atmospheric water can be determined by the isotopic composition of the ocean where evaporation occurs, the SST, the RH, and the wind conditions in the source region (Muller et al., 2015). After evaporation from a water surface, the air parcels move in the atmosphere and are affected by different processes in the hydrologic cycle.

Precipitation is formed under cooling processes and is mostly generated by extra-tropical storms in the warm conveyor belt (Carlson, 1980). Alterations of the isotopic composition in precipitation are connected to fractionation. However, the fractionation related to phase change is not the only factor, the final isotopic composition of precipitation is a function of many different processes depending on the temperature, the altitude or distance from a moisture source, and the precipitation characteristics (Dansgaard, 1964). The isotopic composition of a rain sample is the mass-weighted average of the composition of all the rain drops contained in this sample. The processes which act on a single drop are therefore relevant to the bulk precipitation (Graf et al., 2019).

2.5.1 Temperature-, amount-, altitude, and rain-out effects

Dansgaard (1964) described different atmospheric conditions that affected the isotopic signal in precipitation. One of these is the temperature effect. The isotopic signals are temperature dependent and there is positive correlation between decreasing δ values and decreasing temperatures. The temperature effect can be explained by the Rayleigh distillation model, when temperature decreases, the specific humidity at saturation decreases which lead to a decrease in the isotopic composition of vapor and the subsequent precipitation (Galewsky et al., 2016). The temperature effect is the dominating effect at high latitudes (Dansgaard, 1964), and can also therefore be referred to as a latitude effect where increasing latitude leads to decreasing temperature which leads to decreasing δ values.

The amount effect is the connection between the δ values and the amount of rain (Dansgaard, 1964). This is a negative correlation, which means that heavy rain has depleted values, while light rain has higher less depleted values. This is mostly relevant in the tropics, where evaporation and exchange with the surrounding air influences the light rain, increasing the δ values. Therefore, the amount effect is negligible at high- and mid-latitudes where the temperature effect dominates because of the lower degree of evaporation from falling droplets (Dansgaard, 1964).

Moving away from the ocean, where there is a constant supply of moist, isotope rich, air, the amount of heavy isotopes in the air parcel decreases. This is called the continental or altitude effect (Dansgaard, 1964). The δ values in precipitation becomes more depleted with increasing altitude. Air masses reaching a mountain will lift adiabatically, cool and condense which will cause orographic precipitation (Dansgaard, 1964). This is the rain-out effect, but the rain-out effect is not only synonymous with orographic precipitation. Studies conducted on isotopic composition in orographic precipitation (Smith and Evans, 2007; Stern and Blisniuk, 2002) saw correlations between the depleted values in precipitation and increasing altitude. Stern and Blisniuk (2002) used the Rayleigh distillation model to compare the effects of orographic lifting with observations and found good results. Smith and Evans (2007) looked at the drying ratio of water vapor through isotope samples and looked on how much moisture travelled over a mountain. Their goal was to map the fractionation processes of water vapor and used that to calibrate a physical model for orographic

precipitation.

The rain-out effect is the product of when sufficient precipitation rains out during a front or storm, the heavy water isotopes will rain out first due to fractionation. This makes the isotopic signals less depleted in the beginning of a precipitation event. As more rain precipitates the precipitation reaching the ground becomes more and more depleted (Dansgaard, 1964). The isotopic composition in water vapor decreases when adiabatic condensation occurs and air that is able to move over the mountain will thus have very depleted values.

The isotopic composition of precipitation shows temporal patterns (Gedzelman and Lawrence, 1990; Weng et al., 2021) which are visible with high frequency measurements. Recognisable patterns that are consistent for cyclones in the mid-latitudes have been described in the context of different atmospheric processes. There is a connection between the isotope signals and the different stages of a low pressure system. The isotopic composition of precipitation is an integrated result of the fractionation processes and cloud effects in and below the cloud that occurs during phase changes in the atmosphere (Weng et al., 2021).

The position of the melting level determines where snow melts to rain, which is important for the final isotopic composition. Snow has different properties than precipitation when it comes to fractionation. Snow keeps the isotopic signals from the clouds, and there is no exchange with moisture below the cloud (Gat, 1996). Isotopic equilibrium can be expected from rain formation in warm clouds (Weng et al., 2021) but the snow formation has some contribution from kinetic effects.

Understanding the different components that change the isotopic signals in precipitation is key to understand the broader aspects of the hydrologic cycle. The precipitation is a product of the mid-latitude processes and understanding the large scales helps understanding the small scale.

2.6 Isotopic composition of a front

2.6.1 Front characteristics

A front can be characterized by the horizontal gradients of temperature which distributes the precipitation in bands parallel to the fronts (Wallace and Hobbs, 2006). The initialization of a front which reaches the west coast of Norway is attributed to mesoscale circulation and low pressure systems which are created over the North Atlantic Ocean.

One key factor is to determine the type of front. Different front types are a warm front, a cold front, a stationary front or an occluded front (Wallace and Hobbs, 2006; Carlson, 1980). In a low pressure system, the cold front is located south of the centre, and exhibits stronger wind from west. This front is characterised by cold air moving under warmer air. The lifting of the warm air creates convective clouds. A warm front is located further east and has more subtle temperature gradients compared to the cold front (Wallace and Hobbs, 2006). The warm air moves and is convected over colder air, this creates stratiform clouds. A cold front moves faster than the warm front, and the collision of the two fronts creates the occluded front. A front with little movements indicates a stationary front. Carlson (1980) looked at the evolution of cloud patterns and how different fronts could be determined based on their cloud structures and position dependent on the warm or cold conveyor belts. Conveyor belts are airstreams (Browning, 1994), and the warm conveyor belt (WCB) is an airstream with a high wet-bulb potential temperature which travels along the cold front. The ascent of air in the WCB can be rearward-sloping where air is moving rearward relative to the to the movement of the cold front, or forward-sloping where the air in and above the WCB is moving forward relative to the cold

front, with the main region having a slantwise ascent occurring further downwind at the warm front (Browning, 1994).

Precipitation along the warm front for the forward-sloping ascent has the form of a wide frontal rainband associated with broad scale slantwise ascent (Browning, 1994). Beneath the warm frontal zone lies the cold conveyor belt (CCB). The CCB can be strong relative to the system, especially close to the cyclone center. It begins as a dry air stream and the warm frontal precipitation falling down in it will experience evaporation (Browning, 1994). Precipitation at the upper cold front has a band of heavier precipitation at the leading edge of the dry intrusion. The dry intrusion is part of the cold front in the forward sloping ascent and is a dry air stream from the upper stratosphere. After the warm frontal precipitation and the upper cold frontal precipitation, what follows is an outbreak of shallow convective rain within the shallow moist zone. This type of rain is usually light (Browning, 1994).

2.6.2 Isotopic signals in frontal structures

The precipitation sampled throughout this field work had a place of origin. Tracking of water vapor in the atmosphere is a tool to determine the amount of precipitation. Integrated water vapor (IWV) is the total amount of water vapor in an atmospheric column and can predict the theoretical amount of water which can precipitate and the initiation of precipitation in an area (Labbouz et al., 2015).

The isotopic composition in water vapor and precipitation can be determined partly by the front type because isotopic composition in precipitation is connected to the frontal systems (Gedzelman and Lawrence, 1990). Cloud distributions have an effect on the isotopic composition of precipitation and different types of fronts are connected to different types of clouds. Gedzelman and Lawrence (1990) looked at the relationship between the fronts and isotopic composition in the clouds and the subsequent precipitation generated from different fronts and cloud structures. The cold and warm fronts, their cloud formations, and the isotopic composition of $\delta^{18}\text{O}$ can be sketched for an idealized situation (fig. 3). Determination of the right front and cloud structures could help the understanding the evolution and processes affecting the isotopic signals in precipitation.

Convective clouds connected with cold fronts have less depleted δ values compared to stratiform clouds connected to warm fronts (Gedzelman and Lawrence, 1990). In the cold front, condensations take place at higher levels than in the warm fronts, but these processes are also dependent on the development stage of the cyclone. As a front passes, the different measurements of precipitation will reflect the different stages of the front. Aemisegger et al. (2015) investigated the role of the below-cloud effects during a cold front and found different scales which controls the spatial and temporal evolution of the isotopes in precipitation and vapor. The type of cyclone, for example continental or oceanic, can have an effect on the isotopic effects because of the conditions in the moisture region (calm ocean close to the coast compared to more wind and kinetic effects out over the open ocean). They also noted the microphysical interactions between the ambient vapor and the rain drops below the cloud base are not sufficiently constrained. Under equilibrium between vapor and precipitation the uncertainties were negligible because the errors were at the same magnitude as the measurements uncertainties. The d-excess did not show similar results.

The warm front is characterised by stratiform clouds which are produced by condensation within layers of relatively moist and warm air and undergo large scale slant ascent above colder air. Precipitation is usually wide spread north of the front while the outer edges consist of thin layer of cirrus-type clouds at higher altitudes. In later phases of the cyclone development, shallow stratiform clouds extends west and southwards (Carlson, 1980). In stratiform clouds the precipitation is largely

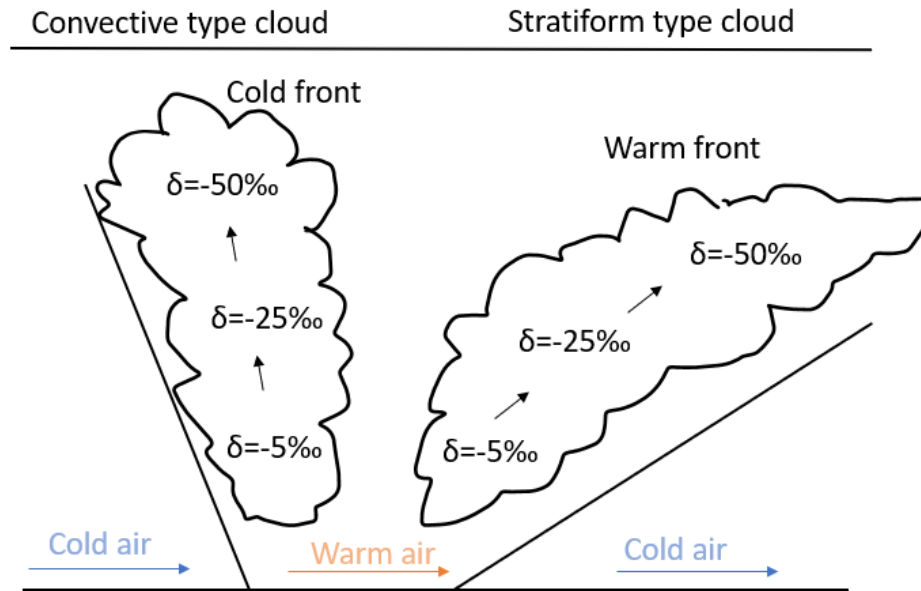


Figure 3: An illustration of a cold and a warm front and the corresponding $\delta^{18}\text{O}$ values in the clouds, after Gedzelman and Lawrence (1990). The blue and orange arrows indicate the direction of the front passage. The black arrows indicate the depletion in $\delta^{18}\text{O}$ as air rises. The cold front has convective type clouds and the warm front has stratiform type clouds.

dependent on the vertical profile of the air column, and this is connected to the cloud-top height. The cloud-top height can be affected locally and temporarily, and if the cloud top increase, the isotope ratio would decrease. In convective clouds the isotope ratios are less depleted than in the stratiform clouds, even when the cloud-dimensions are similar. These less depleted ratios are attributed to the vapor source and that convective clouds undergo little prior fractionation (Gedzelman and Lawrence, 1990). Ignoring below-cloud conditions in a warm front, the δ values will be more depleted if the cloud bases are high and have a high melting level. As the warm front progresses the values will become less depleted as the cloud base height decreases. If below-cloud conditions are non-negligible, the first rain will be dependent on the air conditions, if it is dry or humid it will affect the final composition measured at the ground.

The primary difference between stratiform and convective precipitation is the vapor source. The vapor source in stratiform precipitation is distributed through the cloud while the convective precipitation has its source below the cloud base (Gedzelman and Lawrence, 1990). Convective precipitation will have less depleted δ values than stratiform cloud, even if the dimensions are similar. The isotopic compositing in stratiform cloud are determined by the condensation rate at each level while the convective clouds will have effective fractionation as the parcels rise, and the higher the cloud top, the lower δ values (fig 3). However, as rain falls through the cloud the isotopic content tends to equilibrium with the surrounding vapor, ultimately becoming less depleted as surface precipitation compared to the stratiform precipitation.

During the transitioning from a shallow cloud layer to a deep cloud layers in a warm front, Coplen

et al. (2008) saw that the isotopic composition in precipitation drastically changed becoming more depleted under the span of 1 hour. The change in cloud structures during a front passage alters the isotopic composition of precipitation in short time spans.

Weng et al. (2021) have determined four different stages with distinct changes in isotopic composition during the front passage of an AR-event. At the first stage, below-cloud evaporation could influence the values making the δ values less depleted in surface precipitation. Second stage: gradual weakening of the below-cloud evaporation, as the ambient air becomes more saturated, and other hydrometeors from above the melting layer results in a gradual drop in δ values. Third stage: deep clouds allow the hydrometeors formed at high levels to gain condensate and moisture as they fall, leading to less depleted values again. Fourth and final stage: numerous convective showers that are formed low and locally, leading to the least depleted δ values. The changes between the third and final stage is explained by change in moisture source conditions. This made out a "W" pattern in the isotopic signals (Weng et al., 2021).

The isotopic composition in precipitation is also a product of the conditions at the moisture source. Li et al. (2022) sampled precipitation diurnally and determined different moisture sources for their precipitation. Moisture transported by the warm conveyor belt had high δ values and high d-excess because of high temperatures at the sea surface and low humidity.

2.6.3 Below-cloud effects

The Rayleigh model represents the condensation processes in clouds. If there were no processes altered the isotopic signals below the cloud base, the Rayleigh model could also represent the isotopic signals in surface precipitation. However, the surface precipitation is a combination of the air mass signature, vapor at the surface and the below-cloud processes (Weng et al., 2021). It is therefore important to understand these processes and how they can alter the isotopic composition. Neglecting the below-cloud processes could give false understanding of the isotopic signals.

A rain drop leaving the cloud is subjected to exchanges with underlying environment until it reaches the ground. If the atmosphere is in equilibrium, for example fully saturated when $RH = 100\%$, there would be no exchange between the falling raindrops and the ambient vapor. Since the RH varies, the air can be unsaturated and non-equilibrium effects affect the rain drops and alters the isotopic signals. The underlying environment of the clouds can be affected by the vapor isotopic composition, the formation height of the precipitation, the RH profile in the air, advection and turbulence, or up- and downdrafts of air (Graf et al., 2019). The final isotopic composition measured at the surface can change compared to the cloud composition, and a main contributing processes to fractionation is evaporation. Evaporation is high in dry air and the process is likely in non-equilibrium (Dansgaard, 1964). After a front passage, the near surface atmosphere layer exhibits a higher RH which leads to weaker below-cloud evaporation (Graf et al., 2019).

The rainfall intensity is connected to the raindrop sizes where small droplets exchange more with the surroundings compared to larger droplets with high vertical velocity (Gedzelman and Lawrence, 1990). Larger drops spend less time in the air and is thus less affected by the below-cloud processes (Graf et al., 2019). The surrounding conditions help the growth or decay of the raindrops; warm, thick and humid air layers give light rain the chance to adjust and the δ values equilibrate between air and droplet. Dry, cold air will have more evaporation of the droplet leading to less depleted δ values. The preceding conditions for a precipitation event have an effect on the final composition. In periods with intense rain, the below-cloud effects becomes weaker (Graf et al., 2019).

A sensitivity experiments and comparison with observations conducted by Yoshimura et al. (2010)

found that below-cloud processes altered the final composition of precipitation during the same AR-event as Coplen et al. (2008). There were kinetic exchange between the precipitation and ambient vapor which was responsible for the initial enrichment of the early rain in the precipitation event. The kinetic effects were the large scale condensation which caused a drop in δ values. The increase of δ in vapor was attributed to dynamical processes of up-stream inflow of deuterium-rich water vapor. The mixing of air masses can change the composition of the vapor and subsequent precipitation. Yoshimura et al. (2010) also noted that, in their simulations, the Rayleigh-type fractionation for evaporation was not able to produce the correct enrichment in the beginning of the event. When the RH is almost 100 % and there is intense convection the condensation rate increases and the δ in water vapor and precipitation decrease (Yoshimura et al., 2010). This limits the re-enrichment of rain drops as they fall.

2.7 Snow Isotopes

Snow have different characteristics in isotope hydrology compared to liquid precipitation. Precipitation under $T = 0$ °C experiences an enhanced fractionation factor because of the larger offset between vapor and condensate. The increased fractionation factor leads to more rapid depletion of the vapor and subsequent condensate (Galewsky et al., 2016). Under equilibrium conditions, the Rayleigh model can explain the isotopic composition in snow (Dansgaard, 1964). Cloud vapor turns to solid ice from vapor deposition and is immediately removed from the system as snow or ice(hail). Snow or hail that reaches the ground is not affected by isotopic exchange with the atmosphere and would be more depleted than in an equilibrium situation. The snow would therefore conserves the isotopic composition formed in the cloud (Gat, 1996).

Water vapor deposited onto ice crystals experiences kinetic effects as well (Jouzel and Merlivat, 1984). These kinetic effects are attributed to the different diffusivities. This is present under supersaturation when $RH > 100$ % and can be neglected when $T > 0$ °C (Jouzel and Merlivat, 1984). Vapor deposition also enhances the d-excess in precipitation (Weng et al., 2021), altering the otherwise unchanged d-excess when the snow or ice leaves the cloud.

Formation of snow gives rise to an elevated d-excess in precipitation (Jouzel and Merlivat, 1984). The degree of evaporation from the falling precipitation in winter compared to summer usually overrides the effect of the humidity in the source area. Accumulation of snow on the ground keeps its identity, if it remains unmixed by snowdrifts from high winds, which has enabled the use of ice cores to establish reliable climatic records of isotopic signals in precipitations (Gat, 1996).

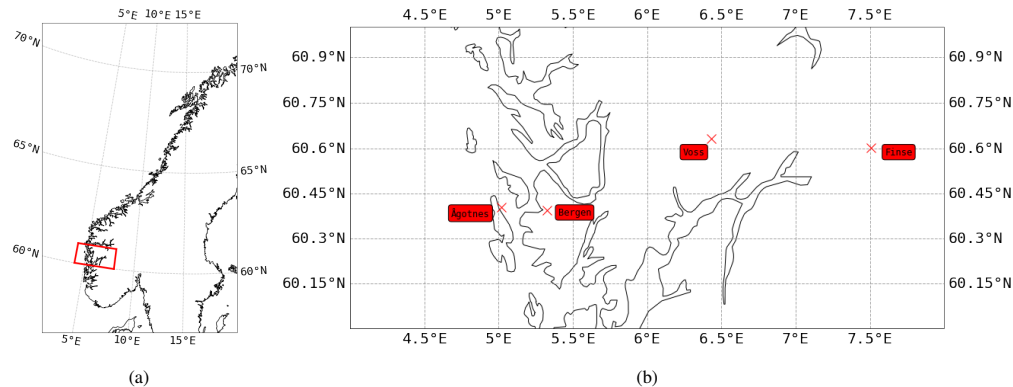


Figure 4: a) Map of Norway, the red square is the area in b) which shows the positions and names of the four stations.

3 Method

The fieldwork part consisted of precipitation samples, AWS measurements, and snow- and rainfall measurements from 4 different stations located at the west coast of Norway (fig. 4). The field work started on the 27/11/22 at 7:30 UTC when the sampling started at Finse. The sampling stopped in the afternoon between 17 and 19.30 UTC depending on when precipitation stopped at the different stations.

3.1 Stations

Four stations were chosen for the field work. They were selected based on availability of people to help take the samples and also for accessibility. At three of the four stations, there were AWSes with available data for temperature and RH. The locations consisted of two coastal stations and two inland stations at the west coast of Norway (fig. 4a). West to east in figure 4b, the stations were: station 1; Ågotnes, station 2; Bergen, station 3; Voss and station 4; Finse. The stations will be referred to by their names, Ågotnes, Bergen, Voss and Finse throughout this thesis.

The first sampling site, at Ågotnes, was located in a private garden (fig. 5a) at 28 m.a.s.l (60.3974 N, 5.0329 E). Ågotnes is located on an island, and has a coastal climate. The second station, Bergen, was at the Geophysical Institute (fig. 5b) (60.3837 N, 5.3320 E). The sampling site was located on the rooftop observatory at 47 m.a.s.l. Bergen is surrounded by mountains and is affected by orographic precipitation. The third station, was located in a private garden in Vossevangen, “Voss” (fig. 5c), at 64 m.a.s.l (60.6280 N, 6.4180 E). Voss sits at the barrier between coastal and inland climate. Voss surrounded by mountains and experiences orographic precipitation. The last station was located at Finsehytta at Finse (fig. 5d) at 1220 m.a.s.l (60.5981 N, 7.5069 E). Finse sits at one of the high points in the mountain range that splits Norway which acts as a natural border between West- and East Norway.

3.2 Instrumentation

Daily precipitation was collected in a mounted rain-collector. The Palmex Rain Sampler RS1 (red circle, fig. 5b) has been specifically designed for precipitation collection for isotope measurements since it avoids re-evaporation (Palmex Ltd). The rain collector is constructed with a funnel with a



(a) Ågotnes



(b) Bergen



(c) Voss



(d) Finse

Figure 5: The different instrument setup for the different stations. All stations were equipped with the same plastic box for precipitation sampling. a) Ågotnes, the green circle is the HOBO rain gauge. b) Bergen, the red circle is the Palmex rain sampler. c) Voss, a HOBO rain gauge was positioned next to the box. d) Finse, the box mounted and secured to a bench to prevent it from blowing over.

protective wire guard around the rim to avoid bird landings. From the funnel, an intake tube runs into a detachable plastic bottle which can hold up to 1 L of water. The plastic bottle was attached inside of a metal housing. For daily precipitation sampling, the bottle inside was detached and the rainfall amount was measured with a precipitation cylinder. A sample was taken with a syringe and transferred into a small 1.5mL vial (548-0907, VWR, USA). These vials were closed off with an open top screw cap with PTFE/rubber septa (548-0907, VWR, USA) which prevented evaporation until analysis.

The rainfall rate was measured by a HOBO Data Logging Rain Gauge (RG2-M)(green circle, fig. 5b). This is a rain-gauge operated by a tipping bucket. The collector consisted of an aluminum house with a funnel on top. The tipping bucket tipped every 0.2 mm of rainfall recorded the time. Each tip was detected by a magnet attached to the tipping bucket that actuated a magnetic switch as the bucket tipped (HOBO, 2001). The spent water drained out the bottom of the housing. The data was stored and collected directly from a memory chip in the instrument. The calibration accuracy of the rain gauge was $\pm 1.0\%$ and the operating range was between $0\text{ }^{\circ}\text{C}$ and $+50\text{ }^{\circ}\text{C}$. Ågotnes and Voss were equipped with the HOBO rain-gauges. The rain gauges were placed close to the sampling boxes at the ground and measured rainfall throughout the sampling period (fig. 5a and 5c). The tipping buckets were fastened during transition to and from the sampling sites to ensure no contamination of the data. The fastener was removed as soon as the box was placed outdoors and put back on when the sampling period ended.

Measurements of humidity, temperature and rainfall in Bergen were gathered from an Automatic Weather Stations (AWS)(AWS 2700, Aanderaa Data Instruments AS, Bergen Norway). The AWS is located at the rooftop observatory of the Geophysical Institute at 45 m.a.s.l. The AWS consists of different sensors used for meteorological data gathering. The ranges, resolutions and accuracies can be found in table 1. The rainfall measurer had a funnel of 200cm. The AWS measurements from Bergen was hourly averaged for easier comparison with the AWS measurements from Voss and Finse.

	Range	Accuracy	Resolution
Air Temperature	$-43\text{ }^{\circ}\text{C}$ to $+48\text{ }^{\circ}\text{C}$	$\pm 0.1\text{ }^{\circ}\text{C}$	$0.1\text{ }^{\circ}\text{C}$
Relative Humidity	0-100%	$\pm 2\text{ }^{\circ}\text{RH}$	
Rainfall	200mm/interval 12mm/min. max	$\pm 2\text{ }^{\circ}\%$	

Table 1: The range, accuracy and resolution from the AWS in Bergen.

Hourly averaged RH and temperature at Voss and Finse was collected from AWS stations operated by the Norwegian Meteorological Institute. Data was retrieved from 00 UTC on the 27/11/22 until 00 UTC on the 28/11/22. The station info and accuracy are given in table 2. The station numbers were 51350 "Vossevangen" for Voss and 25830 "Finsevattn" for Finse (Norwegian Meteorological Institute, personal communications, 2023).

	Accuracy
Temperature	$\pm 0.3\text{ }^{\circ}\text{C}$
Humidity	$\pm 5\text{ }^{\circ}\%$

Table 2: Accuracy for temperature and RH for AWSes at Voss and Finse

3.3 Equipment and techniques for sampling of precipitation

3.3.1 Collecting precipitation

For the precipitation sampling in the field, each station followed the same sampling techniques and had the same equipment. A clear plastic box (40 cm x 60 cm x 60 cm) was used as the precipitation collector. At Ågotnes and Voss they were secured to the ground (fig. 5a and 5c), in Bergen, on the rooftop observatory at GFI (45m) (fig. 5b) and at Finse the box was secured to a bench (ca. 40 cm above ground) with straps (fig. 5d). Squeegees were provided to gather the precipitation and pipettes were used to transfer the precipitate into 8 mL vials (548-0821, VWR, USA). Paper towels were used to dry over the box between each sample. The 8mL vials were stored at room temperature until analysis. A sample was collected every 60-15 minutes dependent on how intense the rainfall was.

Collection snow at Finse went by a different procedure than the other stations. By using a small wooden spoon, the snow was collected in a small plastic bag with a wire for securing the closed bag (Whirl-Pak, Nasco, 58 mL). The snow sample was brought indoors for the snow to melt. The melted snow water was stirred in the bag and transferred into a 8 mL vial by pouring or by a pipette. The samples were stored at room temperature until analysis.

3.3.2 Snowfall rate

Snowfall-rate was manually estimated by placing 10 1m sticks at different places around the sampling site at Finse. They were placed out when the sampling period started (07:33 UTC). When they were placed in snow, the depth was marked on the sticks. After the last sample was taken (19:29 UTC) the sticks were retrieved. Before removing them from the snow, a new line was marked on the sticks. The length between the two marks were measured with a ruler (uncertainty of ± 1 mm) and a mean snow depth was estimated. The snowfall rate was then calculated by taking the mean snow depth over the duration of the field work.

3.4 Lab analysis

The precipitation samples were all transferred from a 8mL vial into 1.5 mL vials (548-0018, VWR, USA) with PTFE/rubber septa screw caps (548-0907, VWR, USA). The precipitation samples were analyzed by FARLAB, University of Bergen, Norway. The procedure was using a L2140-i Picarro ring-down spectrometer (Picarro Inc, 2013). The Picarro analyser is a time-based optical absorption spectroscopy of target gases that determine isotopic composition (FARLAB, 2019).

The instrument consists of an analyser which contains the spectrometer, the sample chamber, the data storage, and an external vacuum pump which draws the sample gas through the instrument. The precision (at 1 standard deviation) for liquid is 0.025‰ for $\delta^{18}\text{O}$ (FARLAB, 2019). The process began with an autosampler (A0325) which retracted 2 μL from 1.5mL vials with rubber/PTFE septa which were injected into a high-precision vaporizer which was then heated to 110 °C. The injection was blended with dry N_2 (<5 ppm H_2O) and this gas mixture was directed into the measurement cavity of the cavity-ring down spectrometer (Picarro Inc, 2013). 8 injections were taken from each sample because of memory effects which caused carry-over between samples, and the average of the last 5 injections were therefore used for further processing. The sampling run started with 5 standards (table 3). DI2 were measured twice during the first 5 standards and after every 8th sample. Ågotnes and Bergen had two runs, while Voss and Finse had one. The two runs showed similar results but only the first run was used for Ågotnes and Bergen because of some missing values in run 2.

Standard	$\delta^{18}\text{O}$
DI2	$-7.6419 \pm 0.0148 \text{ ‰}$
GLW	$-40.0951 \pm 0.0255 \text{ ‰}$
EVAP2	$1.7739 \pm 0.0147 \text{ ‰}$
VSMOW2	$0.0000 \pm 0.0200 \text{ ‰}$

Table 3: Standards for calibration with predetermined values of $\delta^{18}\text{O}$

3.5 Weather Forecasting with MEPS

For this project, the goal was to collect precipitation samples at different stations during the same incoming front to track the evolution of water isotopes in precipitation. To determine when precipitation would start, a suitable front needed to be found.

To forecast a front prior to the field work, the MetCoOP (Meteorological Cooperation on Operational Numerical Weather Prediction) Ensemble Prediction System (MEPS) was used to track an incoming front on the 27/11/22. The MEPS model is an ensemble prediction system developed by the Norwegian, Finnish and Swedish Meteorological Institutes (Müller et al., 2017), and is a cooperation to enhance the numerical weather predictions (NWP) for short range forecasts with high resolution. An ensemble forecast is a forecast which consists of many runs which quantifies the most possible outcomes of the weather development instead of relying on a single forecast (Warner, 2010).

The MEPS model consists of 10 members and has a lead time of 66h and updates hourly. The grid resolution is 2.5km x 2.5km, and the model has 65 vertical levels with a mass-based, terrain following hybrid vertical discretization. The model has a 3-hourly updating cycle where all the atmospheric and land variables at the surface are updated. At every cycle a new 66h forecast is created. The microphysic scheme utilized by the MEPS model is based on the Kessler scheme for the warm, liquid processes and three-class ice parameterization (ICE3) for the cold processes. The ICE3 includes cloud ice, snow and graupel (Müller et al., 2017).

3.5.1 ERA5

To find the potential moisture source, the monthly average SST in November over the North Atlantic Ocean was investigated with the ERA5 reanalysis. The ERA5 reanalysis has a detailed record of the global atmosphere, land surface and ocean waves from 1950 and onward (Hersbach et al., 2020). ERA5 is based on an integrated forecast system (IFS).

3.6 Statistical methods and model verification

Forecast verification evaluates the quality of the forecast (Warner, 2010). Verification of a model implies comparison between different variables and observations of the same variables. The accuracy measures the correspondence of the forecasts values and observed values. Scalar measures of the accuracy gives a summary of the quality of the forecast in the form of a single number.

The accuracy of a model can be estimated by calculating the root mean square error (RMSE) (eq. 15), which conserved the physical dimensions of the forecast and observations (Warner, 2010). f_k and o_k are the k -th and n -th pairs of forecast and observations.

$$RMSE = \sqrt{\frac{1}{n} \sum_{k=1}^n (f_k - o_k)^2} \quad (15)$$

The bias is the measure of the correspondence between the average forecasted values and the average observed values. The bias is calculated using the mean error (ME) (eq. 16) (Warner, 2010). The bias looks at the difference between the average forecast, \bar{f} , and average observations, \bar{o} .

$$ME = Bias = \frac{1}{n} \sum_{k=1}^n (f_k - o_k) = \bar{f} - \bar{o} \quad (16)$$

The mean of a sample with the size n is defined in eq. 17. The standard deviation (std, or σ) measures the widths of the distribution and represents the fluctuation around the mean (Leo, 1994).

When measurement have varying degrees of uncertainties the weighted mean can be used as a more precise tool. The weighted mean (eq. 18) allows weight dependent on different measurements, for example the isotopic composition can be weighted by how much precipitation occurred.

The uncertainty of the weighted mean is given by the standard error of the mean (SEM), and not the standard deviation (Leo, 1994). The standard error of the mean (eq. 19) is defined by the standard deviation and the sample size n.

$$Mean = \frac{1}{n} \sum_{i=1}^n x_i \quad (17)$$

$$x_{weighted} = \frac{\sum_{i=1}^n x_i / \sigma_i^2}{1 / \sigma_i^2} \quad (18)$$

$$SEM = \sigma(\bar{x}) = \frac{\sigma}{\sqrt{n}} \quad (19)$$

The box plot or box-and-whisker plot (fig. 6) is a statistical tool consisting of five sample quartiles showing the full range of the sample (Wilks, 2011). The box part consist of the lower quartile, which included 25 % of the data, the median at 50% of the data and the upper quartile at 75%. The whole box-and-whisker plots includes 100 % of the data, with the whiskers including he minimum and maximum values (Wilks, 2011). A box plot shows an overview of the distribution of the data. The data can be determined as symmetrical depeding on the position of the median. A median placed in the middle of the box indicating a symmetrical distribution, while if it is closer to the lower or upper quartile it indicates a skewed distribution.

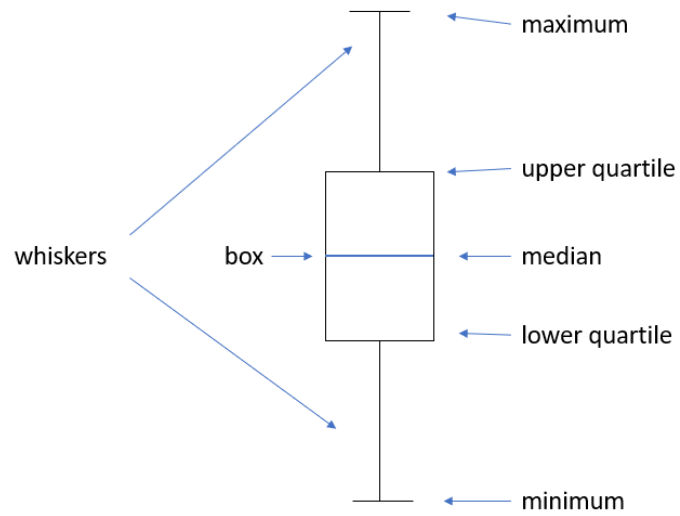


Figure 6: Schematic of a simple box plot, after Wilks (2011)

4 Results

4.1 The incoming front on the 27/11/22

For the field work, a suitable front seemed to arrive at the west coast of Norway on the 27/11/22. To further investigate this, I used the MEPS model to look at the forecasted accumulated precipitation and wind direction (fig. 7). This was also used to determine the starting time for collecting precipitation samples at each station. The wind arrows were added to indicate the wind direction and strength. At 8 UTC (fig. 7a) the accumulated precipitation was located off the coast and in patches over south-eastern Norway and had not reached at any of the stations (red crosses). At 10 UTC (fig. ??) the accumulated precipitation band had moved closer to Ågotnes which was furthest west. Some patches in mid-Norway were also more prominent, and approached Finse. At 12 UTC (fig. 7c) the accumulated precipitation had reached the coast. The patches of precipitation inland were prominent over Voss and Finse and from this (fig. 7c) it was assumed that all station had precipitation from 12 UTC and going forward. At 14 UTC (fig. 7d) the accumulated precipitation band outside the coast increased, and the accumulated precipitation at all station got a darker color which indicated increase in precipitation.

Another way to look at the front evolution was to look at a cross section of temperature and cloud area fraction (fig. 8). This could establish the type of front from the isotherms and cloud structures. The incoming clouds resembled the stratiform clouds connected to a warm front in figure 3. At 6 UTC (fig. 8a) the high cloud could be spotted which evolved, and at 8 UTC (fig. 8b) the cloud base became lower and the cloud fraction increased. The cloud front seemed to have reached Ågotnes and Bergen at this point. At 10 UTC (fig. 8c) the cloud fraction had increased and moved eastward and reached Voss. Throughout the day, the evolution of the cloud structures were investigated at 12, 14 and 16 UTC. An overview of the cloud fraction would help to determine possible factors which could affect the final isotope signal in precipitation.

The horizontal isotherms showed irregularities prior to the cloud front. The isotherms became more stable in the clouds with less horizontal change. The front had higher temperatures in the clouds, which could indicate the arrival of a warm front.

Over Finse, there were low, shallow clouds present from the morning hours at 8 to 10 UTC. At 12 UTC, stratiform type clouds from the incoming front seemed reach this station and at 14 UTC and 16 UTC a deeper cloud structure was visible which seemed to diminish with time. The vertical irregularities in the isotherms between Voss and Finse could be attributed to the changing topography because of the mountains and the subsequent ascent and descent of air masses.

4.2 Model verification

To verify the MEPS model I compared the available AWS data from Bergen, Voss and Finse with the MEPS model variables of RH and surface temperature (fig. 9) and made a comparison to look at the accuracy and bias (table 4) during the 24h period between 27/11/22 00 UTC and 28/11/22 00 UTC. The MEPS model was initialized at 27/11/22 at 00 UTC with a hourly outputs for the next 24 hours.

The root mean square error (RMSE) looked the average difference between the MEPS model and the observations from the AWS measurements. All values in table 4 showed the accuracy and bias for temperature and RH for each station. The bias was similar for temperature, which was around -2 °C at all the stations. There were some variations in RH, with Voss having the lowest bias, but largest

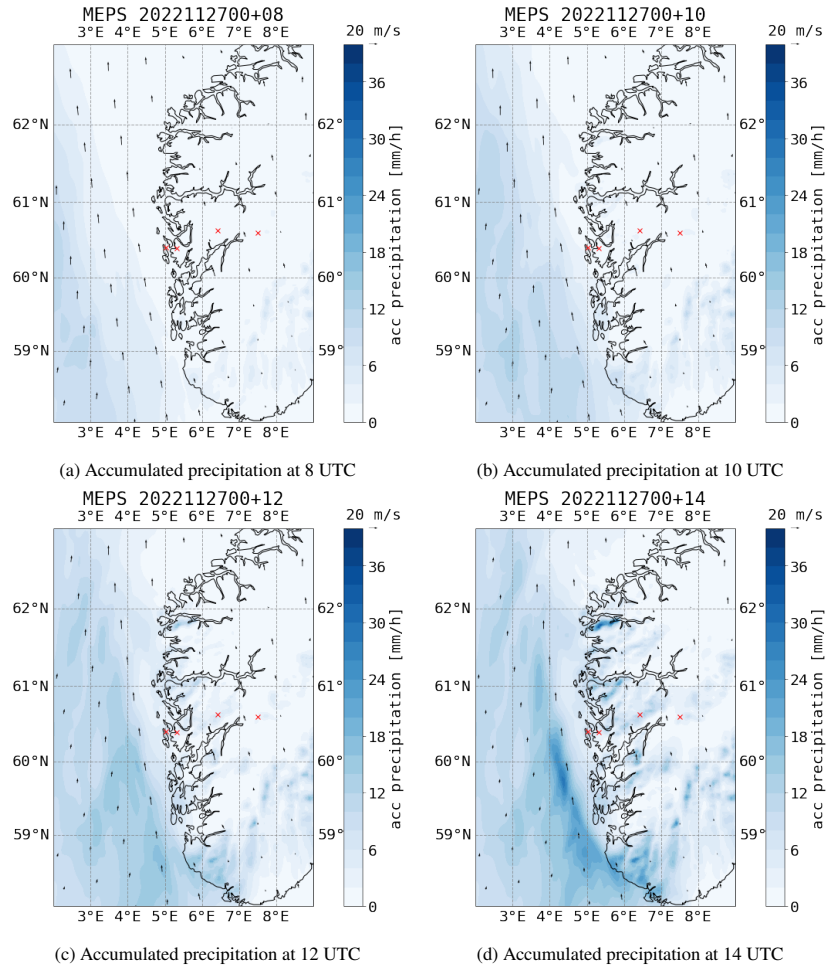


Figure 7: The evolution of accumulated precipitation (filled blue contours) and wind direction (arrows) to indicate the evolution of a front approaching the west coast of Norway. a) is 8 UTC, b) is 10 UTC, c) is 12 UTC and d) is 14 UTC.

RMSE. Bergen and Finse had a RH bias of around 10 %. Negative bias indicates that the MEPS model had lower outputs than the observed measurements.

Station	RMSE T	RMSE RH	Bias T	Bias RH
Bergen	2.1 °C	10.6 %	-2.1 °C	9.8%
Voss	2.7 °C	11.3 %	-2 °C	-5.9 %
Finse	1.9 °C	10.4 %	-1.9 °C	10.3 %

Table 4: RMSE and Bias for temperature and RH between the MEPS model and observations from AWS

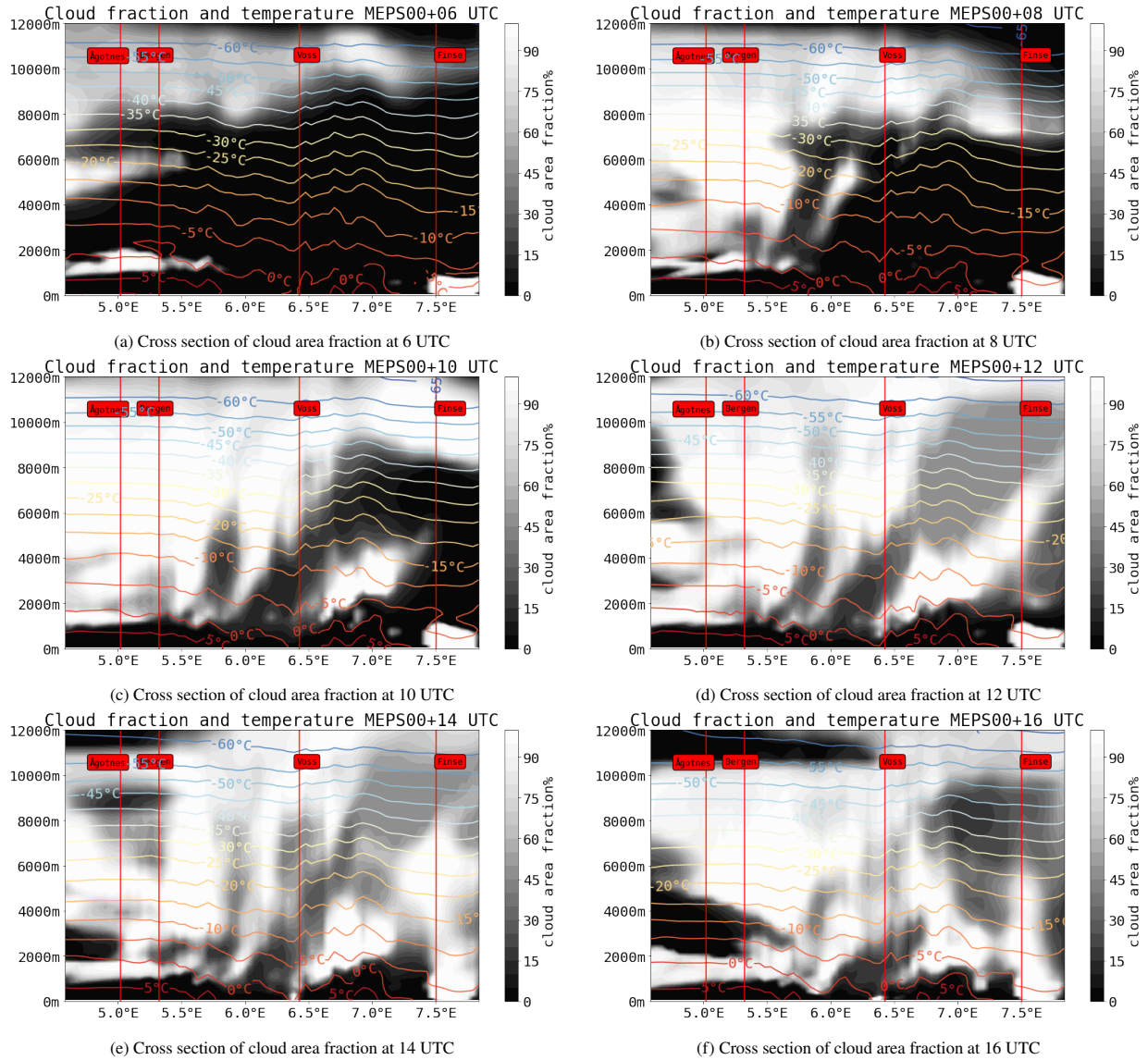


Figure 8: Cross section of the cloud area fraction [%] and temperature [°C] from 6-16 UTC on 27/11/22, stations are marked as red horizontal lines. The isotherm has a gradient from red to blue indicating warm to cold. The cloud area fraction is the filled contour, whiteness indicates higher cloud fraction

4.3 Daily precipitation measurements

Apart from the field work samples of precipitation, daily precipitation was sampled at the Geophysical Institute in Bergen. I was in charge of collecting precipitation in the autumn of 2022, but samples have been collected regularly since 2016. The aim was to compare the daily measurements with the high-frequency measurements and investigate the effects of seasonality on the isotopic signals. Prior to the field work on November 27th, between November 14th to 25th there was a long dry period.

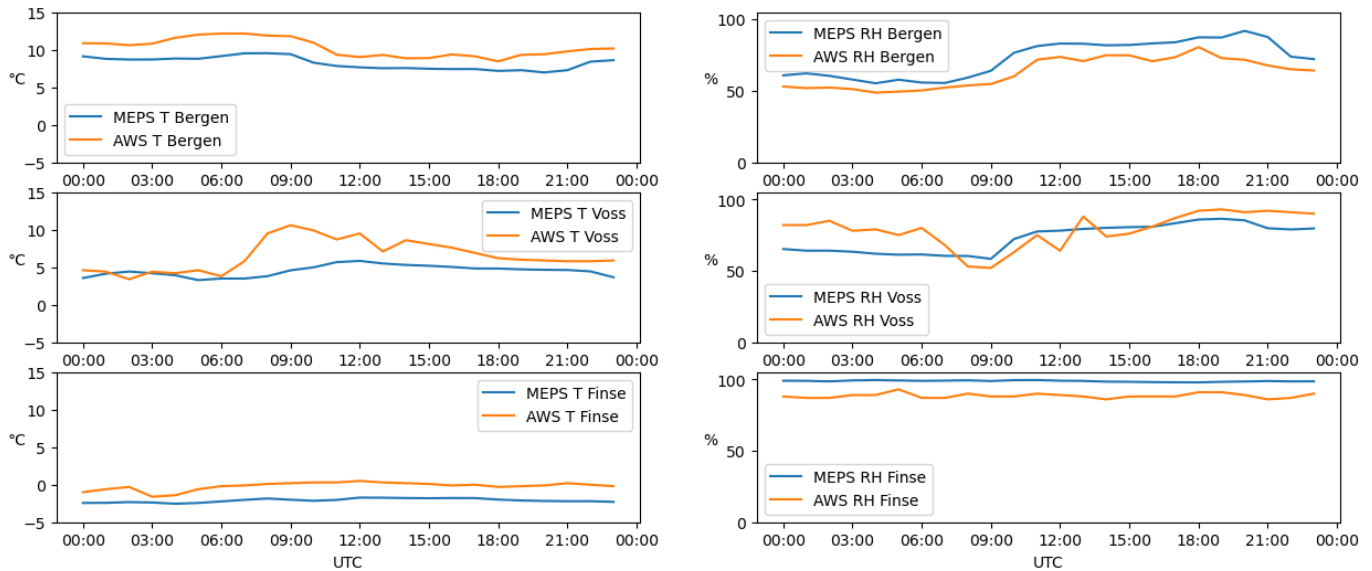


Figure 9: Comparison between the MEPS model (blue lines) and AWS data (orange lines). The top row is Bergen, left is temperature and RH is right. Middle row is Voss, left side is temperature and right is RH. Bottom row is Finse, left side is temperature and right is RH. The time span was from 00 UTC on the 27/11/22 until 00 UTC on the 28/11/22.

Daily precipitation for stable isotope analysis was sampled in Bergen with the Palmex rain sampler (green circle, fig.5b). The $\delta^{18}\text{O}$ were monthly averaged to observe the seasonal variations. There were no samples taken in April. The whisker indicates the minimum and maximum values and the orange line is the median.

The daily precipitation samples could extend over more days depending on how much it rained, therefore the amount of daily precipitation (mmday^{-1}) was estimated. The precipitation amount was monthly averaged to investigate the seasonality (fig. 10a). A sample starting at the end of a month and expanding into the other would be put into the month of when the sample ended. The high variability from July to November could be explained by several extreme precipitation events. March had 3 samples which could explain the low spread. The median showed no clear seasonal indication in the precipitation data. March, May and August had the least amount of daily precipitation which could indicate some seasonality, but June and July had increased amount. There was some more precipitation in January and February compared to November and December. The reason December was low could stem from snow measurements which were only measured for isotopic composition.

The isotopic composition of the daily precipitation measurements had high day to day variability in some months dependent on the amount of samples taken. The monthly averages of the $\delta^{18}\text{O}$ (fig. 10b) smoothed out these variabilities, and an indication of seasonality became visible. The evolution from February and forward showed that there was an increase towards the summer months which peaked in June and then a decrease towards December. The high median in November could be caused by the extreme weather in the beginning of the month and the dry period which lasted for a couple of days between the 14th and 25th of November prior to the field work. The highest values in January coincided with two samples with short intervals taken on the 12th of January. The low isotopic values in December were from the snow samples.

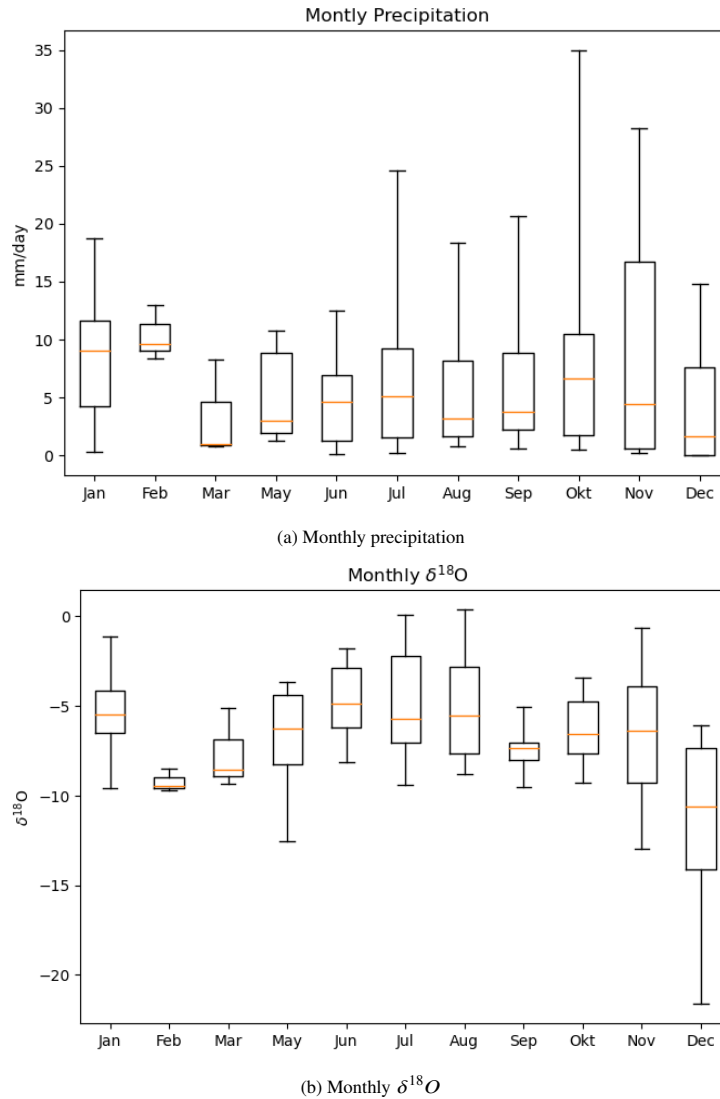


Figure 10: Box plots of monthly averages of daily precipitation samples for year 2022. a) is the monthly precipitation amount [mm day^{-1}]. b) is the $\delta^{18}O$ [‰] from the precipitation samples. The orange lines are the median, the whiskers indicates the spread of the samples

4.4 Meteorological ground observations during the fieldwork

All samples and measurements were collected during an incoming eastward front on the 27/11/22. The conditions during this sampling period varied from station to station. The start time (table 5) was based on the MEPS forecast, and collecting began prior to the forecasted precipitation to catch potential early rain or snowfall. Finse had snow in the morning and therefore the sampling started earlier than first estimated. The ending of the field work corresponded to the end of precipitation at Ågotnes and Bergen. Voss and Finse experienced rain and snowfall when the field work ended. The sampling stopped at Finse at 19:30 UTC because of bad wind conditions and nighttime. Voss had

some light precipitation with breaks when the sampling ended while Finse had increasing snowfall and high winds which continued throughout the night.

Station	Start of sampling	End of sampling	Number of samples
Ågotnes	9 UTC	16:30 UTC	10
Bergen	9 UTC	17 UTC	10
Voss	9 UTC	18 UTC	17
Finse	7:30 UTC	19:30 UTC	16

Table 5: Start and end times for the precipitation sampling at the different stations

At Ågotnes there were observed light windy conditions in the morning accompanied with light rain. Rain started around 9 UTC with the first precipitation sample being collected at 09:56 UTC. The rain continued until 13 UTC and afterwards there were period of sparse rain and precipitation breaks until 16:26 UTC. The last sample was collected after a longer period of no rain. The conditions in Bergen were similar to Ågotnes, with light windy conditions and light rain. In Bergen, it started raining between 10 UTC and 11 UTC and the first sample was collected at 11:08 UTC. Light rain continued during the day, and at 14 UTC the rain intensity increased, and the sampling went from every 30 min to every 15 min. The rain intensity decreased around 15 UTC and light rain continued until the last sample was collected at 16:29 UTC when the rain stopped for long periods. At Voss there was light rain from the morning when sampling started around 9 UTC. There was a sampling error so the measured rain rate between 10 UTC and 12 UTC was corrupted. There was a misunderstandings of the sampling procedure, so samples were collected from the box and the rain gauge as two separate samples. When the samples were retrieved from the rain gauge, it flipped the tipping bucket. The samples from the tipping bucket were not further included. The problem was cleared right before 12 UTC. The light rain at Voss continued during the day and increased in the afternoon between 16 UTC and 17 UTC. At Finse the conditions were very windy the forecasted wind gusts were over 20 m/s around 13 UTC. The sampling period began around 07:30 UTC but the first sample was collected at 10:00 UTC. There was light snow in the air, but most of the snow blew out of the box. The winds prevailed around 15-16 UTC at the same time the snowfall became more intense and the snowflakes came in chunks. The heavy snowfall continued after the last sample was collected at 19:30 UTC.

4.5 Fieldwork samples and measurements

The results from the field work consisted of the precipitation samples at each station, the rain-gauges at Ågotnes and Voss, and the AWS at Bergen, Voss and Finse. Snowfall was also measured and calculated at Finse.

4.5.1 Ågotnes

Ågotnes had no AWS measurements, therefore the results from this station consisted of rainfall rate calculated from the rain-gauge measurements (blue bars, fig. 11) and the isotopic composition of the precipitation samples (black lines, in fig. 11). The length of each black $\delta^{18}\text{O}$ line represents the duration of that sample. The rain rate showed light drizzle in the morning hours around 08:00 UTC, and at 10 UTC it increased to light rain ($< 2.5 \text{ mmh}^{-1}$).

The first sample started at 09:02 UTC and was collected at 09:56 UTC. The first sample had a $\delta^{18}\text{O}$ value of -2.9‰ . The following 5 samples were sampled between 10 and 12:30 UTC, during

which the $\delta^{18}\text{O}$ values decreased and rain continued. Around 12:30 UTC there was a short break in the precipitation. The rain started again at 13:30 UTC, a precipitation sample was collected which included this break and showed an increase in $\delta^{18}\text{O}$ compared to the previous sample. This increase was going from -12.4‰ to -11.1‰ during the break and then down to -12.8‰ when it started to rain again, between 12:40 and 13:59 UTC. The rain intensity peaked at 13:50 UTC with 2.4mmh^{-1} , during this the $\delta^{18}\text{O}$ values reached the minimum $\delta^{18}\text{O}$ value of -13.1‰ sampled at 14:52 UTC. The rain stopped again after 15 UTC, with a long sample starting at 14:55 UTC and ending 16:26 UTC, during this sample, a small amount of rain fell after 16:00 UTC contributed to the sample. The average $\delta^{18}\text{O}$ value during this sampling period was -9.8‰ (standard deviation (std): 3.3‰). The variations in $\delta^{18}\text{O}$ was 9.5‰ at Ågotnes.

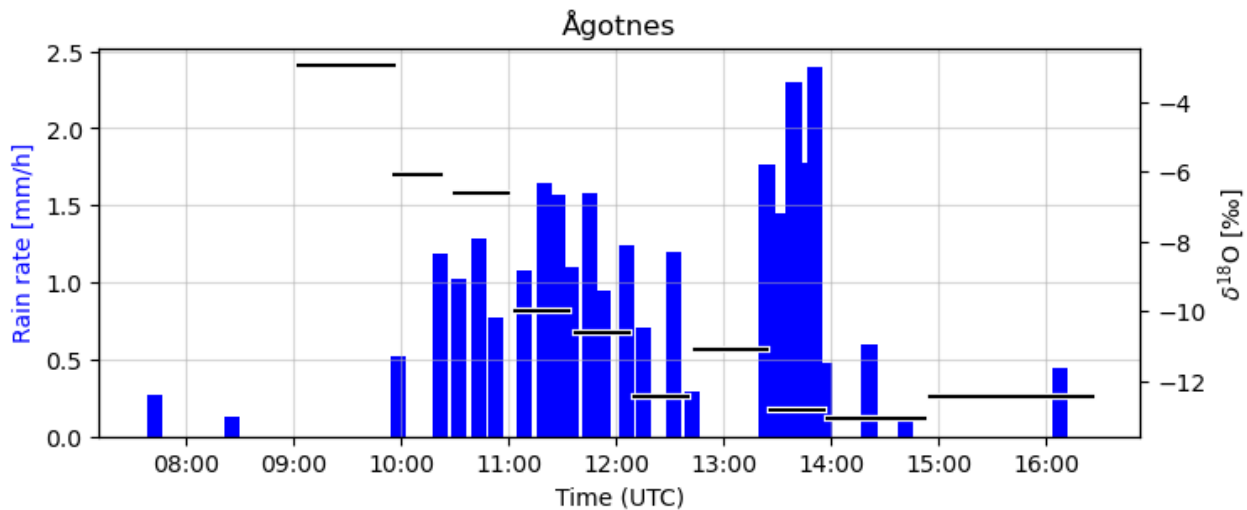


Figure 11: The rainfall rate [mmh^{-1}] at Ågotnes is indicated by blue bars. $\delta^{18}\text{O}$ [‰] in precipitation are indicated by the black lines. The length of the black lines indicates the duration of a precipitation sample.

4.5.2 Bergen

Bergen had hourly averaged temperature and relative humidity measurements from the AWS (fig. 12a) and rain rate calculated from the AWS and $\delta^{18}\text{O}$ from the precipitation samples (fig. 12b). The rain started around 11 UTC and the temperature decreased from 11 °C to 9 °C (red line, fig. 12a) while the RH increased from 55 to 74 % (gray line, fig. 12a). Both the temperature and RH remained stable with small variations throughout the sampling period. The small increases of temperature and decreases of RH were connected to the precipitation breaks. The first precipitation sample was collected at 11:08 UTC when the rain rate increased. The following sample had the maximum value of $\delta^{18}\text{O}$ at -2.3‰ . The $\delta^{18}\text{O}$ values decreased as the rain continued with the following samples at -5.0‰ and a drop to -10.0‰ at 11:45 and 12:22 UTC, respectively. There was a break in precipitation at around 13 UTC similar to Ågotnes. The break lasted less than an hour and the sample collected at 14:17 UTC consisted of precipitation from the second peak visible in figure 12b. The change from the sample at 13:02 UTC right before the break and the sample after the break at 13:41 UTC was small, it went from -10.2‰ to -10.3‰ . The following samples showed more depleted $\delta^{18}\text{O}$ values at -12.5‰ at 14:17 UTC and -12.4‰ at 14:39 UTC. An observed increase in rain intensity caused the sampling frequency to increase to every 15 minutes. The minimum $\delta^{18}\text{O}$

was collected at 15:01 UTC with $\delta^{18}\text{O}$ at -12.5‰ . The rain intensity decreased and the next sample had a slightly increased value of -12.2‰ at 15:53 UTC. The last sample was collected at 16:29 UTC where the $\delta^{18}\text{O}$ value had increased to -8.9‰ . The mean $\delta^{18}\text{O}$ value was -9.6‰ (std: 3.3‰) during the sampling period and the variation in $\delta^{18}\text{O}$ was 10.2‰ in Bergen.

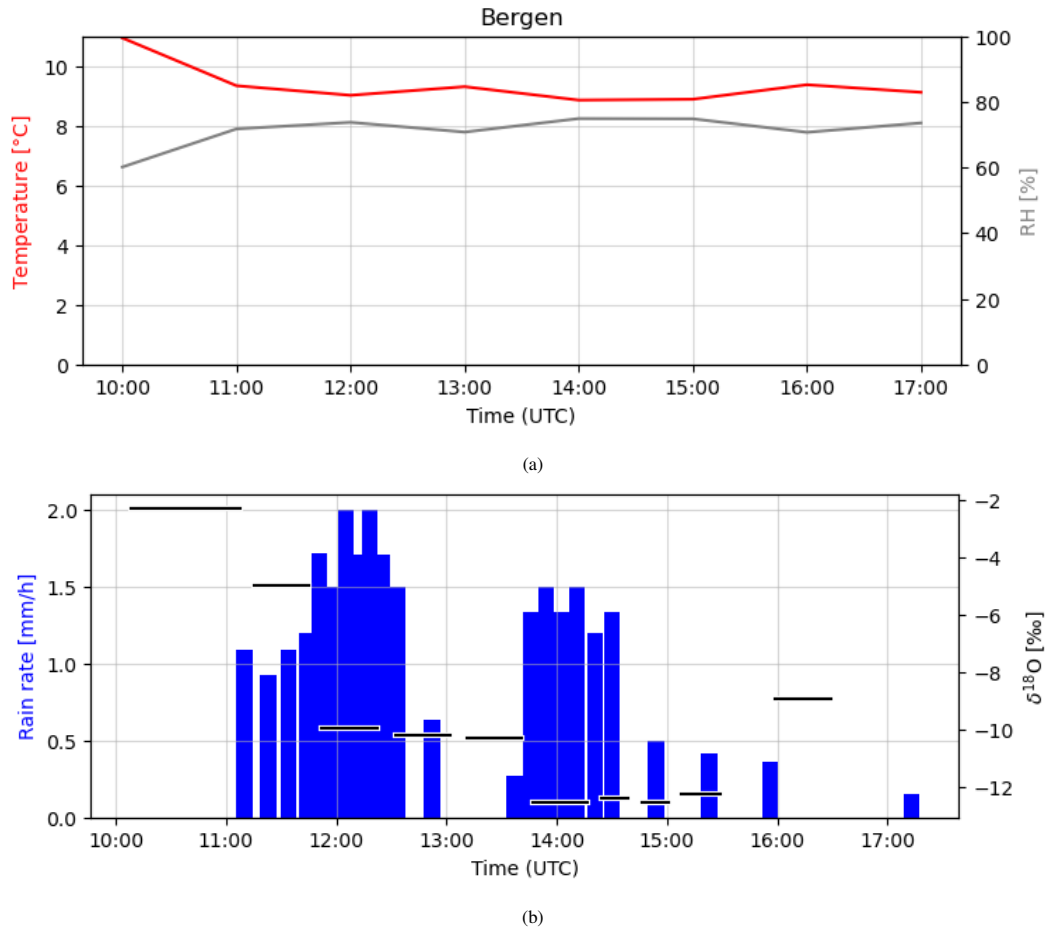


Figure 12: a) Hourly AWS measurements from Bergen. The red line is the temperature [°C] and gray line is the RH [%]. b) rainfall and $\delta^{18}\text{O}$ [‰]. Black lines indicate the $\delta^{18}\text{O}$, the length of the line is the duration of a sample. The blue bars is the precipitation rate. Measurements were taken in Bergen between 10 and 17 UTC on the 27/11/22.

4.5.3 Voss

The precipitation sampling at Voss started around 9 UTC. There was light precipitation until noon, and the precipitation rate (blue bars, fig. 13b) were measured from the HOBO rain gauge. The lack of rainfall rate between 10 and 12 UTC was due to the sampling error, so the precipitation during this period was removed. The temperature (red lines fig. 13a) and RH (gray lines, fig. 13a) were retrieved from the local AWS station at Voss (section. 3.2). The RH between 8 UTC and 11 UTC increased, going from 52 % at 8 UTC and up to 75 % at 11 UTC, while the temperature sank. The peaks in RH and subsequent drops in temperature was connected to the precipitation.

The RH had a peak at 13 UTC at 88 % before dropped down to 74 % at 14 UTC. The RH steadily increased during the afternoon and reached a maximum at 19 UTC of 93 %. The temperature showed a general decrease, anti-correlated with the RH. There were several smaller precipitation breaks, which occurred regularly between 12 and 15 UTC.

The first sample was collected at 09:45 UTC and had a $\delta^{18}\text{O}$ value of -4.9 ‰. The following sample had the maximum $\delta^{18}\text{O}$ value of -3.4 ‰ at 10:15 UTC. The values decreased to -4.4 ‰ at 10:45 UTC and further to -5.3 ‰ at 11:15 UTC and 11:45 UTC. At 12:30 UTC the $\delta^{18}\text{O}$ increased to -4.1 ‰. The precipitation became more consistent around 13 UTC, with less and smaller breaks. The $\delta^{18}\text{O}$ then decreased to -5.1 ‰ at 13:00 UTC. The light precipitation persisted and at 13:30 UTC the $\delta^{18}\text{O}$ had decreased down to -5.4 ‰. The following two samples stayed consistent at -5.8 ‰ at 14 UTC and 14:30 UTC. There was a noticeable drop in and the three following samples, which had the values -8.8 ‰, -9.6 ‰ and -10 ‰ between 15 to 16 UTC. At around 15 UTC the rainfall intensity increased simultaneously as the temperature decreased and the RH increased. A short break in rainfall at 16 UTC corresponded to a slight increase in $\delta^{18}\text{O}$ from -10.0 ‰ at 16:30 UTC to -9.2 ‰ at 17 UTC. The maximum rain rate was measured at 17:09 UTC with 5.1 mmh^{-1} and the minimum $\delta^{18}\text{O}$ values of -14.3 ‰ was measured at 17:30 UTC. The rain intensity decreased and the last sample, measured at 18 UTC had $\delta^{18}\text{O}$ values at -12.9 ‰. The mean $\delta^{18}\text{O}$ value for this station was -7.3 ‰ (std: 3.2 ‰). The variation in $\delta^{18}\text{O}$ was 10.9 ‰.

4.5.4 **Finse**

Finse had snowfall from the morning and 10 sticks were deployed in the accumulated ground snow to measure change in snow depth after the sampling period. The snowfall rate was calculated from the mean depth of accumulated snow over the duration of the field work. The mean snowfall rate was 4.9 mmh^{-1} . These measurements were highly uncertain due to different factors like the wind, the snow intensity was not homogeneous, and no density measurements of snow were collected. The subsequent accumulated snowfall calculations would also be uncertain due to the sampling uncertainties.

The AWS data from Finse showed little fluctuations in temperature (red lines, fig.14a) and RH (gray line, fig.14a) throughout the day. The temperature was on average at $0.1 \text{ }^\circ\text{C}$ with the maximum temperature of $0.5 \text{ }^\circ\text{C}$ at 12 UTC, and a minimum temperature of $-0.3 \text{ }^\circ\text{C}$ at 18 UTC. The RH had an average of 88.7 %.

The first sample had a long sampling interval (2h and 27min) due to strong winds which blew the snow out of the collection box. This sample, collected at 10 UTC, had a $\delta^{18}\text{O}$ value of -8.1 ‰, and the following sample at 11:13 UTC had the maximum value of -6.6 ‰. At around 12 UTC, the wind reached a maximum at 20.9 m/s and the snowfall intensified. There was a drop in the $\delta^{18}\text{O}$ down to -13.4 ‰ at 12:22 UTC. The snowfall increased and the sampling frequency decreased down to 30 min intervals. At 12:45 UTC the $\delta^{18}\text{O}$ value was -14.7 ‰ which increased a little to -14.6 ‰ at 13:24 UTC. The meteorological observations noted that the snowfall intensity had increased around 14 UTC, and the sample collected at 13:57 had $\delta^{18}\text{O}$ values at -13.2 ‰. At 15 UTC the snow intensity had continuously increased and the sampling frequency went to every 15-20 min. There was another drop in the $\delta^{18}\text{O}$ values down to -16.4 ‰ at 15:37 UTC and the two following samples had -16.6 ‰ and -16.7 ‰ at 15:56 UTC and 16:12 UTC, respectively. The minimum $\delta^{18}\text{O}$ of -18.6 ‰ was collected at 16:30 UTC. The next samples showed some increase in $\delta^{18}\text{O}$ at -15.1 ‰ at 16:45 UTC, which decreased to -16.0 ‰ at 17:08 UTC. Then there was again an increase to -15.1 ‰ at 17:23 UTC before the next sample decreased down to -17.9 ‰ at 17:56 UTC. The two last samples showed

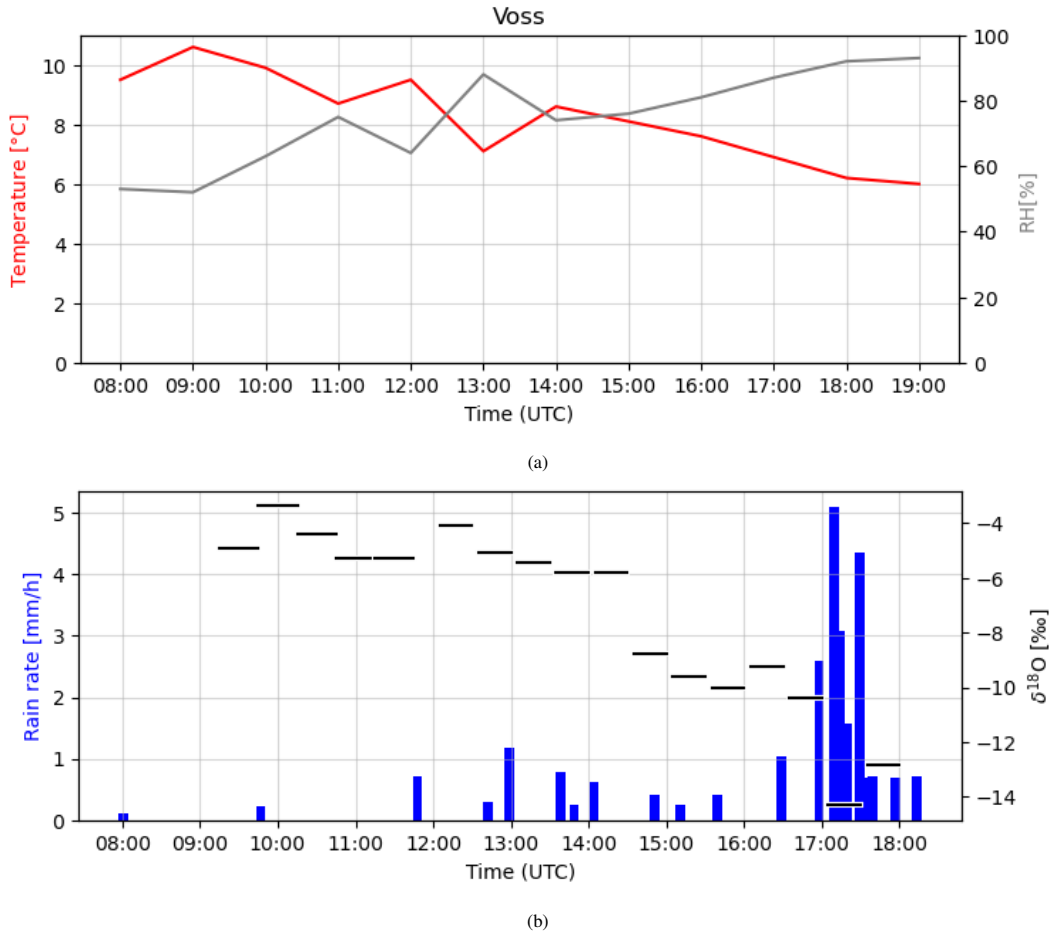


Figure 13: a) Hourly AWS measurements from Voss The red line is the temperature [°C] and gray line is the RH [%]. b) rainfall and $\delta^{18}O$ [‰]. Black lines indicate the $\delta^{18}O$, the length of the line is the duration of a sample. The blue bars is the precipitation rate. Measurements were sampled in Voss between 8 and 18 UTC on the 27/11/22.

an increase from this second minimum, with -17.0 ‰ at 19:58 UTC and -16.7 ‰ at 19:29 UTC. The mean $\delta^{18}O$ value was -14.8 ‰ (std: 3.2 ‰). The variation in $\delta^{18}O$ was 12 ‰ at Finse

4.6 Precipitation weighted mean and rain intensity

There was a connection between the rain intensity and the $\delta^{18}O$ values at each station. The precipitation weighted average for each station (table 6) indicated a pattern of decreasing values from station to station when moving away from the coast and increasing the altitude.

The total amount of precipitation at each station was also calculated from the precipitation measurements. Finse had the highest accumulated amount at 60.1 mm, however, due to the sampling uncertainties connected with the snowfall measurements, this value is uncertain. Voss had the most rain at 12.1 mm total, followed by Ågotnes at 9 mm rain and lastly Bergen at 7.1 mm rain. The MEPS model showed similar values of accumulated precipitation for Ågotnes, Bergen and Voss

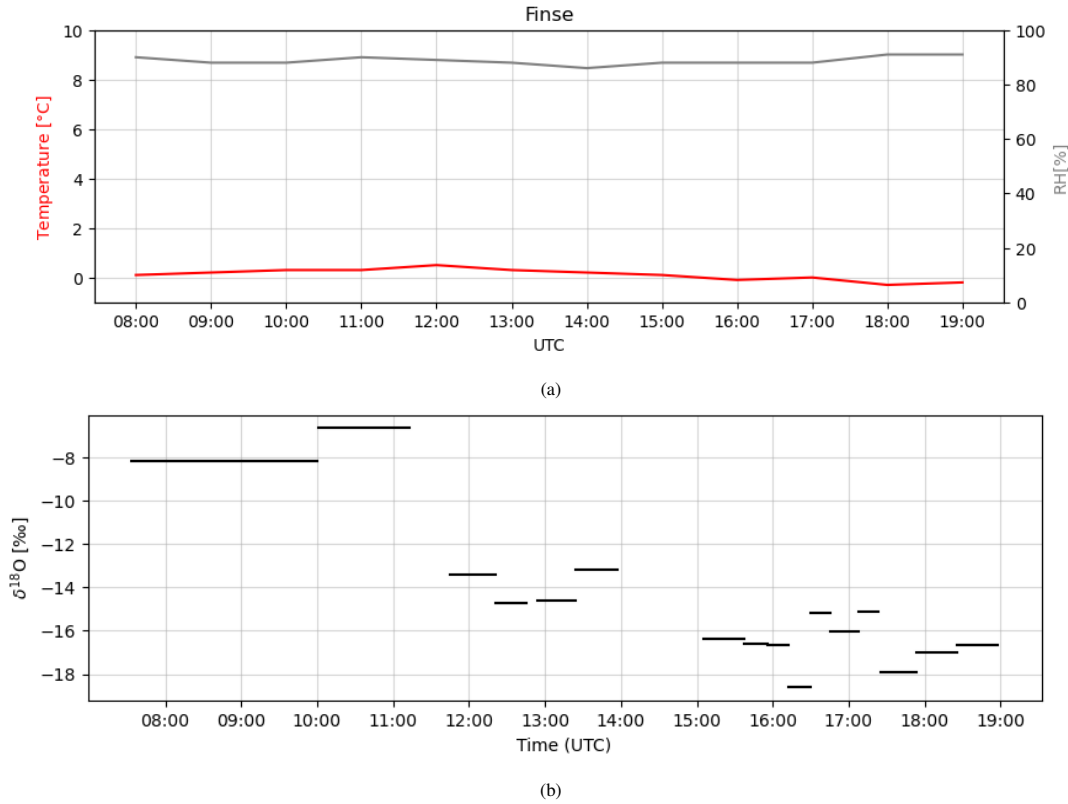


Figure 14: a) Hourly AWS measurements from Finse. The red line is the temperature [°C] and gray line is the RH [%]. b) rainfall and $\delta^{18}\text{O}$ [‰]. The length of the black lines indicates the duration of a sample. The blue bars is the precipitation rate. Measurements were sampled at Finse between 7 and 19 UTC on the 27/11/22.

(table 6).

Station	$\delta^{18}\text{O}$ [‰]	SEM	Precipitation [mm]	Precipitation MEPS [mm]
Ågotnes	-3.8	1.034	9	10.7
Bergen	-5.7	1.037	7.1	8.2
Voss	-6.7	0.764	12.6	12.4
Finse*	-8.4	0.788	60.1	18

Table 6: The weighted average of $\delta^{18}\text{O}$ in precipitation at the four stations and the calculated precipitation amount from the rain rates and the accumulated precipitation from the MEPS model. *The values from Finse are highly uncertain because of the uncertainties connected with snowfall rate measurements. SEM indicates the standard error of the mean for each station and was calculated with eq. 19.

Comparing the hourly averaged rain intensities measured the different stations with the MEPS model could give an insight on how well the model forecasted rainfall and rain intensity (table 6). The hourly values for the MEPS model (blue bars, fig.15) was compared with the hourly averaged rain at the different stations (red bars, fig. 15) to investigate the timings of the rain events and at the precipitation rates. The hourly averaged precipitation smoothed out the irregularities in the instantaneously measured rain. The precipitation breaks were not visible for Bergen and Ågotnes.

However, the MEPS model allowed an insight in the snowfall which had uncertain observations. The meteorological ground observations at Finse confirmed the increase in snow intensity which was visible around 15 UTC in the MEPS model and the increase towards the evening.

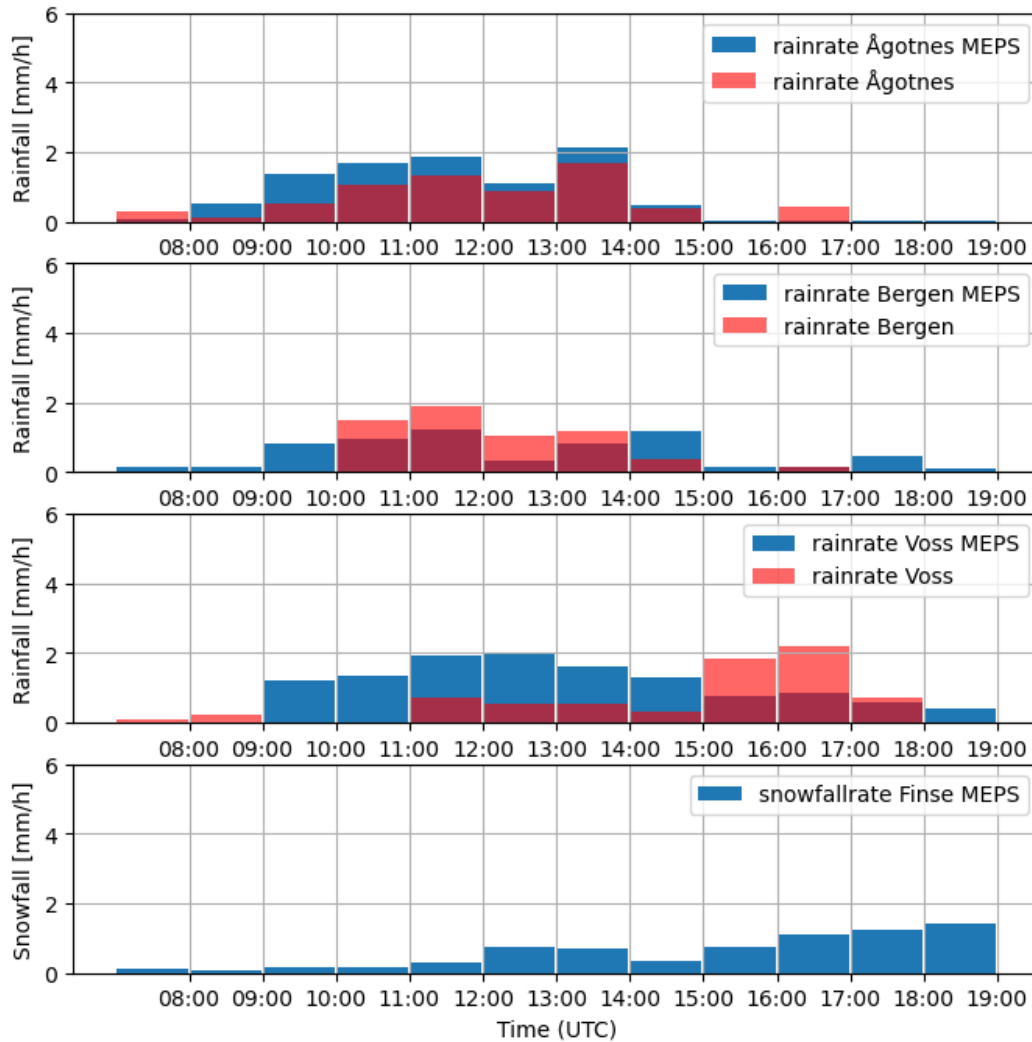


Figure 15: Comparing the hourly averaged rain intensity [mmh^{-1}] at the different stations (red bars) with the rain intensity [mmh^{-1}] from the MEPS model (blue bars). Panels top to bottom: Ågotnes, Bergen, Voss and Finse. Ågotnes, Bergen and Voss were the only stations with reliable rainfall observations. The snowfall rate [mmh^{-1}] for Finse (bottom) panel have been obtained from the MEPS model.

The peaks in precipitation were more diffuse when the rain rates were hourly averaged. Ågotnes and Bergen had similar distribution, and the peaks were represented at similar times. The MEPS model had generally higher rain rates than the hourly averaged observations at Ågotnes. In Bergen the rain started earlier and lasted longer according to the MEPS model and the overall rain rate was lower than the observations between 10 and 14 UTC. The MEPS model failed to forecast the afternoon precipitation at Voss. The precipitation intensity at Voss peaked in the model at 12 UTC, which had

a small increase in the measurements around 12-13 UTC, but this could be uncertain because of the sampling error. At 17 UTC, when the observed rainfall rate was at a maximum at Voss, the MEPS model showed decreasing trends.

4.7 Integrated water vapor

The integrated water vapor (IWV) was calculated from the specific humidity variable in the MEPS model and integrated over the atmospheric column. IWV allowed investigation on the evolution of the water vapor in the atmospheric column above each station during the front on the 27/11/22. There was a noticeable time offset of the peak values which could indicate the front passage.

Ågotnes (blue line, fig.16) had the highest values, where the maximum IWV was 22.1 kgm^{-2} at 9 UTC. It gradually decreased throughout the day, and from 15 UTC to 16 UTC there was a sharp drop from 19.1 kgm^{-2} to 14.6 kgm^{-2} . After 16 UTC there was a more gentle decrease, ending up at 12.6 kgm^{-2} at 19 UTC. This could indicate the arrival of new, dry air masses. The arrival of drier air masses could also explain why the precipitation stopped at 16:30 UTC.

Bergen (orange line, fig.16) had a similar decrease to Ågotnes, only the decrease was less steep. The maximum value was 19.3 kgm^{-2} at 8 UTC, and the minimum value was at 14.2 kgm^{-2} at 19 UTC. The same dry air masses seemed to have reached the station, but the drop in IWV was less steep than at the drop at Ågotnes.

Voss (green line, fig.16) had an increase from 8 UTC to 10 UTC of IWV from 12.5 kgm^{-2} to 16.9 kgm^{-2} . This could indicate that moist air masses arrived at Voss around 10 UTC. The maximum value was 17 kgm^{-2} , and the average was 16.7 kgm^{-2} between 9 UTC and 19 UTC. The IWV was stable and consistent, with very little change throughout the day. The dry air mass drop at Ågotnes and Bergen was not visible for Voss.

Finse (red line, fig. 16) had the lowest amount of IWV. This station started with increasing values from 8 UTC to 13 UTC following the same pattern as Voss, although with a larger time offset of the peak value. This would indicate the arrival of the front at this station, which fit well with observations of increases snow around noon. The maximum of 13.2 kgm^{-2} was reached at 13 UTC and the conditions were stable throughout the rest of the sampling period and decreased to 12.3 kgm^{-2} at 19 UTC.

There was a general decrease in IWV between the stations from west to east along the forecasted trajectory of the front. The front, and peak of IWV, passed Ågotnes and Bergen around 8-9 UTC and seemed to reach Voss at 10 UTC and Finse between 11 and 13 UTC. At 15 UTC the abrupt shift at Ågotnes might have been caused by new dry air masses entering over the station, this drop was also noticed in Bergen. The continuous decreasing indicated that water vapor was leaving the system at Ågotnes and Bergen. Voss and Finse experienced increase in water vapor, meaning moist air masses advected to these stations, keeping the water vapor levels stable.

The water vapor tended to be concentrated inside the clouds close to the cloud base (fig.17), as indicated by the green shaded area close to the cloud base (black lines, fig.17). The water vapor in the atmosphere at 10 UTC (fig.17a) fit the west-east gradient with decreasing IWV towards east. There was a high concentration of water vapor above Ågotnes and Bergen at 10 UTC. The arrival of dryer air masses was visible over these stations at 16 UTC (fig.17b). The arrival of the dryer air masses coincided with the end of the precipitation at Ågotnes and Bergen. At the end of the sampling interval, around 19 UTC, the dry air masses had not reached Voss yet (fig.17c). However, size of

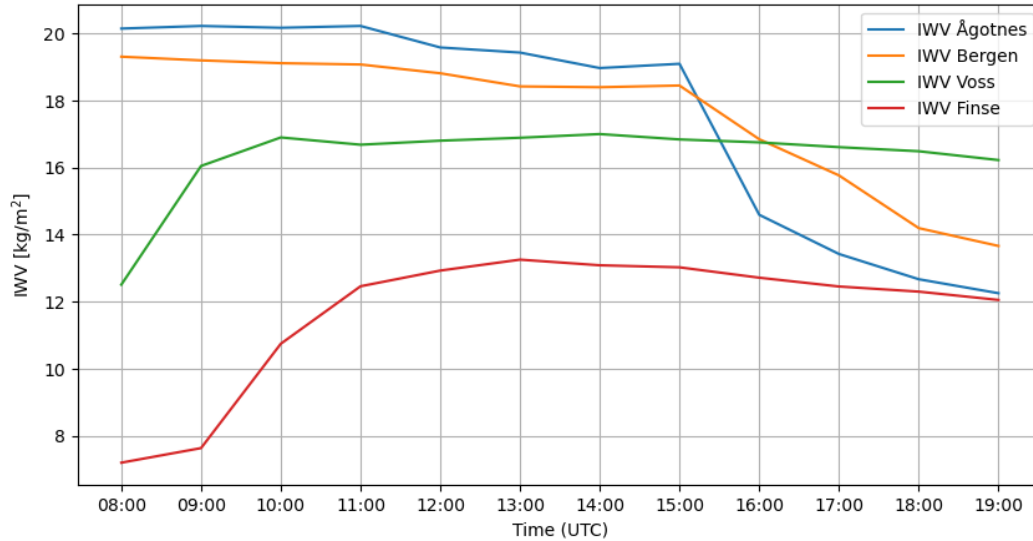


Figure 16: IWV [kgm^{-2}] at each station from 8 UTC to 19 UTC on the 27/11/22, retrieved from the MEPS model. The blue line is Ågotnes, the orange line is Bergen, the green line is Voss and the red line in Finse.

the local maximum of the water vapor contours was diminishing. This could be from the continuous rain-out with no new moisture coming in to the system to re-moisten the air.

4.8 Rayleigh distillation model

To investigate the observations through the Rayleigh framework, the precipitation weighted $\delta^{18}\text{O}$ values (table 6) was used. Each station had one representative $\delta^{18}\text{O}$ value. The chosen diagrams were the IWV and saturation mixing ratios. To estimate the fraction of moisture left in the reservoir, f (eq. 9) was adjusted to the source region conditions of w_{s0} and initial amount of IWV to fit with the Rayleigh framework. The assumptions were that the condensation process was from vapor to liquid, and no rain-out or mixing of air masses occurring between the moisture source and the first rain at Ågotnes.

4.8.1 Rayleigh model from an IWV framework

The IWV presented the available water vapor in the atmosphere during the field work. The IWV could be used as a reference for the amount of theoretically available precipitation at any time. Assuming there were no rain-out prior to the rain at Ågotnes, the maximum IWV at the start of the field work was equal to the initial IWV in the source region. The precipitation weighted mean for the IWV was calculated, and each station had one representative value of IWV. The weighted averaged was applied to match the weighted $\delta^{18}\text{O}$ values. The hourly precipitation rate from the MEPS model was used as weight. The uncertainties were calculated from the SEM values at each stations (table 6 for $\delta^{18}\text{O}$ and table 7 for the IWV). The IWV showed the decrease of moisture from station to station in the remaining moisture amount in table 7. According to the unweighted IWV from the MEPS model, 40 % of the moisture left the air parcel between Ågotnes and Finse.

The Rayleigh distillation process is temperature dependent and I needed to determine the temperature

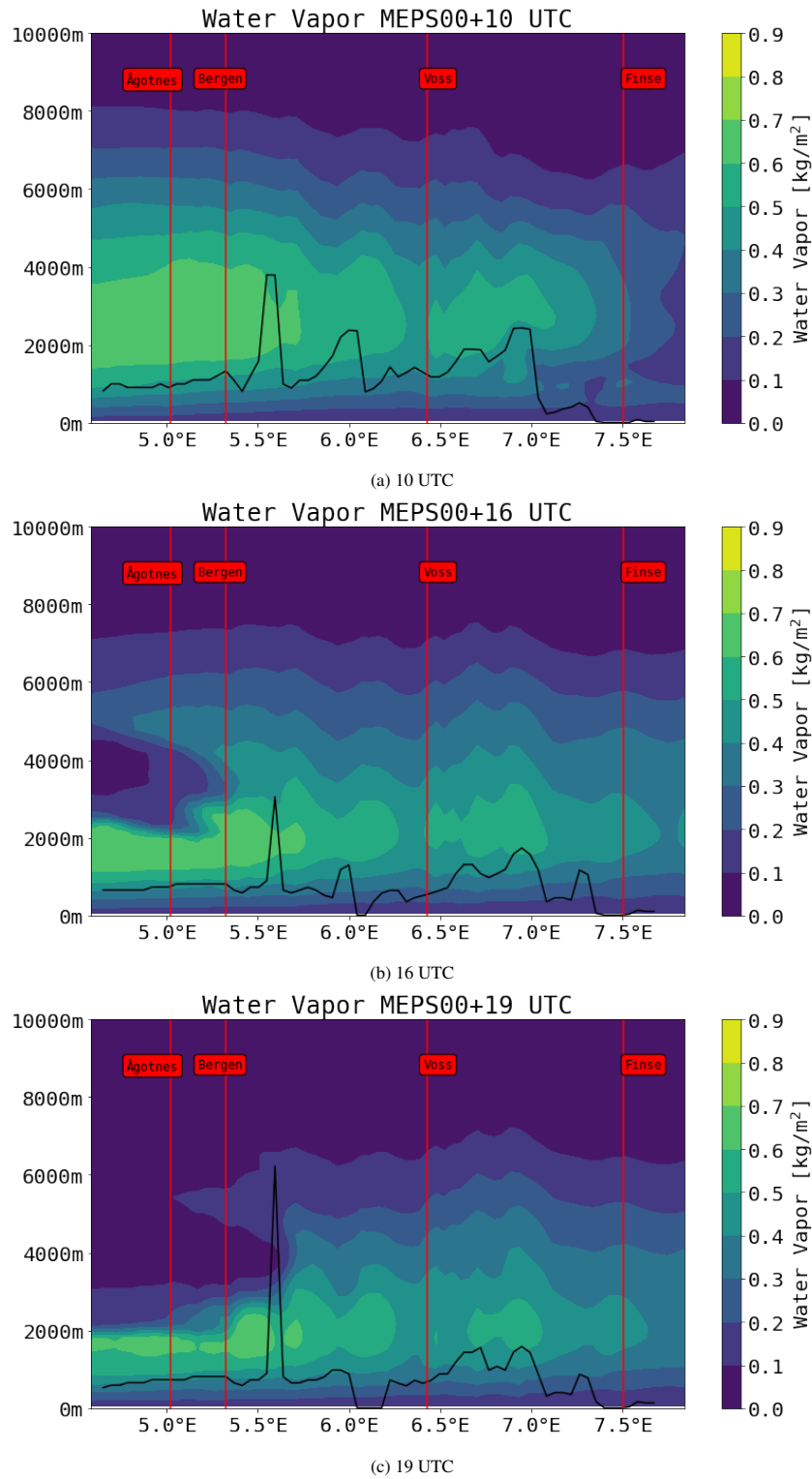


Figure 17: Water vapor in the atmosphere at a) 10, b) 16 and c) 19 UTC from the MEPS model. The filled contours is the water vapor [kgm^{-2}] in the atmosphere. The black line the cloud base height [m]. Stations are marked in red.

Station	Weighted IWV [kg/m^2]	SEM	Precipitation [mm]	Remaining moisture [%]
Ågotnes	16.2	0.903	10.66	100 %
Bergen	14.9	0.555	8.16	87 %
Voss	14.5	0.339	12.4	77 %
Finse	10.5	0.576	18.1	60 %

Table 7: Precipitation weighted mean for IWV at each station weighted with the precipitation rate from the MEPS model. The accumulated precipitation amount indicated by the MEPS model, and the remaining moisture [%] indicates how much moisture is lost between each station and was calculated from the unweighted IWV. SEM was calculated with eq. 19

during the cloud condensation process. Under the assumptions of the Rayleigh model, the newly formed condensate falls as rain. The instantaneous rain could be explored with the MEPS model (red shaded area, fig. 21), and the rain generation was located between the 0 °C and 5 °C isotherms. Assuming the Rayleigh distillation occurs close to the cloud base (black line, fig. 21), the temperature was close to 5 °C. The temperature was therefore assumed to be 5 °C during the condensation process.

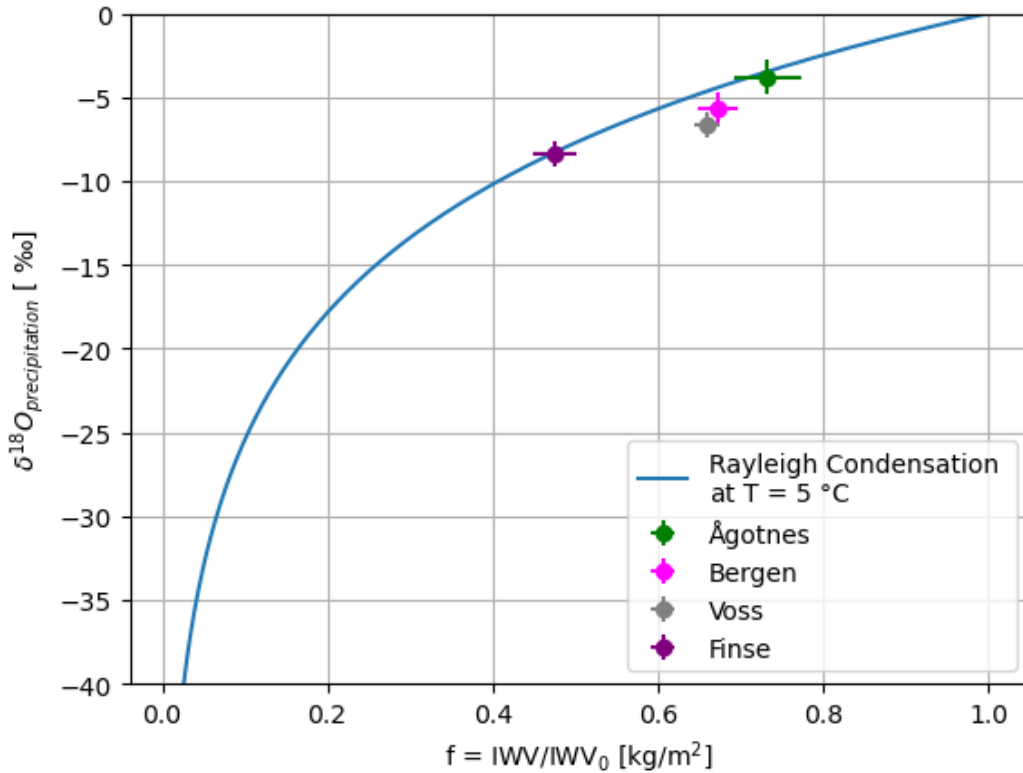


Figure 18: Precipitation weighted mean for $\delta^{18}\text{O}$ [‰] and IWV [kgm^{-2}] for the different stations (Ågotnes = green, Bergen = pink, Voss = gray and Finse = purple). The blue line is the Rayleigh curve plotted for the condensation temperature of $T = 5$ °C. $f = \frac{\text{IWV}}{\text{IWV}_0}$ with the IWV remaining unchanged from the source region. Horizontal lines was the SEM for the precipitation weighted IWV and vertical lines was the SEM for the precipitation weighted $\delta^{18}\text{O}$

The Rayleigh curve was calculated with eq. 10 (fig. 18). The stations, with their respective weighted

means of IWV and $\delta^{18}O$ values, were plotted in the same diagram (fig. 18). The fraction f was adjusted to the unweighted IWV under the assumption that the reservoir was full at 8 UTC at Ågotnes. The unweighted IWV was 22.1 kgm^{-2} (fig.16) at 8 UTC and thus $N = 22.1 \text{ kgm}^{-2}$ and since there was assumed no rain-out prior to Ågotnes, $N_0 = 22.1 \text{ kgm}^{-2}$ in the source region. The curve matched well with Ågotnes and Finse, but the values from Bergen and Voss were below the curve. The horizontal lines at each point were the SEM from IWV and the vertical lines indicated the SEM for the $\delta^{18}O$ values. Ågotnes had the highest IWV SEM, which could be explained by the arrival of the new dry air masses giving large variations in the IWV at this station.

4.8.2 Rayleigh model from a mixing ratio framework

The saturation mixing ratios were retrieved with the MEPS model at the cloud base height under the assumption that the condensation temperature was 5°C throughout the whole process. Following eq. 13 and eq. 14 with p as the pressure at the cloud base height, the saturation mixing ratios w_s at cloud base height were calculated for the different station for the duration of the field work between 8 and 19 UTC (fig. 19).

Ågotnes and Bergen had similar patterns (blue and orange lines, fig. 19), with Bergen (orange) having a higher w_s compared to Ågotnes (blue). Voss (green line, fig.19) had initially higher values than Ågotnes. Voss peaked above the value in Bergen at 12 UTC, before decreasing until 18 UTC when it increased slightly at 19 UTC. Finse (red line, fig. 19) had the lowest values overall, which started with a decrease until 10 UTC, before increasing and peaking at 13 UTC. The saturation mixing ratio at Finse was stable between 12 UTC and 17 UTC before decreasing.

The Rayleigh model could be expressed as a function of the saturation mixing ratio $f = \frac{w_s}{w_{s0}}$. Figure 20 displays the weighted $\delta^{18}O$ values with their respective weighted saturation mixing ratio for each station. The precipitation weighted saturation mixing ratios $w_{sweighted}$ (table 8) were calculated along with their respective SEM.

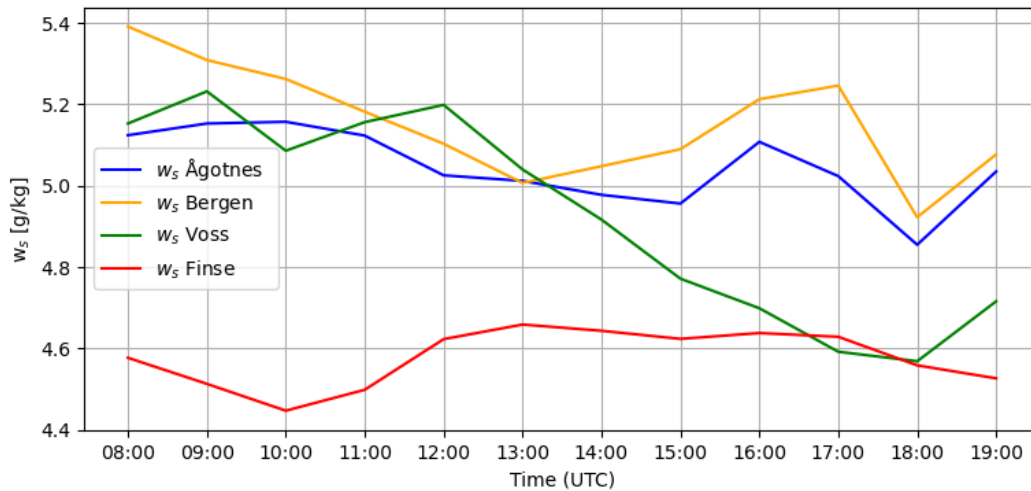


Figure 19: Evolution of the saturation mixing ratios (w_s) [gkg^{-1}] at the cloud base height for the different stations between 8 UTC and 19 UTC retrieved from the MEPS model. The blue line is Ågotnes. The orange line is Bergen. The green line is Voss and the red line is Finse.

To fit the Rayleigh curve to the observations, the w_{s0} in the source region was needed. Assuming $w_{s0} = 9 \text{ gkg}^{-1}$ along with the condensation temperature of $5 \text{ }^\circ\text{C}$, revealed a Rayleigh curve which fit for Bergen, Voss and Finse (fig. 20). Ågotnes was positioned above the curve.

With the assumption that $w_{s0} = 9 \text{ gkg}^{-1}$ in the source region, the CC-relation could be used to calculate the initial condensation temperature by using eq. 14. The condensation temperature in the source region could therefore be estimated to be $12.5 \text{ }^\circ\text{C}$.

Station	w_s weighted [g/kg]	SEM	precipitation amount [mm]
Ågotnes	4.9	0.028	10.66
Bergen	5.3	0.042	8.16
Voss	5.2	0.077	12.4
Finse	4.5	0.021	18.1

Table 8: Precipitation weighted mean for w_s at each station weighted with the precipitation amount from the MEPS model. SEM was calculated with eq. 19

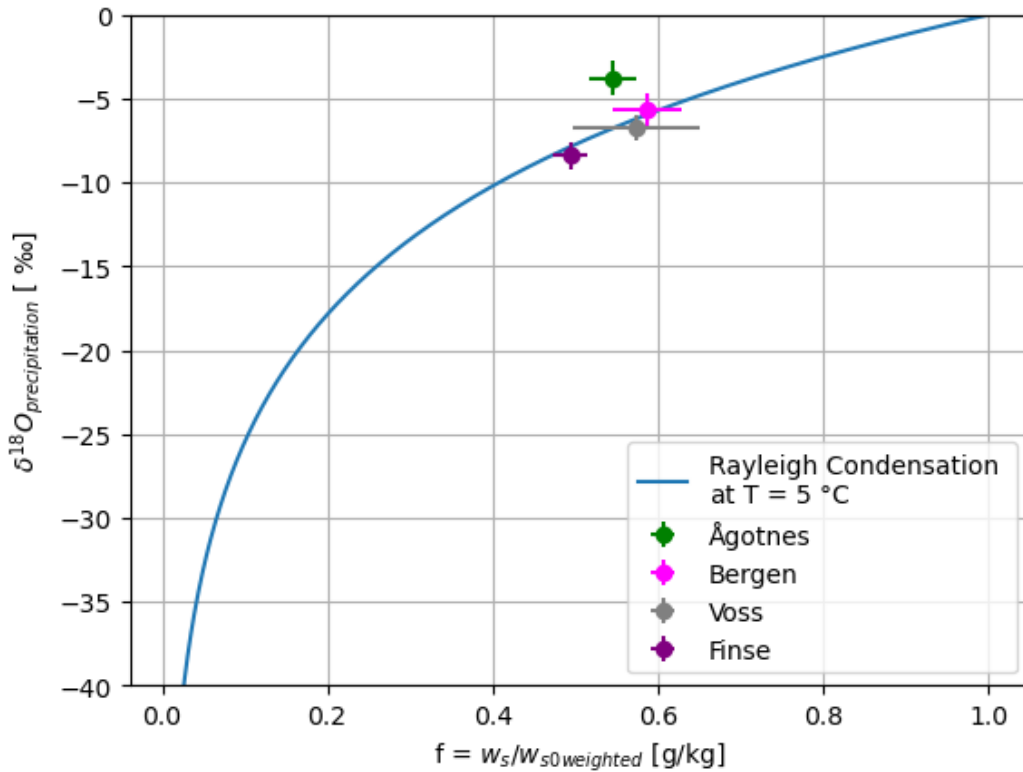


Figure 20: Rayleigh curve at $T = 5^\circ\text{C}$ for the precipitation weighted $\delta^{18}\text{O}$ and the precipitation weighted saturation mixing ratios $[\text{gkg}^{-1}]$ at the different stations. Ågotnes is the green dot, Bergen is the pink, Voss is the gray and Finse is the purple dot. Horizontal lines was the SEM for the precipitation weighted saturation mixing ratios and vertical lines was the SEM for the precipitation weighted $\delta^{18}\text{O}$

4.9 Generation of precipitation with the MEPS model

The instantaneous rain gave indicated when and where rain was generated. The extent of the instantaneous rain also showed if the rain reached the ground before re-evaporation.

There were no measurements taken of the atmosphere except for the AWS measurements at the surface. The below-cloud processes were therefore investigated by using the MEPS model. A way to look at the possible extent of the below-cloud processes, was to compare the atmospheric conditions to when the below-cloud effects were most likely prominent and when they were mostly absent. The highest rainfall rates was for Ågotnes at 12 and 14 UTC (fig. 11), in Bergen at 12 and 14 UTC (fig. 12) and Voss at 17 UTC (fig. 13). In these cases, the $\delta^{18}\text{O}$ values were most depleted. The highest $\delta^{18}\text{O}$ values were measured early in the sampling period. The precipitation sampling began around 10 UTC (fig. 21a) at Ågotnes and this was used as the reference time to observe the atmosphere when the below-cloud processes dominated. The variables used for determining the possible below-cloud effects were the instantaneous rain (red shaded area, fig. 21), the instantaneous snow (blue shaded area, fig. 21) and the cloud condensate (green contours, fig. 21). The instantaneous snow was prominent on higher levels and inside the clouds, and the boundary between snow and rain could indicate the height of the melting layer. The isotherm at 0 °C could also indicate the potential position of the melting layer, and the black lines in the cross sections represents the cloud base heights.

The rain above Ågotnes and Bergen was created around the cloud base at temperatures between 0 °C and 5 °C which persisted until 17 UTC when there was no rain. The rain generation at Voss was located closer to the ground, which could indicate more solid precipitation and a lower melting layer over this station. Over Voss, the 0 °C isotherm was located closer to the surface. Further east the surface temperatures was below 0 °C. The amount of instantaneous snow above Finse increased with time, which could indicate the eastward movement of the front.

The rain generation at 10 UTC showed little change compared to 12 UTC above Bergen and Ågotnes. There was no notable areas of precipitation which disappeared before reaching the ground and throughout the day, the cloud base height became lower. Over Voss, at 10 UTC the cloud base was high with instantaneous snow below the cloud base and some instantaneous rain which increased with time. The difference in the instantaneous rain amount changed little between 10 and 14 UTC, there was some increase in the rain and the cloud base became lower. The snow generation between Voss and Finse seemed to increase, reaching a peak indicated by the darkest shaded area at 12 UTC before gradually decreasing. Simultaneously, there was a decrease in rain generation. This decrease in rain could be explained by the eastward movement and adiabatic lifting initially creating more available moisture from condensation (visible in the blue shaded area at 12 and 14 UTC). The cloud condensation contours showed that there was cloud condensation above Ågotnes and Bergen without any rain generation at 17 UTC. The precipitation intensity at Voss reached its maximum amount of 5.1 mmh^{-1} around 17 UTC. This was not the case according to the MEPS model, rather Voss lied between two maximum of instantaneous snow. These maximums seemed to be the same maximums observed above Ågotnes and Bergen at 10 and 12 UTC, which at 17 UTC had advected further eastward. The precipitation intensity at Voss reached its maximum amount of 5.1 mmh^{-1} around 17 UTC. This was not the case according to the MEPS model, rather Voss lied between two maximum of instantaneous snow. These maximums seemed to be the same maximums observed above Ågotnes and Bergen at 10 and 12 UTC, which at 17 UTC had advected further eastward.

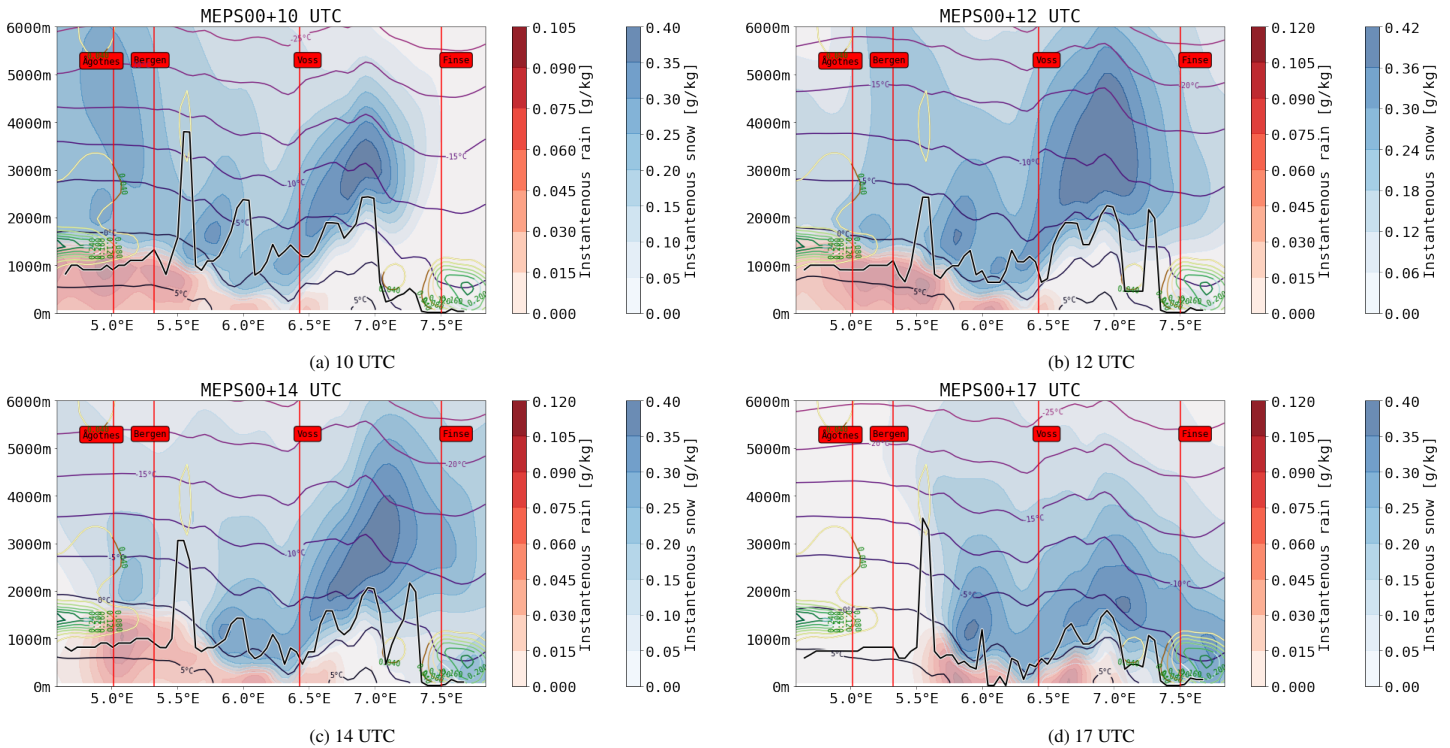


Figure 21: Cross section of the atmosphere showing different variables from the MEPS model. The variables are instantaneous rain (red shaded area), instantaneous snow (blue shaded area), cloud condensate (green contours) and temperature (purple isotherms) at a) 12, b) 14 and c) 17 UTC. Stations are marked in red. The black line indicates the cloud base height. The reference size of the wind arrows is the arrow of 20 m/s located above the colorbar.

4.10 *d*-excess

The *d*-excess (fig. 22) was calculated at each station following eq. 2 from the measurements of $\delta^{18}\text{O}$ and δD in the precipitation samples.

Ågotnes had an overall increasing trend, which started with negative values just under 0 ‰ and became positive towards the end of the sampling. Bergen had negative values, with some increasing values around 12 UTC and 14 UTC, which corresponded to the period of most intense rain at this station. Voss started with negative values which became positive towards the end of the field work. The increase in *d*-excess at Voss also corresponded to the increased rainfall and intensity. The light precipitation at Voss gave a negative *d*-excess while the heavy more intense precipitation gave positive values. Finse was the outlier with a high *d*-excess from the beginning. There was a sharp drop in *d*-excess at Finse between 13 and 14 which became positive again after 15 UTC. Toward the end of the sampling, the *d*-excess at Finse had alternating values.

Table 9 lists some of the properties of the *d*-excess. The mean values showed no patterns and the standard deviation at Voss and Finse were high. There was a large variability between the station with Ågotnes had the lowest and Finse the highest variation in *d*-excess. The variations in the *d*-excess increased with each station going west to east. The minimum values seemed to occur earlier in the field work for Ågotnes, Bergen and Voss, simultaneously with the observations of light rain.

Station	Mean d-excess	std(σ)	Min. value	Max. value	Variation
Ågotnes	1.16 ‰	1.7 ‰	-1.2	4.6 ‰	5.8 ‰
Bergen	-10.8 ‰	3.6 ‰	-15.4 ‰	-4.3 ‰	10.7 ‰
Voss	-8.6 ‰	5.6 ‰	-16.1 ‰	1.5 ‰	17.6 ‰
Finse	6.7 ‰	7 ‰	-12.9 ‰	15.2	28.1 ‰

Table 9: the mean values, minimum values, maximum values and variation of d-excess at the different stations.

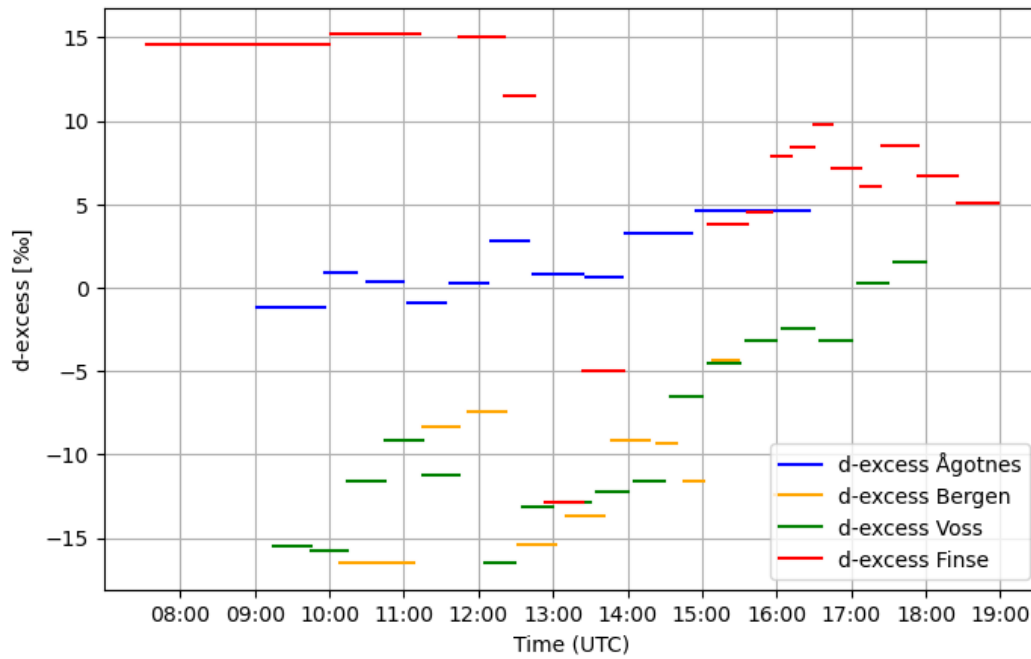


Figure 22: The d-excess at each station. Ågotnes (blue lines), Bergen (orange lines), Voss (green lines) and Finse (red lines), the length of the lines indicate the duration of a sample

5 Discussion

The observations from the different stations along with the MEPS model data allowed some insights in the isotopic evolution of precipitation at the west coast of Norway. This discussion will look at the different components of the field samples, measurements and MEPS model outputs and I will compare and discuss the results and the uncertainties.

5.1 MEPS model verification and weather forecast

To verify the MEPS model, the accuracy and bias was calculated. The unit conservation of RMSE gave an easy overview of the differences. Lower values indicates a better forecast (Warner, 2010). The RMSEs (table 4) were generally low for the temperatures, around 2°C, with Finse having the lowest of 1.9°C. The MEPS model had consistent lower temperatures compared to the observations. The bias was similar for all the stations, of about -2°C. The MEPS model looked at a grid of 2.5km x 2.5km, with the the grid closest to my stations being chosen as the representative location for each station. This could result in some of the differences because of the grid scaling. The AWS accuracy for Bergen for temperature was ± 0.1 °C, while Voss and Finse had an accuracy of ± 0.3 °C. This meant that the differences was not likely caused by measurement errors. The instrument accuracy was ± 2 % for the AWS at Bergen and ± 5 % for Voss and Finse. The humidity measurements at Voss and Finse was closer to their accuracy, therefore some irregularities could be explained by instrument uncertainties. At Finse, the MEPS model had very constant values of high RH. There seemed to be a connection between the high RH and the low clouds at Finse (fig. 8). The differences in RH at each station could stem from the same problem as the temperature, that small variations were not picked up by the grid resolution. Having higher resolution might have helped to include more small-scale processes, but would have had higher computational cost (Warner, 2010). Many small scale atmospheric processes need parameterization and they are still difficult to reproduce accurately with a model. The shape of the time series for both temperature and RH (fig. 9) were smoother for the MEPS model. This indicated that the AWSes picked up smaller variations at the surface which could have increased the differences between the model and observations.

The meteorological ground observations at each station (section 4.4) was compared with the forecasted front and the anticipated start time for the precipitation at the different stations. At Ågotnes the front and precipitation was anticipated to reach the coast around 10 UTC which corresponded well to when rain and sampling started at this station. The sampling was thought to start at a similar time in Bergen, but there was some delay and the first sample was collected after 11 UTC. All stations had anticipated precipitation at 12 UTC, but for Voss there was already light precipitation from around 9 UTC. At 8 UTC (fig. 8b) the stratiform clouds were visible above Voss and the cloud front must have reached Voss earlier than first anticipated. There was a lower cloud formation positioned between Voss and Finse at 10 UTC (fig. 8c) which could have been caused by adiabatic lifting because of increasing topography. This could indicate some orographic precipitation at Voss. For Finse, some small patches of accumulated precipitation were visible at 10 UTC (fig. ??) which became more prominent at 12 UTC (fig. 7c). From the observations there was snow from the early morning and sampling began at 07:30 UTC. However, there was a lot of wind at Finse, which the MEPS model did not capture at the same magnitude. The wind could have contributed to more turbulence and movement of snow locally at this station, giving the illusion of snowfall.

The front was assumed to be a warm front. The arrival of the front brought stable temperatures which were indicated by the isotherms. Prior to the front, irregular isotherms of increasing and decreasing temperatures could be seen in figure 8. This could be explained by adiabatic expansion and cooling of

air masses when they rose over mountains, and the subsequent warming from adiabatic compression when air masses descent on the leeway side (Stern and Blisniuk, 2002). The warm front assumption was also reinforced by the cloud shape, which consisted of high clouds in the beginning, which grew to deep clouds and resembled a stratiform type cloud.

5.2 Role of daily precipitation

The average $\delta^{18}\text{O}$ values in precipitation indicated some seasonality, with higher averages in the summer and lower in the winter. The box plots (fig. 10b) had an indication of a higher medians in summer. The range between the higher and lower $\delta^{18}\text{O}$ was also lower in the summer months, while the precipitation (fig. 10a) had larger ranges. One uncertainty with the box plot is that the median is not equivalent to the average, it only tells of the distribution. The higher values in summer would mostly be explained by the temperature effect, where increasing temperatures in summer lead to increasing $\delta^{18}\text{O}$ values (Dansgaard, 1964). The winter months had lower δ values, and December had snow. The snow measurements consisted of samples for isotope analysis and not for accumulated snowfall. The snow measurements were the lowest recorded $\delta^{18}\text{O}$ values, indicated by the minimum whisker in December (fig. 10b).

To put the field work in this thesis into a context of the weather prior to the field work, I investigated the month on November 2022 in more detail. During November 2022, there was a long period of dry weather prior to the field work. Between the 14/11/22 and 25/11/22 there was one sample, which was collected during a small precipitation event on the 25th prior to the field work on the 27th. The average value during this period was -4.8‰ , while the average during the fieldwork at Bergen was -9.6‰ . The next sample, on the 29th of November had similar depleted value of -9.1‰ . The small rain event on the 25th could have contributed to a more saturated atmosphere, but since there was no rain on the 26th and the RH in the morning of the 27th was low, it was unclear how the prior conditions could have affected the isotopic signals in this precipitation event, and if the dry period had an effect.

The isotopic signals during the precipitation event on the 27th compared to seasonality indicated that this event was more depleted than the monthly average. The median in Bergen in October and November was -6.5‰ and -6.4‰ , while the average was -6.4‰ for both months. There was a noticeable shift in December with the arrival of snow, the median sank to -10.6‰ and the average $\delta^{18}\text{O}$ was -11.8‰ . The day to day variability, especially if there was little precipitation, seemed to have little information on the isotopic variation. Even within the short precipitation event sampled in this thesis there was high variability which was not represented in the daily measurements. The seasonal variations were also less prominent compared to other mid-latitude stations (Dansgaard, 1964; Gat, 1996). The most prominent change and indication of seasonality came from the snow measurements in December, which would not have been affected by below-cloud evaporation (Jouzel and Merlivat, 1984).

5.3 The evolution of the isotopic in precipitation

Several studies (Weng et al., 2021; Aemisegger et al., 2015; Gedzelman and Lawrence, 1990; Dansgaard, 1964) have conducted research on the temporal patterns of water isotopes in precipitation. A recent study by Weng et al. (2021) described a “W” pattern in their high-frequency precipitation measurements during an AR-event in Bergen. They looked at the different stages in the precipitation event, which corresponded to different isotopic values in the precipitation. During stage 1, in the beginning of the precipitation event, the δ values were higher before they entered stage 2 and became

more depleted because of the weakened below-cloud processes which was present at stage 1. At stage 3 there was an increase in δ values because of moisture gained from developing deep clouds. When the deep cloud passed, stage 4 entered and local convective showers influenced the final δ values of precipitation. Since the precipitation event sampled in this thesis was not an AR event, the intensities of precipitation are not at the same magnitude. Nevertheless, an AR-event is a strong warm front and the different stages defined by Weng et al. (2021) are a good base for discussing the evolution of $\delta^{18}\text{O}$ in time and at each stations.

5.3.1 Patterns and evolution of isotopic signals at Ågotnes

Starting by looking at Ågotnes, from the pattern of the isotopic values it seemed like this station followed a similar "W" pattern (fig. 11) as Weng et al. (2021) found. However, when looking closer it was revealed that the stages they defined were not suitable to explain the isotopic composition for this precipitation event. In the beginning there were less depleted values mirroring stage 1, and the increase in depletion as more precipitation occurred mirrored stage 2. The break at around 13 UTC made the sample collected at 13:15 UTC less depleted compared to the previous samples. This differs from precipitation event in Weng et al. (2021) where they had increased precipitation from deep clouds which increased the δ values. When the precipitation break ended the first rain would have experienced below-cloud evaporation which increased the $\delta^{18}\text{O}$ value of the sample.

The connection between rain intensity and isotopic composition of precipitation can be explained by when a raindrop falls through unsaturated air, evaporation would cause the lighter isotopes to re-evaporate leaving the heavier isotopes in the droplets causing less depleted values. The rain drop will become enriched compared to the surrounding vapor. When the rainfall is more intense, the air will become more saturated and the lessen exchange between the droplet and the surrounding air (Graf et al., 2019). The decrease in $\delta^{18}\text{O}$ could also be explained by the Rayleigh distillation model, where the heavies isotopes condense and rain out. This makes the remaining vapor and subsequent cloud condensate more depleted.

There were no RH measurements from this station, so there was no clear indication of how saturated the air was at the surface. There was evidence that some below-cloud evaporation occurred because of d-excess. Equilibrium processes do not alter the the d-excess (Dansgaard, 1964). Ågotnes had a negative d-excess initially, which gradually increased throughout the day (blue lines, fig. 22). The increase could be caused by less below-cloud alterations when the rain drop left the cloud base. However, the arrival of dry air at around 15 UTC do not support this assumption. At 15 UTC, dry air arrived at this station, indicated by the drop in IWV (fig. 16) and water vapor contours (fig.17b). Some rain fell around 16 UTC, and the final sample showed an increase compared to the previous samples. Because of the arrival of new dry air, the mixing of air masses can also be a reason for the altered d-excess. Mixing of air masses, with different isotopic signals will further deplete or increase the δ values which is dependent on the isotopic composition of the arriving air.

Without additional measurements at this station, like AWS or vapor measurements, it was difficult to make clear conclusions and quantification on the below-cloud processes at Ågotnes. With measurements of RH, the saturation of the atmosphere could be better understood to see how much evaporation could have affected the rain drops. Vapor measurements could quantify the evaporate from the difference between the rain drops and the vapor. The vapor would have enrichment of HDO and positive d-excess compared to the rain drops. From the measurements, the clearest result was the connection between light rain and less depleted values. The $\delta^{18}\text{O}$ values became more depleted with time as rain intensity increased and rain-out of heavier isotopes which increasingly depleted the remaining vapor in the clouds.

5.3.2 Patterns and evolution of isotopic signals in Bergen

Comparing the Weng et al. (2021) AR-event in Bergen to a non AR-event in Bergen showed little similarities. In the beginning there were higher $\delta^{18}\text{O}$ values which could be explained by below-cloud effects and atmospheric conditions prior to the rain, mirroring stage 1 from Weng et al. (2021). The RH measurements indicated an increase in RH connected to the increasing rain. This could mark the beginning of stage 2, where more rain and more depleted values of $\delta^{18}\text{O}$ could be explained by the rain-out effect. The isotopic pattern in Bergen showed similarities to Ågotnes with the same pattern of precipitation. The two precipitation rate peaks were present at both stations. This precipitation break was shorter than the one at Ågotnes, and there was a light amount of rain which contributed to the sample collected at 13:41 UTC which did not show a significant increase of the $\delta^{18}\text{O}$ compared to the previous sample. The following sample, on the other hand showed a significant drop connected to the intensification of the rain.

The second precipitation event which include the minimum values of -12.5 ‰ at 15:01 UTC could be explained by rain intensity and the rain-out effect. When the rain stopped around 16 UTC, the last sample collected at 16:29 showed an increase which was likely caused by below-cloud evaporation of the droplets when it stopped raining. The dry air masses were visible in the water vapor (fig.17) and IWV (orange line, fig. 16) which approached Bergen around 16 UTC. The dry air masses could have amplified below-cloud evaporation of the last samples. The RH increased in the afternoon, this could indicate that the dryer air masses was situated higher in the atmosphere and did not affect the surface humidity to the same degree.

The pattern in Bergen did not mirror the clear increase which was visible in the precipitation break at Ågotnes. One explanation could be that the rain at this station, independent of rain intensity, experience some below-cloud exchange. Bergen had the least amount of precipitation of all the stations, so it is not unreasonable to assume that below-cloud processes affected the more intense rain too. This could additionally be supported by the d-excess measurements. The d-excess indicated that significant evaporation of HDO occurred, because of the negative values. Bergen had a negative d-excess throughout the whole field work (yellow line, fig. 22). The highest d-excess values were at the same time the precipitation was most intense, so there could be a connection between the light rain and negative d-excess.

To further understand the atmospheric influences on the $\delta^{18}\text{O}$ and d-excess, the cross section in (fig.21d) was investigated over Bergen. At 17 UTC, according to the MEPS model, there was no generation of rain in the atmosphere above Ågotnes or Bergen. There was some cloud condensate, and some water vapor which could be seen in the water vapor cross section at 16 and 19 UTC (fig.17b and 17c). This indicated some water vapor was still present in the air. The presence of cloud condensate without rain, made the Rayleigh distillation model assumption of immediate removal of condensate wrong. Which highlights that the Rayleigh model, by fault of its own simplification, is flawed for an open system. If the cloud condensate would immediately be removed from the system, there would be no clouds.

Another explanation for the high d-excess, especially compared to the d-excess at Ågotnes could be an error. The error could stem from a sampling error which could have caused evaporation after a sample was taken, for example improper storing before the analysis. The caps of the vials, if not closed properly, can leak. The sample vials were stored under room temperature and if the caps were not properly sealed, some evaporation could have occurred.

5.3.3 Patterns and evolution of isotopic signals at Voss

The $\delta^{18}\text{O}$ values at Voss decreased gently compared to Ågotnes and Bergen (fig.13b). According to the precipitation measurements, Voss experienced the most amount of rain through out the day, and most fell after 16 UTC. There was an increase in RH and drop in temperature likely caused by the precipitation. The gentle decrease of $\delta^{18}\text{O}$ could be attributed to below-cloud effects continuously re-evaporating parts of the precipitation and causing less depleted values. The RH values at Voss were low between 8 and 14 UTC which could indicate that the air was unsaturated during this period. The peak in RH at 13 UTC seemed to be connected to some increase in precipitation, but this was not visible in the isotope signals at this time. In unsaturated air, there would be a net transfer of water molecules from the rain drops to the surrounding vapor. Lower RH leads to non-equilibrium fractionation, because of the the slower diffusion of H_2^{18}O compared to HDO. The d-excess is sensitive to non-equilibrium conditions (Graf et al., 2019). The d-excess at Voss (green lines, fig.22) followed a similar path as Bergen with negative d-excess. This could be explained by the light rain and below-cloud processes which would alter the d-excess. When the rain intensity increased, and below-cloud effects became weaker because of less exchange between the drops and the unsaturated air. The d-excess increased and the final two samples had a positive d-excess.

The stages defined by (Weng et al., 2021) had less footing for the precipitation event at Voss. The altering intensities of light precipitation corresponded to altering $\delta^{18}\text{O}$ values, and there were a lot of precipitation breaks. In the afternoon, from 16:30 UTC, the rain intensity increased and more depleted values occurred for the last samples. There could have been less exchange between the rain drops and the surrounding atmosphere and according to the high surface RH the atmosphere could have been more saturated. The most depleted values occurred when the rain intensity was the most intense, and reached a maximum precipitation amount of 5.1 mmh^{-1} .

The MEPS model failed to forecast the intense rainfall at Voss around 17 UTC, so the below-cloud processes at 17 UTC were difficult to interpret with the MEPS model. Figure 21d showed almost no instantaneous rain above Voss at 17 UTC, but there was some snow generation in the atmosphere. Throughout the duration of the field work, there was an amount of instantaneous snow between Voss and Finse. This could have contributed to the precipitation at Voss, by melting on the way down. There was also an increased amount of water vapor between Voss and Finse, which was visible in the filled contours at all times (fig.17).

Another scenario could be that the air parcels in the front, visible above Ågotnes and Bergen at 10 UTC, reached Voss around 17 UTC. This is in contrast to what the IWV showed (green line, fig.16), but since the MEPS model already failed to capture the precipitation at Voss, other explanations could be possible. The potential adiabatic ascent of the air parcels could have caused the increased amount of orographic rainfall at Voss before the front moved further east. The amount of vapor and snow could be the product of adiabatic lifting caused by topography. There was a small amount of cloud condensate which supports the adiabatic lifting, cooling and condensation of vapor and subsequently creating on ice particles, or super cooled droplets. Super cooled droplets can exist in cloud down to $-15 \text{ }^\circ\text{C}$ (Jouzel, 1986) and has event been observed at temperatures down to $-35 \text{ }^\circ\text{C}$ (Sherwood et al., 2010).

It needs to be noted that there was an error connected to the rain sampling at this station, so there was missing rain rate data between 10 UTC and 12 UTC. There were still precipitation samples taken during this time. From the meteorological ground observations in section 4.4 the light rain persisted throughout this period.

5.3.4 Patterns and evolution of isotopic signals at Finse

The wind conditions at Finse were strong, with the highest measured wind at 20.7 m/s at 14 UTC. In the beginning the first samples consisted of snow that was blown into the sampling box. There were small pieces of dead grass present which lead to the conclusion that most of the snowfall was blown up from the ground. The first two samples had a long duration because of this since the snow would also continuously blow out of the box. It was difficult to interpret the relationship between depleted $\delta^{18}\text{O}$ signals and precipitation amount because of the uncertainties connected to snowfall measurements. The accumulated snowfall measurements calculated from the sticks located around collection box gave an overall estimation of the accumulated snowfall amount. From this, the average of the snowfall rate was calculated throughout the day under the assumption that snowfall was constant, which from the ground observations and MEPS model was proved to be wrong.

The snow samples collected after 12 UTC were more depleted compared to the first two samples. This could be the product of longer sampling intervals which missed the larger variations picked up by higher frequency samples, or that the increase in snowfall would lead to less contamination from wind blown ground snow. Later, the sampling frequency switched from every approximately every 30 minutes down to approximately every 15 minutes due to the increase in snow intensity.

Looking at the MEPS model for snowfall, it started snowing more after 12 UTC, which corresponded to the meteorological ground observations. The increased snowfall could be explained by moister air masses arriving, which was visible from the IWV (red line, fig.16). After the peak at 13 UTC, the IWV amount persisted throughout the day without major change. The MEPS model's snowfall rate could explain some changes when accompanied by the IWV. However, in the afternoon, when the snowfall increased, there were no notable changes in IWV. A small decreasing trend in IWV was visible around 19 UTC, while the snowfall increased.

Between 12 UTC and 14 UTC there was a "U" shape made up from 4 samples. One explanation for the altering $\delta^{18}\text{O}$ values could be explained by the high wind conditions. Wind could still blow snow from the ground into the box and mixing with the snow sample. Connecting high wind with decreasing snowfall around 14 UTC, could indicate the two samples making up the latter two samples of the "U" were contaminated by snow from the ground. This mixing between snow from the air and ground could lead to the less depleted $\delta^{18}\text{O}$ values. The wind decreased in the afternoon and the isotopic values taken between 15 UTC and to the end of the sampling period at 19:30 UTC still showed varying $\delta^{18}\text{O}$ values.

The saturation mixing ratio at Finse (red line, fig.19) increased at 13 UTC, the same time as IWV peaked. The arrival of new air masses around 13 UTC could therefore have altered the isotopic signals. Looking at the forecasted accumulated precipitation at 14 UTC there was spots coming from the south-east (fig.7d). This could indicate other air masses from the south or east arriving. The direction of the wind was mostly from south, with some indication of south-eastern winds. The winds were persistent throughout the day, and could have transported air masses from the south-eastern part of Norway (fig.7). Air masses could have brought additional moisture and changed the overall composition of the precipitation. The increasing and decreasing values at Finse could therefore be attributed to the mixing of air masses from both west and east. From the IWV (red line, fig.16) there were no increasing values indicating arrival of new air masses, it stayed consistent only decreasing slightly around 19 UTC. The new air masses could have held a similar amount of moisture, but contain a different isotopic composition. This would have altered the isotopic signal in the snow without altering the IWV.

Under the Rayleigh model assumption, snow is formed in isotopic equilibrium with the vapor phase

and immediately removed from the cloud (Dansgaard, 1964). Snowfall is not affected by exchange below the cloud base to the same degree as liquid precipitation. The RH at Finse was high throughout the field work, and the $\delta^{18}\text{O}$ samples were the lowest of all the stations. Solid phases do not exhibit exchange between the snow crystals and the ambient vapor, the snowfall conserves the isotopic signals from the clouds (Gat, 1996).

Jouzel and Merlivat (1984) found that for mixed and polar clouds between 0 °C to -25 °C, if there is coexistence of solid and liquid phases, the water vapor saturation mixing ratio takes a value between the mixing ratios of supersaturation over water and saturation over ice. This explains why droplets tends to evaporate while snow formation can get additional growth from condensation of vapor on the growing ice crystals. Formation of snow is a non-equilibrium process which gives rise to a high d-excess. The high d-excess is connected the kinetic effect during vapor deposition which lead to snow formation inside the clouds (Jouzel and Merlivat, 1984). Finse had a high d-excess with exception of two samples (red line fig.2). The sharp drop and two negative values around 12 UTC were the outliers. From the $\delta^{18}\text{O}$ samples, they were not noticeably different than the other samples. The drop corresponded with the two samples of less depletion in the $\delta^{18}\text{O}$ measurements that made up the latter part of the "U" shape. The $\delta^{18}\text{O}$ values became more increasingly depleted again after this occurrence and the d-excess became positive. This drop in d-excess could be explained by a sampling error, new air masses mixing, or contamination from wind blown snow from the ground. Temperature were around 0 °C, and if there was partial melting of ground snow, the melted snow water could become more enriched before freezing again. If the conditions at Finse allowed for partially melting and re-freezing, the increased values could be a combination of this and new snowfall. Mixing can give d-excess values that are lower than expected for Rayleigh distillation (Galewsky et al., 2016). Therefore, the drop in d-excess further the conclusion that mixing of snow occurred, since there was no notable change in IWV or RH, the mixing was from ground snow.

The sampling procedure of snow was different than the sampling for rain. Snow was collected in small bags and brought inside for melting. The sampling of the snow outdoors could be more dominated by recent snow than earlier snow. When collecting snow from the box, the snow on top could be over-represented in the snow sample compared to snow at the bottom of the box. Stirring and mixing of the snow in the box was done before sampling. However, improper mixing of all the snow inside the box could misrepresent the true isotopic signals. Failing to remove all the leftover snow before starting the next sample could also contaminate the samples with "old" snow.

5.3.5 Impacts of humidity and temperature

The AWS measurements from Bergen, Voss and Finse showed that conditions at Finse and Bergen were stable during the most sampling period. The RH at Bergen increased steadily throughout the day and was between 60 % at the beginning of the sampling period and almost 80% at the end. The temperature in return, decreased a little from 11 °C to 9 °C in the afternoon. After 11 UTC there was little change in both temperature and RH in Bergen, the only notable increases in temperature and decreases in RH was during the precipitation breaks. This made sense since precipitation has a cooling effect on the atmosphere (Wallace and Hobbs, 2006). At Finse the RH was almost around 90% during the whole fieldwork and the temperature was around 0 °C. The temperature could have affected the snow by melting, but during the sampling there were no noticeable sleet, and the snow was not noticeably wet. At Voss there were more irregularities, the RH increased towards the afternoon which was connected to the increase in precipitation, this was also represented in the temperature change which was anti-correlated to the RH. The temperature decrease could therefore be the product of increasing RH, higher precipitation rates and also the shorter diurnal cycle in

November. The temperature and RH measurements could help the reasoning of the extent of the below-cloud processes at the different stations. The below-cloud evaporation is affected by humidity and temperature which determines how saturated the air is. Drier air leads to more evaporation of falling droplets. Bergen experienced lower humidity compared to Voss and Finse, laying below 80 % throughout the sampling time. This could mean that even during the more intense rainfall, because of little humidity fluctuations, the below-cloud evaporation could still influence the final isotopic composition in precipitation.

5.4 Processes expanding on the evolution of isotopic signals within the front

The variations and evolution of the precipitation events at the individual stations could also be studied and compared together and reveal the spatial distribution of the isotope signals in a passing front. The different processes altering the isotopic signals in the atmosphere became more visible when investigating the changes from station to station.

5.4.1 Amplitudes of the variations of the isotopic composition

The variability in isotopic composition at each station showed the extent of the depletion. In the beginning there were less depleted $\delta^{18}\text{O}$ values, and with increasing rain and RH depletion increased. The interpretation of variability could be based on the increase in rain-out, the below-cloud effects or as for Coplen et al. (2008) the changing of cloud height.

Weng et al. (2021) had a variability of δD_v of 85 ‰ for vapor, but mentioned that the variability for δD in precipitation was similar. The shape of the isotopic evolution of $\delta^{18}\text{O}$ was similar to that of δD so using the linear relationship $\delta D = 8 \cdot \delta^{18}\text{O}$ gave a variation of $\delta^{18}\text{O}$ 10.6 ‰ from Weng et al. (2021).

During this field work, the variability in Ågotnes was 9.5 ‰. In Bergen it was 10.2 ‰, which was similar to the findings by Weng et al. (2021). The amplitude variation at Voss was 10.9 ‰ and at Finse the variation was 12 ‰. The variations in $\delta^{18}\text{O}$ increased going eastward, and similarly for the d-excess (table 9). Following the MEPS model, between Bergen and Finse there was an increasing amount of accumulated precipitation which mean the the increasing rain-out between the stations could have attributed to the increasing variability. High levels of below-cloud evaporation and lower RH prior to the field work could have worked together with the increasing rainfall to make the variability larger. Low RH would increase the amount of below-cloud evaporation making the $\delta^{18}\text{O}$ values less depleted. The decrease in variability and the similarities between Weng et al. (2021) and the variation at Bergen could be explained by local conditions or seasonality. More investigation on the changing variabilities are needed to make a clear conclusion. This might have been a coincidence, but there could also connection for the increasing variability with the below-cloud effects, rain-out, seasonality, increasing altitude or the local climate.

5.4.2 Precipitation weighted mean and precipitation intensity

The precipitation weighted means of $\delta^{18}\text{O}$ gave an insight on the evolution from station to station which was not visible wit the unweighted means. The mean values of the $\delta^{18}\text{O}$ at each station showed that Voss had a higher average than Ågotnes and Bergen, even though this station laid further away from the coast and further east in the trajectory of the front. Bergen and Ågotnes had similar averages, but Bergen had a higher average than Ågotnes. Finse had the lowest average, which is explained by the snow and the high altitude.

The gradual decrease eastward visible from the precipitation weighted mean of $\delta^{18}\text{O}$ showed the extent of rain-out effect over the west coast of Norway. The weighted averaged compared to the averages showed the connection between higher rain rates and lower isotopic signals. By diminishing the stations down to one value, the evolution through a Rayleigh framework was easier applicable.

Comparing the hourly average of the observed precipitation rates (red bars, fig.15) with the instantaneous rain rates (fig.11 for Ågotnes, fig.12b for Bergen and fig.13b for Voss) revealed that the hourly averaged smoothed out the variations. The precipitation break that was visible at Ågotnes and Bergen was not covered by the hourly averages which only produced lower averages for 12 UTC. Comparing the $\delta^{18}\text{O}$ values with the hourly averaged precipitation rate (not shown) failed to reproduce the connection between the isotopic signals and the increasing and decreasing rainfall on a scales $< 1\text{h}$. This indicated that the $\delta^{18}\text{O}$ was affected by changes on a small scale and the hourly averages are too large to capture all the fluctuations.

One of the limitations with the MEPS forecast was visible from the rainfall rates. The precipitation intensity and distribution by the MEPS model fit for Ågotnes and Bergen. The two peaks were represented in the hourly forecasts, although more diffuse. For Ågotnes, the only difference from the observations were that rain appeared earlier than forecasted, and that the hourly averaged observations were lower than the forecasted. For Bergen, the differences was firstly, the start and end times of the precipitation which was too early forecasted in the MEPS model compared to when it actually started to rain. Secondly, the amount of rain was higher in the observations than in the forecast. The model, most notably, failed to forecast the rainfall at Voss around 17 UTC, even though the accumulated amount of rainfall between the measurements and model were similar, the timing and intensity of the precipitation events were unsatisfactory. The meteorological observations noted an increase in snowfall in the afternoon, which coincided with increased snowfall forecasted by the MEPS model. However, since the snowfall rate measurements have high uncertainties and there was only one measurement of snowfall rate, it was not reliable to compare the model with the observation.

The IDF curves are used to forecast intense precipitation and predict the frequency, duration and intensity of future precipitation (Sun et al., 2019). Lack of high frequency data over longer period makes forecasting of IDF curves for large parts of Norway uncertain (Dyrrdal, 2021). IDF curves are used in urban planning and it is therefore a demand for statistics on rainfall. Throughout this thesis, there was tracking of isotopic signals in an incoming front, and there were measurements of rain. The uncertainties connected to moisture source determination and only tracking precipitation during one day leaves the influences isotope signals could have on IDF curves beyond the scope of this thesis. According to the IWV, around 40 % of the moisture left the front passage between Ågotnes and Finse, and this could be incorporated in tracking the moisture, but it hold no information on the rain intensity. Between Voss and Finse, the largest amount of moisture was lost, going from 77 % over Voss to 60% remaining moisture over Finse. This is not accounting for new moisture potentially entering the system from south or south east. Using the IWV could tell the amount of potential precipitation over an area even when the full amount from the source region is unknown. Since there was a way to track the remaining amount compared to Ågotnes, it was possible to look at the evolution between each station. More research would need to be conducted with measurements over longer times to fully grasp the potential connections. More measurements of precipitation is needed, and if these are verifiable with the IWV, the IWV could be used to track moisture and precipitation which could be used for IDF curves.

5.4.3 Altitude effect

Going from Ågotnes and eastward to Finse, the surface elevation increases to about 1220 m.a.s.l (Finse). The altitude effect of decreasing $\delta^{18}\text{O}$ values that Stern and Blisniuk (2002) and Smith and Evans (2007) discovered in the Andes could explain the gradual decrease from station to station given by the precipitation weighted mean of $\delta^{18}\text{O}$. Between Bergen and Voss there are mountains even though the altitudes are similar (measurements taken at 47 m.a.s.l in Bergen and at 64 m.a.s.l in Voss). An air parcel would experience adiabatic lifting, expansion and cooling between these stations, which was not picked up by my measurements. The orographic rain could have caused the loss of water vapor in the atmosphere. This was visible from the IWV (fig.16) decreasing eastward. The time offset between the maximum values of IWV for each station showed that the moisture which arrived at Voss around 10 UTC had significantly less moisture than Bergen. This indicated that moisture was lost between these station most possibly to rain-out caused by orographic precipitation. Finse is positioned at the one of the highest point in the mountain range that splits east and west Norway. The $\delta^{18}\text{O}$ was the lowest and the IWV was the lowest of all the stations. These low values could mean that moisture traveling from Voss experienced rain-out caused by adiabatic lifting of the air masses.

Finse is located at the top of the mountain and was the station furthest east. There were no leeway side measurements of isotopic composition. Stern and Blisniuk (2002) noted no altitude change in the δ values in the Andes and explained it by the restricted moisture sources in the area. The map of the front at 14 UTC (fig. 7d) indicated patches of moisture which originated from east of the mountain as well as the west. The possibility of other moisture sources limits the assumptions about the $\delta^{18}\text{O}$ values on the leeway side of this front.

The orographic effects lifting the air masses could have caused the increased rainfall at Voss. This would have further depleted the air masses that eventually reached Finse. The orographic precipitation seemed more influential at Voss than in Bergen, which could have been attributed to the height of the cloud base and where precipitation was formed. The cloud base height was lower over Voss towards the afternoon.

5.4.4 Cloud shape and evolution

Stratiform and convective cloud give different isotopic signals. Cloud structures could also give insight in possible processes that occurred. During two storms, Gedzelman and Lawrence (1990) found similar patterns that were consistent for both. The local and temporary increases in cloud thickness was often accompanied by decreasing isotope signal. Convective clouds showed less depletion, while stratiform clouds had isotope ratios determined by the vertical profile of the vertical velocity of cloud (Gedzelman and Lawrence, 1982). To some extent the isotopic ratio was directly determined by the cloud top height (Gedzelman and Lawrence, 1990). However, without any direct measurements from the cloud conditions, the type of clouds were difficult to verify since the only determination of cloud structures were from the MEPS model. The MEPS model offered an alternative solution to look at the cloud fraction and evolution of the clouds and cloud base. This is not without fault, and there are uncertainties connected to modelling clouds, and one uncertainty noted by Müller et al. (2017) was the frequency bias of low clouds bases and the second highest cloud class (1500-4000m heights) which under-predicted low clouds. Throughout the field work, the cloud base remained low after precipitation started both for the deep and shallow clouds present at the different stations (fig. 8). The low cloud base was prominent over Finse, with heights < 100 m, according to the MEPS model. Towards the end of the field work, the clouds became shallow over Ågotnes and Bergen along with visible higher clouds in the MEPS model. This corresponded to the

end of precipitation and arrival of new dry air masses indicated by the IWV. This was also noticed by the low cloud fraction.

The evolution of cloud and subsequent change in isotopic signal in precipitation was investigated by Coplen et al. (2008). They noted an increased depletion when the cloud changed from high to low clouds during warm front with a stratiform cloud shape. During this field work, the MEPS model forecast had stratiform shaped clouds (fig.8) at the beginning of the precipitation event. After 10 UTC the clouds had a low base over Ågotnes and Bergen, resembling more convective type structures. The stratiform pattern reached Voss around 12 UTC. The change from high and mid cloud to low cloud between 6 and 10 UTC where accompanied by light rain according to the MEPS model (fig. 15). From 10 to 12 UTC the precipitation increased and the cloud became deeper and thicker over Ågotnes and Bergen. The cloud optics on Voss were more uncertain, it looked like there were one higher and deeper cloud approaching while a more stratiform-shaped cloud was situated below. The clouds seemed to merge and become thick and opaque around 14 UTC over Voss and Finse. At 16 UTC the cloud base height increased at Voss. The deep, convective type cloud had moved further east and was visible over Voss and Finse.

The increased drop in δ values that Coplen et al. (2008) experienced from deepening of clouds could be an explanation for the increased depletion in $\delta^{18}\text{O}$ observed at the different stations. However, the increased drop in $\delta^{18}\text{O}$ values at the different stations seemed more connected to the rainfall intensity and below-cloud processes. Differences could come from the different intensity of the Coplen et al. (2008) event, which was an AR event. An AR-event has significantly more moisture and intense rainfall. The cloud optics presented by the MEPS model showed changing cloud thicknesses and areas of lower cloud fraction.

Another way to determine if the change in cloud type and cloud base height had an impact, was to investigate where in the cloud the rain was generated. Precipitation could be formed in convective type clouds at higher altitudes with high depletion (fig. 3). The droplet would then travel through the cloud and the isotopic composition would change through coalescence and collisions with other droplets (Gedzelman and Lawrence, 1990). This would alter the composition even before the drop left the cloud base. The instantaneous rain (fig. 21) indicated that rain generation only occurred close to the cloud base. Snow generation would not have the same mixing processes as liquid precipitation, and the isotopic signals would not change. There could have been super cooled droplets in the clouds. Microphysical modifications in the MEPS model are needed on supercooled liquid in clouds (Müller et al., 2017), and could therefore provide uncertainties connected to the in-cloud snow or rain amount.

Therefore, due to lack of observations in the clouds, it is difficult to confirm if the drop in $\delta^{18}\text{O}$ was connected to changing cloud heights or thickening to more convective structured clouds. This conclusion is similar to the conclusions made by Yoshimura et al. (2010) which attributed the changes in isotopic signals to the below-cloud processes. The absence of extreme weather, which is the case in many of the studies, made the conclusions around cloud cover and isotopic signals inconclusive. More studies are needed, with addition of satellite or weather balloon measurements, to get a clearer picture of cloud structures and the isotope signals during an event like this.

5.5 Rayleigh model

Stern and Blisniuk (2002) used the Rayleigh model in comparison with observations of isotopic signals in orographic precipitation. The increasing altitude correlated with more depletion of $\delta^{18}\text{O}$, although they also mentioned some flaws with this framework. Some of the flaws were that the

Rayleigh model fails to include influences by mixing of air masses, or cloud water vapor exchange, or below-cloud effects, or radiative cooling or heating. Nevertheless, their model results still fit with the observations. The Rayleigh framework seems more suitable for convective events on a small scale (Yoshimura et al., 2010) and adiabatic lifting (Stern and Blisniuk, 2002) where there is one moisture source and the orographic lifting dominates. With the field observations, using the precipitation weighted means, minimized the potential influence from the below-cloud processes when using one representative value for each station. The Rayleigh model was then able to explain the gradual decrease of $\delta^{18}\text{O}$ values from station to station going east.

The Rayleigh curve was chosen at 5 °C based on the position of the instantaneous rain close to the cloud base (fig. 21). The instantaneous rain was used to determine rain generation from the newly formed condensate from the Rayleigh distillation. One assumption behind this was that the condensation process was from vapor to liquid only, and not including possible vapor to solid. Super cooled droplets could exist in clouds down to temperatures of -15 °C (Jouzel, 1986) or even down to -35 °C (Sherwood et al., 2010). Under this assumption, most instantaneous precipitation was formed under the -15 °C isotherm according to figure 21. Calculating the Rayleigh curve at 5 °C for all the stations undermines the different condensation temperatures which would be present at the different station, and how the condensation temperature changes in time. In reality, the condensation temperature was not constant, which is not accounted for in these results. The Rayleigh model is a distillation model, and the distillation controls the role of the condensation temperature.

Several studies have described the flaws around the use of the Rayleigh distillation model (Weng et al., 2021; Yoshimura et al., 2010; Stern and Blisniuk, 2002). The Rayleigh model failed to reproduce the isotopic composition in precipitation in many cases due to the simplifications. Weng et al. (2021) concluded that rain generated at different heights would each need individual Rayleigh processes, and introduced the "Rayleigh Stack". The Rayleigh stack looks at a stack of air parcels, which each has their own Rayleigh model to better represent the fractionation processes in stratiform clouds. Yoshimura et al. (2010) noted a flaw with their simulation from assumption that the immediate removal of condensate fell to the ground as precipitation. This was one of the key assumptions for the Rayleigh model according to Dansgaard (1964), but in reality the condensed water could remain in the air as clouds, water or ice (Yoshimura et al., 2010). There was visible cloud condensate at 17 UTC (green contours, fig. 21d) when there was no noted rainfall above Ågotnes and Bergen. The immediate removal of clouds condensate would also indicate that clouds would disappear as soon as they are created, which is not the case in nature.

The lack of snowfall measurements were an uncertainty for the precipitation weighted average at Finse. The true snowfall rate could alter the position and overall fit on the Rayleigh curve. The MEPS model forecasted 18.1 mm of accumulated snowfall which was around 1/3 of what the snowfall observations were at 60mm. Gat (1996) also noted that the removal of snow from an air mass which is not in isotopic equilibrium does not satisfy the Rayleigh process. Since there was no measurements of ambient vapor to confirm the conditions during the snow removal, there are more uncertainties connected to the Rayleigh framework for snow.

Both the weighted averaged of IWV and saturation mixing ratio fit on the Rayleigh curve, but there were some deviations from the curves, which were different for the two frameworks. For future work, it could be useful to include more stations to potentially get a clearer pattern. The inclusion of both frameworks help comparison and determine possible uncertainties connected to the Rayleigh framework. The condensation temperature of 5 °C fit for both stations, and therefore this temperature proved to be satisfactory. The difference became more visible when looking at the potential conditions in the source region. The saturation mixing ratio was better framework than the

IWV when it came down to determine the source region.

5.5.1 IWV perspective

Water vapor has been used as a tracer of atmospheric moisture (Sodemann and Stohl, 2013). The IWV was used as a tool in the MEPS model to look at the water vapor in the atmosphere during this field work. There was a noticeable gradient going west to east both in the cross section and time series (fig.16 and fig.17a). An explanation for this was the incoming front providing new moist air to the system, and the decrease was the rain-out processes. The noticeable offset in the peak values indicated when the front reached the different stations at different times, which was most noticeable at Finse and Voss. Using the IWV in an isotope perspective gave an indication in where the moisture was in the atmosphere, but gave no direct insight on the isotopic signals.

Most IWV was located inside the clouds, close to the cloud base. The peak value of IWV (22.1 kgm^{-2}) during this field work was at 8 UTC, and this became the reference point for the Rayleigh processes along with the same value as the source region condition, $\text{IWV} = \text{IWV}_0$. In this assumption lied the notion that the full amount of water vapor from the source region was still in the air masses, and that there was no prior rain-out or addition of new moisture before Ågotnes. This in itself revealed a flaw with this assumption since there was no previous knowledge of the rain-out history. The IWV in the source region was most likely be different than 22.1 kgm^{-2} which would alter the Rayleigh curve and the curve might potentially have fit closer to the values for Bergen and Voss. Additional moisture and mixing of air masses after evaporate left the source region was also an uncertainty, which was difficult to verify without measurements.

The weighted mean of the IWV followed the similar decreasing trend from east to west and the decision to use the IWV as a reference on the Rayleigh model allowed the reservoir to be defined by the IWV. The overall fit between the Rayleigh curve and the weighted averages for each station was good, with Finse and Ågotnes having a good fit while Bergen and Voss was below the curve but following a similar curve shape (fig.18). The deviations from the curve could stem from additional depletion caused by mixing of air parcels. Orographic ascend could have altered the composition (Smith and Evans, 2007; Stern and Blisniuk, 2002) and there could be deviations the precipitation estimates and at what time the rain was most intense for each station. The MEPS model lacked the ability to forecast the intense precipitation event at Voss which could have affected the real IWV amount and the weighted IWV calculations. Uncertainties on the IWV amount and the exact amount water vapor that left the atmosphere after the air mass left Voss would also rise uncertainties connected to the precipitation weighted IWV at Finse.

The field measurements of precipitation was used as weight for the $\delta^{18}\text{O}$, while the IWV used the precipitation rate from the MEPS model. Since there already was a noticeable deviation between the precipitation forecast and observation (fig.15), the two were kept separated to minimize overlapping errors connected to sampling errors and model errors. The "mixing" of errors could warp the final outcome and give false information on what the MEPS model forecasted if the observed precipitation was used as a weight.

5.5.2 Saturation mixing ratio perspective

The Rayleigh curve as a function of the precipitation weighted saturation mixing ratio under the assumption that the initial saturation mixing ratio in the source region was 9 gkg^{-1} , fit well with the observations for Bergen, Voss and Finse. The ability of the simple Rayleigh framework on the

w_s - δ pairs gave satisfying results for Noone (2012), who suggested that parts of the atmospheric hydrologic cycle could be explained by the Rayleigh distillation model.

Ågotnes had higher values and was situated above the Rayleigh curve (fig. 20). Explanations of the deviations could stem from exchange during rain evaporation. This position was an identifier if data fell below the Rayleigh curve, and according to Noone (2012) exhibit super-Rayleigh behavior. Another explanation could be that the saturation mixing ratios at Ågotnes was uncertain. Figure 19 showed that Bergen had higher saturation mixing ratio than Ågotnes. The mixing ratios were calculated at the cloud base height with cloud base temperature and pressure, therefore the low value of Ågotnes could be attributed to uncertainties connected to how moist the MEPS model assumed the air masses was at this height. The MEPS model cloud base height might therefore have caused some problems in the final calculations. If the saturation mixing ratio had been higher at Ågotnes, which is what would have been expected based on the IWV, Ågotnes might also have fit on the Rayleigh curve. Without measurements of cloud base humidity, the saturation mixing ratio at Ågotnes could not be verified.

Voss had uncertainties connected to the precipitation weighted mixing ratio, the SEM was 0.077, the highest for any station. This could be a product of the high variability of the saturation mixing ratio at Voss. During the intense precipitation the saturation mixing ratio decreased. However, since this was from the MEPS model, the decrease in saturation mixing ratio could be explained by the decrease in precipitation according to the model, both saturation mixing ratio and precipitation rate peaked at 12 UTC. The precipitation weighted means for the saturation mixing ratio were weighted on were the precipitation data from the MEPS model, the same as for IWV.

5.6 Locating the moisture source

The assumptions of the saturation mixing ratio in the source region made it possible to estimate the position of the source region. By using the CC-relation under the assumption that the saturation mixing ratio was 9 gkg^{-1} in the source region, the condensation temperature in the source region was calculated to $12.5 \text{ }^\circ\text{C}$. This was calculated under the assumption that there was saturation, i.e. RH = 100% in the source region. Models approximate saturation at RH $\approx 80 \%$, and similar approximations were made here to find the potential source region. This means that the temperature in the source region could vary slightly from $12.5 \text{ }^\circ\text{C}$, and the real temperature could be closer to $15 \text{ }^\circ\text{C}$.

Southern Norway have moisture sources which could shift 15° to 20° depending on if it was an AR-event or not (Sodemann and Stohl, 2013). The largest moisture contribution during the AR event investigated by Sodemann and Stohl (2013) was attributed to moisture originating between 30°N to 50°N . The moisture source of this front, which was a non-AR event, could then be located at higher and more local latitudes from 45°N to 70°N . According to Sodemann and Stohl (2013) around 80 % of the moisture tracked during a non-AR event originated from latitudes between 50 to 70°N .

To investigate the temperature over the North Atlantic Ocean in November, the ERA5 reanalysis for monthly averages was used to investigate the sea surface temperature (fig. 23). The SST over the North Atlantic had temperatures around 12 - $15 \text{ }^\circ\text{C}$ around 50°N . The potential source region could therefore be narrowed down to the red box in figure 23, and this area resonates with the findings from Sodemann and Stohl (2013). Weng et al. (2021) looked at the IWV evolution in the North Atlantic prior to the AR-event, but since the domain of the MEPS model is too small, the IWV evolution was not investigated for this thesis. Investigating the evolution of the water vapor from the same source region would be a topic for further research. The moisture source could be investigated with water vapor tagging.

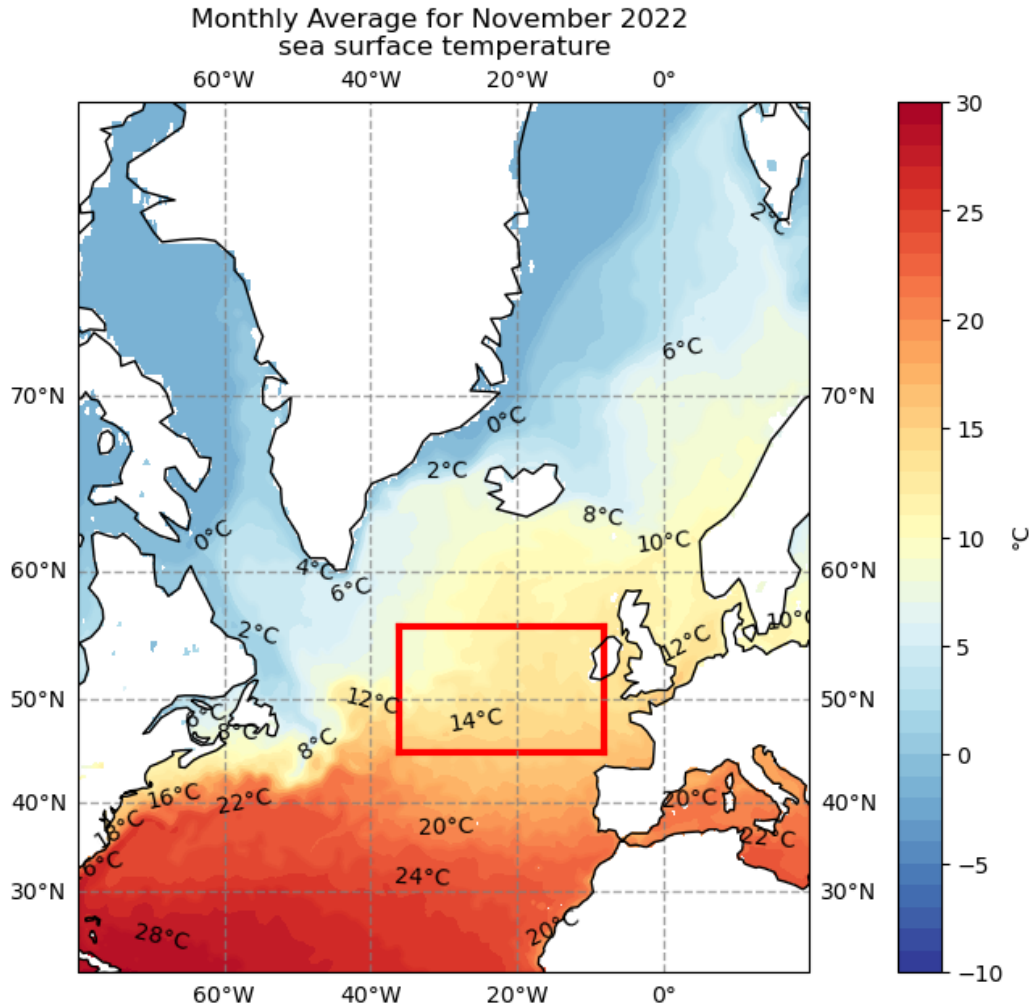


Figure 23: ERA5 reanalysis of monthly mean SST for November 2022 over the North Atlantic Ocean. The red square indicates the potential moisture source region for the precipitation event of the 27/11/22.

The ERA5 reanalysis monthly mean for November provided a tool to narrow down the potential source region but it is not without limitations. Some limitations are the monthly averaging which limits local fluctuations, and only looking at one variable, SST. Nevertheless, with the limited amount of data and measurements from the field work, the combination of measurements, the MEPS and ERA5 models provided a potential source region which was satisfactory.

5.7 What happens when a rain drop leaves the cloud base?

The below-cloud evaporation which affected the falling rain drops have been described as an explanation for the increased isotopic signals early in the field work and during the rain breaks. The d-excess was also notably more negative when precipitation was light and the RH was low. Merlivat (1978)

found that the molecular diffusivity of the heavy isotopes relative to H_2^{16}O was $\frac{HDO}{H_2^{16}O} = 0.9755$ and $\frac{H_2^{18}O}{H_2^{16}O} = 0.9732$. HDO is lighter and thus have a higher molecular diffusivity compared to H_2^{18}O , this makes the HDO molecules evaporates easier from the rain drop, making the raindrop relatively more enriched in $\delta^{18}\text{O}$ compared to δD , while the ambient vapor will be relatively more enriched in δD than $\delta^{18}\text{O}$. With vapor measurements, the confirmation of evaporation would be shown if the vapor d-excess was positive relative to d-excess in precipitation. The evaporation of rain drops is dependent on how saturated the air is, higher RH leads to less evaporation. When the air is dry, the RH gradient between the droplet and surrounding vapor increases, and a larger gradient increases the role of the diffusion rates

Since there was no vapor measurements, one way to determine if there were any below-cloud effects is to look at the correlations between light rain and low d-excess and heavy rain and high depletion of $\delta^{18}\text{O}$ and then compare them with the change of RH throughout the field work. Investigating the correlation between the $\delta^{18}\text{O}$ values and the d-excess in Bergen with the amount of precipitation which fell over Bergen for each sample revealed that the correlation between d-excess was $r = 0.2$ while for $\delta^{18}\text{O}$ $r = 0.07$. This indicated that d-excess could have some connection with the rain intensity, but there was not a clear correlation and no correlation for $\delta^{18}\text{O}$. Calculating the correlation between rainfall amount and d-excess for Voss had a higher correlation of $r = 0.6$ while the correlation between rainfall and $\delta^{18}\text{O}$ was $r = -0.7$. The difference in the correlations between Bergen and Voss could be attribute to the higher RH and more rain at Voss, which could have contributed to the increase in the d-excess (green lines, fig. 22) which became positive in the two last samples. Increased RH would mean higher saturation and less below-cloud evaporation. Although, there were few samples, so the sample size makes it hard to draw a conclusion. More samples and significance testing would be necessary to determine if there is a correlation between the light rain and d-excess, or if the high correlation at Voss was a coincidence.

The negative correlation between rainfall and $\delta^{18}\text{O}$ at Voss could look like the amount effect, where increased depletion of $\delta^{18}\text{O}$ was connected to increase in rainfall. The amount effect is not noticeable during winter at higher latitudes (Dansgaard, 1964), so the high correlation was most likely the product of less below-cloud evaporation and significant depletion from rain-out.

The measurements of d-excess did not show any similarities from station to station, indicating that if the precipitation at the different stations came from the same source region, below-cloud processes and mixing of air masses had altered the final composition. The high difference between each station gave inconclusive results on which to determine the moisture source conditions. A better quantification of below-cloud processes would be needed to determine the d-excess without alteration for more satisfactory results. With the limited amount of data collected during the field work, it is difficult to make any clear conclusions and more data would need to be sampled. Each station had between 10-17 precipitation samples, which is a small sample size to make assumptions about. Along with the lack of additional measurements, most notable vapor, the processes affecting the isotopic signals remain speculative.

Several studies(Graf et al., 2019; Aemisegger et al., 2015; Weng et al., 2021)) have looked at the isotopic composition for precipitation and its difference compared to the isotopic composition of ambient vapor. This was a way to determine the below-cloud processes. Since there were no vapor measurements for this field work, one possibility was to look at the below-cloud effect when it was absent. Graf et al. (2019) showed that precipitation samples from the highest rain rates were least affected by the below-cloud processes. Therefore, precipitation would retain their initial isotopic composition from the clouds better. Weak rain rate and small droplet sizes (Gedzelman and

Lawrence, 1990) reflected more influence from evaporation and the below-cloud processes. There were no measurements that looked at the droplet sizes, fall velocity or the distribution of droplets, the only descriptions of the rain were from the meteorological ground observations. The meteorological ground observations consisted mostly of notes on the "lightness" of the rain. This was not a indicator for the droplet size or fall velocities.

The precipitation samples showed that for Ågotnes, the highest rain rates were recorded at between 11-12 UTC and again around 14 UTC. Similar for Bergen, the highest rain rates peaked at 12 and 14 UTC. Voss recorded the highest rain rate at 17 UTC. The least amount of rainfall, and when the below-cloud processes would have the highest effect was at 10 UTC. 10 UTC was right before or when precipitation started. Looking at 12 , 14 and 17 UTC as representative times for when the below-cloud processes were mostly absent (the cross sections in fig.21) gave some implication on the atmospheric conditions. However, since the MEPS model and the precipitation measurements, especially for Voss, was disagreeing on the rain intensity, the 17 UTC cross section gave little information on the processes other than the absence of any rain or snow generation over Ågotnes and Bergen. This made the cross section at 12 and 14 UTC better representations of the potential atmospheric processes which affected the surface precipitation. The highest rain rates corresponded with some of the lowest $\delta^{18}O$ values at the stations, which could indicate the absence of below-cloud evaporation.

Looking at the $\delta^{18}O$ from Ågotnes, they were more depleted than Bergen which was counter-intuitive from the Rayleigh model perspective. These less depleted values in Bergen could be explained by below-cloud processes still interfering with the isotopic composition in precipitation even during higher rain intensities. The cross section at 10 UTC (fig.21a) showed little difference from 12 and 14 UTC. Any significant quantification on the below-cloud processes was impossible because of lack of observations.

6 Summary and conclusion

The goal of the field work was to collect data and samples to gain a better understanding of the spatial and temporal patterns of heavy water isotopes in precipitation at the west coast of Norway. Field observations of $\delta^{18}\text{O}$, temperature, humidity and rainfall along with the MEPS model created a picture of the different processes that altered the isotopic signals in precipitation. The temporal patterns at the stations did not resemble the "W" pattern found by Weng et al. (2021), but revealed that evaporation of light rain gave less depleted values and increasing rainfall and RH the $\delta^{18}\text{O}$ values resulted in larger depletion. The precipitation weighted averages of $\delta^{18}\text{O}$ had a decreasing trend going eastward. The decreasing isotopic signal from station to station was the product of the rain-out, the decrease of water vapor connected to increase in altitude, and distance from the coast. The source region was narrowed down to a region around 50 °N in the North Atlantic Ocean.

Combining the MEPS model with the Rayleigh distillation model provided the observations with a reference for IWV and saturation mixing ratio. This was an important part since the MEPS model provided information on the moisture amount of the atmosphere. The condensation temperature of 5 °C, which was retrieved from the MEPS model, fit reasonably for both frameworks. There were some deviations from the Rayleigh curve which raised the uncertainties of having few stations.

The different perspectives of IWV and saturation mixing ratio showed the difficulty in determining the source conditions without prior knowledge of the rain-out history. The assumptions that the IWV had experienced no rain-out or additional moisture gain prior to reaching Ågotnes was unlikely, and tracing water vapor needs to be investigated further to determine the source region from the IWV perspective. The initial saturation mixing ratio assumption of 9 gkg⁻¹ was on the other hand a suitable assumption for the source region. From this, the estimated source region had a condensation temperature of 12.5-15 °C. And with the ERA5 Reanalysis monthly average for November the possible source region was narrowed down to around 50 °N, this was in agreement with earlier studies (Sodemann and Stohl, 2013).

The qualitative nature of interpreting the below-cloud effects revealed the difficulties and uncertainties when conducting field work with limited samples. The few samples collected at each station were satisfactory in showing a gradual decrease which fit in the Rayleigh framework, but had a lot of uncertainties. The different uncertainties, which have also been touched upon in this thesis are the below-cloud processes (Graf et al., 2019), the mixing of air masses (Noone, 2012; Weng et al., 2021) and the assumption that condensate left the cloud immediately after it was created (Yoshimura et al., 2010). The Rayleigh model's simplicity gave rise to many uncertainties which is also recognised in several papers. The quantification of the below-cloud processes was difficult without vapor measurements, because it could give an indication of the isotopic signals in the vapor, which could determine the evaporation of HDO and explain the d-excess.

Further investigation on the d-excess for Bergen and Voss showed that, along with RH as a guide for how saturated the air, there was a positive correlation between rain intensity and d-excess. However, the small sample size and difference from the two stations highlights the uncertainties and need more data to further investigating the significance of this relationship. The conclusion which could be drawn from this is that the below-cloud processes became limited down to light rain and low RH indicated more below-cloud evaporation while more intense rain was less affected by below-cloud processes. More measurements need to be taken to properly quantify and understand these processes, most notable the addition of vapor measurements. The limits connected to the below-cloud processes and limited information from the d-excess reduced the chances of confirming the moisture source conditions with the d-excess.

There were challenges connected to field samples and sampling errors could affect the final outcome. Along the way, from field to data the precipitation samples underwent storage before analysis in a lab were problems that might have occurred. The uncertainties connected to sampling errors are always a risk with field measurements. However, without observations from the field, verification and improvements of measuring techniques and models would not be possible. Without observations of clouds and atmospheric processes above the surface, the validation of the MEPS model was difficult. The largest difference between the observations and the forecast was revealed by the precipitation forecast. The rain forecast from the MEPS had a similar accumulated precipitation amount, but the hourly averages made it impossible to catch the short intense showers. The intense rainfall measured at Voss in the afternoon was not picked up by the model and rises the need for more accurate forecasts of small intense precipitation events.

The main take away from this thesis is the need for further research and larger samples sizes to accurately portray the isotopic evolution in a front. In this thesis I have determined a decreasing pattern of $\delta^{18}\text{O}$ in precipitation which was connected to rain-out and increasing altitude, but many uncertainties are connected to sampling and lack of verification for the different variables from the MEPS model. Further research is needed to verify the isotopic pattern, and more sampling stations needs to be included and water vapor tagging could further investigate the moisture transport from the moisture source.

References

- F. Aemisegger, J. K. Spiegel, S. Pfahl, H. Sodemann, W. Eugster, and H. Wernli. Isotope meteorology of cold front passages: A case study combining observations and modeling. *Geophysical Research Letters*, 42:5652–5660, 7 2015. ISSN 19448007. doi: 10.1002/2015GL063988.
- L. Araguas-Araguas, K. Froehlich, and K. Rozanski. Deuterium and oxygen-18 isotope composition of precipitation and atmospheric moisture. *Hydrological Processes*, 14:1341–1355, 2000.
- K. A. Browning. Airflow and structure of precipitation systems in extratropical cyclones. *The Life Cycles of Extratropical Cyclones*, 1:210–219, 1994.
- T. N. Carlson. Airflow through midlatitude cyclones and the comma cloud pattern. *Monthly Weather Review*, 108, 1980. doi: [https://doi.org/10.1175/1520-0493\(1980\)108<1498:ATMCAT>2.0.CO;2](https://doi.org/10.1175/1520-0493(1980)108<1498:ATMCAT>2.0.CO;2).
- T. B. Coplen, P. J. Neiman, A. B. White, J. M. Landwehr, F. M. Ralph, and M. D. Dettinger. Extreme changes in stable hydrogen isotopes and precipitation characteristics in a landfalling pacific storm. *Geophysical Research Letters*, 35, 11 2008. ISSN 00948276. doi: 10.1029/2008GL035481.
- W. Dansgaard. The abundance of o 18 in atmospheric water and water vapour. *Tellus*, 5:461–469, 11 1953. ISSN 00402826. doi: 10.1111/j.2153-3490.1953.tb01076.x.
- W. Dansgaard. Stable isotopes in precipitation. *Tellus*, 16:436–468, 11 1964. ISSN 00402826. doi: 10.1111/j.2153-3490.1964.tb00181.x.
- A. V. Dyrørdal. Dimensjonerende nedbør, 5 2021. URL https://snl.no/dimensjonerende_nedb%C3%B8r.
- M. Dütsch, S. Pfahl, and H. Sodemann. The impact of nonequilibrium and equilibrium fractionation on two different deuterium excess definitions. *Journal of Geophysical Research: Atmospheres*, 122:12,732–12,746, 2017. ISSN 21698996. doi: 10.1002/2017JD027085.
- I. FARLAB. Protocols and routines, 2019. URL <https://www.uib.no/en/FARLAB/119780/protocols-and-routines>.
- J. Galewsky, H. C. Steen-Larsen, R. D. Field, J. Worden, C. Risi, and M. Schneider. Stable isotopes in atmospheric water vapor and applications to the hydrologic cycle. *Reviews of Geophysics*, 54: 809–865, 12 2016. ISSN 19449208. doi: 10.1002/2015RG000512.
- J. R. Gat. Oxygen and hydrogen isotopes in the hydrologic cycle, 1996.
- S. D. Gedzelman and J. R. Lawrence. The isotopic composition of cyclonic precipitation. *Journal of Applied Meteorology (1962-1982)*, 21:1385–1404, 1982. ISSN 00218952, 2163534X. URL <http://www.jstor.org/stable/26180756>.
- S. D. Gedzelman and J. R. Lawrence. Isotopic composition of precipitation from two extratropical cyclones. *Monthly Weather Review*, 118:495–509, 1990.
- P. Graf, H. Wernli, S. Pfahl, and H. Sodemann. A new interpretative framework for below-cloud effects on stable water isotopes in vapour and rain. *Atmospheric Chemistry and Physics*, 19: 747–765, 1 2019. ISSN 16807324. doi: 10.5194/acp-19-747-2019.
- H. Hersbach, B. Bell, P. Berrisford, S. Hirahara, A. Horányi, J. Muñoz-Sabater, J. Nicolas, C. Peubey, R. Radu, D. Schepers, A. Simmons, C. Soci, S. Abdalla, X. Abellan, G. Balsamo, P. Bechtold, G. Biavati, J. Bidlot, M. Bonavita, G. D. Chiara, P. Dahlgren, D. Dee, M. Diamantakis, R. Dragani,

- J. Flemming, R. Forbes, M. Fuentes, A. Geer, L. Haimberger, S. Healy, R. J. Hogan, E. Hólm, M. Janisková, S. Keeley, P. Laloyaux, P. Lopez, C. Lupu, G. Radnoti, P. de Rosnay, I. Rozum, F. Vamborg, S. Villaume, and J. N. Thépaut. The era5 global reanalysis. *Quarterly Journal of the Royal Meteorological Society*, 146:1999–2049, 7 2020. ISSN 1477870X. doi: 10.1002/qj.3803.
- HOBO. Data logging rain gauge manual part rg2 and rg2-m, 2001. URL www.onsetcomp.com.
- J. Jouzel. Isotopes in cloud physics: Multiphase and multistage condensation processes, 1 1986.
- J. Jouzel and L. Merlivat. Deuterium and oxygen 18 in precipitation: modeling of the isotopic effects during snow formation. *Journal of Geophysical Research*, 89, 1984. ISSN 01480227. doi: 10.1029/jd089id07p11749.
- L. Labbouz, J. V. Baelen, and C. Duroure. Investigation of the links between water vapor field evolution and rain rate based on 5 years of measurements at a midlatitude site. *Geophysical Research Letters*, 42:9538–9545, 11 2015. ISSN 19448007. doi: 10.1002/2015GL066048.
- W. R. Leo. Techniques for nuclear and particle physics experiments, 1994.
- X. Li, R. Kawamura, A. Sugimoto, and K. Yoshimura. Isotopic composition and moisture sources of precipitation in midlatitude regions characterized by extratropical cyclones’ route. *Journal of Hydrology*, 612, 9 2022. ISSN 00221694. doi: 10.1016/j.jhydrol.2022.128047.
- M. Majoube. Fractionnement en oxygène 18 et en deutérium entre l’eau et sa vapeur. 1 1971. doi: <https://doi.org/10.1051/jcp/1971681423>.
- L. Merlivat. Molecular diffusivities of h216o, hd16o, and h218o in gases. *The Journal of Chemical Physics*, 69:2864–2871, 1978. ISSN 00219606. doi: 10.1063/1.436884.
- L. Merlivat and J. Jouzel. Global climatic interpretation of the deuterium-oxygen 18 relationship for precipitation. *Journal of Geophysical Research*, 84:5029–5033, 1979. ISSN 01480227. doi: 10.1029/JC084iC08p05029.
- C. L. Muller, A. Baker, I. J. Fairchild, C. Kidd, and I. Boomer. Intra-event trends in stable isotopes: Exploring midlatitude precipitation using a vertically pointing micro rain radar. *Journal of Hydrometeorology*, 16:194–213, 2015. ISSN 15257541. doi: 10.1175/JHM-D-14-0038.1.
- M. Müller, M. Homleid, K. I. Ivarsson, M. A. Køltzow, M. Lindskog, K. H. Midtbø, U. Andrae, T. Aspelien, L. Berggren, D. Bjørge, P. Dahlgren, J. Kristiansen, R. Randriamampianina, M. Ridal, and O. Vignes. Arome-metcoop: A nordic convective-scale operational weather prediction model. *Weather and Forecasting*, 32:609–627, 4 2017. ISSN 15200434. doi: 10.1175/WAF-D-16-0099.1.
- D. Noone. Pairing measurements of the water vapor isotope ratio with humidity to deduce atmospheric moistening and dehydration in the tropical midtroposphere. *Journal of Climate*, 25: 4476–4494, 7 2012. ISSN 08948755. doi: 10.1175/JCLI-D-11-00582.1.
- Palmex Ltd. Palmex rain sampler s1. URL <http://www.rainsampler.com/portfolio-page/rain-sampler-rs1/>.
- S. Pfahl and H. Sodemann. What controls deuterium excess in global precipitation? *Climate of the Past*, 10:771–781, 4 2014. ISSN 18149332. doi: 10.5194/cp-10-771-2014.
- Picarro Inc. Operation, maintenance, and troubleshooting l2140-i, l2130-i or l2120-i analyzer and peripherals user’s manual picarro analyzer user’s manual, 2013. URL www.picarro.com.

- S. C. Sherwood, R. Roca, T. M. Weckwerth, and N. G. Andronova. Tropospheric water vapor, convection, and climate. *Reviews of Geophysics*, 48, 4 2010. ISSN 87551209. doi: 10.1029/2009RG000301.
- R. B. Smith and J. P. Evans. Orographic precipitation and water vapor fractionation over the southern andes. *Journal of Hydrometeorology*, 8:3–19, 2 2007. ISSN 1525755X. doi: 10.1175/JHM555.1.
- H. Sodemann and A. Stohl. Moisture origin and meridional transport in atmospheric rivers and their association with multiple cyclones*. *Monthly Weather Review*, 141:2850–2868, 2013. doi: 10.1175/MWR-D-12-00256.s1. URL <http://dx.doi.org/10.1175/MWR-D-12-00256.s1>.
- L. A. Stern and P. M. Blisniuk. Stable isotope composition of precipitation across the southern patagonian andes. *Journal of Geophysical Research Atmospheres*, 107:ACL 3–1–ACL 3–14, 2002. ISSN 01480227. doi: 10.1029/2002JD002509.
- Y. Sun, D. Wendi, D. E. Kim, and S. Y. Liang. Deriving intensity–duration–frequency (idf) curves using downscaled in situ rainfall assimilated with remote sensing data. *Geoscience Letters*, 6, 12 2019. ISSN 21964092. doi: 10.1186/s40562-019-0147-x.
- J. M. Wallace and P. V. Hobbs. *Atmospheric Science: An Introductory Survey*. Elsevier, 2nd edition, 2006.
- T. T. Warner. *Numerical Weather and Climate Prediction*. Cambridge University Press, 12 2010. ISBN 9780521513890. doi: 10.1017/CBO9780511763243.
- Y. Weng, A. Johannessen, and H. Sodemann. High-resolution stable isotope signature of a land-falling atmospheric river in southern norway. *Weather and Climate Dynamics*, 2:713–737, 8 2021. doi: 10.5194/wcd-2-713-2021.
- D. S. Wilks. *Statistical Methods in the Atmospheric Sciences*, volume 100. Elsevier, 3rd edition, 2011.
- J. Worden, D. Noone, K. Bowman, R. Beer, A. Eldering, B. Fisher, M. Gunson, A. Goldman, R. Herman, S. S. Kulawik, M. Lampel, G. Osterman, C. Rinsland, C. Rodgers, S. Sander, M. Shephard, C. R. Webster, and H. Worden. Importance of rain evaporation and continental convection in the tropical water cycle. *Nature*, 445:528–532, 2 2007. ISSN 14764687. doi: 10.1038/nature05508.
- K. Yoshimura. Stable water isotopes in climatology, meteorology, and hydrology: A review. *Journal of the Meteorological Society of Japan*, 93, 2015. ISSN 00261165. doi: 10.2151/jmsj.2015-036.
- K. Yoshimura, M. Kanamitsu, and M. Dettinger. Regional downscaling for stable water isotopes: A case study of an atmospheric river event. *Journal of Geophysical Research Atmospheres*, 115, 2010. ISSN 01480227. doi: 10.1029/2010JD014032.